

A Thesis Submitted for the Degree of PhD at the University of Warwick

Permanent WRAP URL:

<http://wrap.warwick.ac.uk/78616>

Copyright and reuse:

This thesis is made available online and is protected by original copyright.

Please scroll down to view the document itself.

Please refer to the repository record for this item for information to help you to cite it.

Our policy information is available from the repository home page.

For more information, please contact the WRAP Team at: wrap@warwick.ac.uk

THE SEMICLASSICAL THEORY OF HOPPING CONDUCTIVITY

by

KENNETH JOHN HAYDEN

A thesis submitted to the University of Warwick
for admission to the degree of Doctor of Philosophy
July, 1978.

TABLE OF CONTENTS

<u>CHAPTER</u>	<u>TITLE</u>	<u>PAGE NUMBER</u>
1	INTRODUCTION	1
2	SEMICLASSICAL FORMALISM	
2.1	Linearized Rate Equations	9
2.2	Formal Expression for AC Conductivity	11
2.3	The DC Limit	13
3	THE DC CONDUCTIVITY	
3.1	Equivalent Conductance Network	15
3.2	Formal Expression of the DC Conductivity	18
3.3	The Percolation Aspect of Hopping Conductivity	21
3.4	The High Density and High Frequency Limits	25
4	NON-DEGENERATE HOPPING IN VERY NARROW ENERGY BANDS	
4.1	Analytical Formulae	27
4.2	Comparison with Computer Data	30
4.3	Comparison of the Analytical Formulae with Data for Three-Dimensional Systems	33
4.4	Discussion	36

5	DEGENERATE HOPPING IN VERY WIDE ENERGY BANDS	
5.1	Formulae for Hopping in Wide Bands	37
5.2	Comparison with Computer Data	41
5.3	Universal Curves and Comparison with Experimental Data for Three-Dimensional Systems	43
5.4	Universal Curves and Comparison with Experimental Data for Two-Dimensional Systems	48
5.5	Discussion	50
6	HOPPING IN ENERGY BANDS OF INTERMEDIATE WIDTH	
6.1	General Formulae	52
6.2	Comparison with Experiment	57
6.3	Discussion	59
7	REVIEW OF ALTERNATIVE DC FORMULAE	
7.1	Introduction	61
7.2	Alternative Formulae for the Exponent	61
7.3	Alternative Formulae for the Prefactor	64
8	AC CONDUCTIVITY	
8.1	The Pair Approximation	66
8.2	Comparison with Computer Data	68
8.3	Conductivity of Degenerate Systems	68
8.4	Comparison with Experimental Data	70
8.5	Discussion	71

<u>CHAPTER</u>	<u>TITLE</u>	<u>PAGE NUMBER</u>
9	DISCUSSION	
9.1	Introduction	73
9.2	Basic Formalism	73
9.3	The Equivalent Network and Percolation	74
9.4	Comparison with Computer Data	76
9.5	Interpretation of Experimental Data	77
9.6	The Transition Rates	78
9.7	The AC Conductivity	81
9.8	Future Work	82
9.9	Conclusion	84
REFERENCES		85
APPENDICES		
A1	EVALUATION OF $2B$, σ_p AND $\sigma(\infty)$ FOR VERY WIDE BANDS	
A1.1	Evaluation of $2B$	89
A1.2	Evaluation of σ_p	90
A1.3	Evaluation of $\sigma(\infty)$	91
A2	EVALUATION OF s_p and σ_p FOR BANDS OF FINITE WIDTH	
A2.1	Fermi Level Lying at the Centre of the Band	93
A2.2	Fermi Level Lying off Centre of the Band	94
A3	THE TRANSITION RATES	97

LIST OF FIGURES

<u>FIGURE NO.</u>	<u>TITLE</u>	<u>FOLLOWS PAGE NO.</u>
1	Schematic Diagram of Impurity Conduction in an n-type Semiconductor	3
2	Schematic Diagram of Density of States in Amorphous Semiconductors	4
3	Schematic Diagram of an Inversion Layer in a p-type Semiconductor	5
4	Charge Density in Inversion Layers	6
5	Schematic Diagram of Density of States in an Inversion Layer	6
6	The Equivalent Network	15
7	High and Low Conductances in the Conductance Network	23
8	Comparison of Theory with the Three- Dimensional Data of Seager and Pike	30
9	Comparison of Theory with the Three- Dimensional Data of McInnes	31
10	Comparison of Theory with the Two- Dimensional Data of McInnes	32
11	Comparison of Theory with Data Obtained from n-type Germanium	33
12	Comparison of Theory with Data Obtained from p-type Germanium	34
13	Comparison of Theory with Data Obtained from Doped Amorphous Germanium	35
14	Schematic Diagram of the Contours $q(\epsilon_1, \epsilon_2) = q$	39
15	Comparison of Theory with the Two- Dimensional Data of Seager and Pike	42
16	Comparison of Theory with the Two- Dimensional Data of McInnes	42
17	Comparison of Theory with the Three- Dimensional Data of Seager and Pike	43

<u>FIGURE NO.</u>	<u>TITLE</u>	<u>FOLLOWS PAGE NO.</u>
18	Comparison of Theory with the Three- Dimensional Data of McInnes	43
19	Plot of R_p against R_{po}	44
20	Plot of Logarithmic Conductivity against R_{po} for Three Dimensions	44
21	Plot of Logarithmic Conductivity against R_{po} for Two Dimensions	48
22	Graph Illustrating the Temperature Dependence of s_p	54
23	Plot of Logarithmic Conductivity against T^{-1}	56
24	Plot of Transition Temperature θ against $s_{p\infty}$	56
25	Plot of Logarithmic Conductivity against s_{po}	56
26	Comparison of Theory with the Experimental Data of Fowler and Harstein	58
27	Graph Showing Logarithmic Conductivity against Frequency	68
28	Plot of the Frequency Dependent Conductivity against R_{po}	70
29	Graph Illustrating the AC and Dc Domains	71
30	Constant s Surfaces in the Percolation Space	75
31	Schematic Diagram of the $q(\epsilon_1, \epsilon_2) = q$ Contours with a Variable Fermi Level	93
32	Plot of the Transition Rates against Site Separation	99

LIST OF TABLES

<u>TABLE NO.</u>	<u>TITLE</u>	<u>PAGE NO.</u>
1	Parameters in the Approximate Linear Relationship $R_p = MR_{po} + C$	44
2	Values of ρ_F and g_o Derived from 3D Experimental Data	46
3	Alternative Formulae for Degenerate Hopping	65
4	Table Indicating s_p and σ_p for Energy Bands of Finite Width	96
5	Characteristic Temperatures and Energies for Hopping in Energy Bands of Finite Width	96

ACKNOWLEDGEMENTS

I wish to express my sincere gratitude to Professor P. N. Butcher for his excellent supervision throughout the course of this work. I would also like to thank all the members of the Department of Physics and, in particular, those members associated with the Theoretical Group for many useful discussions.

I gratefully acknowledge the financial support given to me by the Department of Physics and the Science Research Council.

I wish to thank Miss Wendy Hampson for her excellent typing of the thesis and her close attention to detail.

Finally, I want to thank my wife Susan for her continued support and encouragement throughout the period of my study.

DECLARATION

Except where indicated, the work reported in this thesis is the result of my own independent research. No details of this work have appeared in any thesis or dissertation at this, or any other, institution. Various aspects of the research reported herein have been published:

"Analytical Formulae for DC Hopping Conductivity" Butcher P N, Hayden K T and McInnes J A 1977 Phil. Mag. Vol 36 No 1 19-32.

"Analytical Formulae for DC Hopping Conductivity II. Degenerate Hopping in Wide Bands" Butcher P N and Hayden K J 1977 Phil. Mag. Vol 36 No 3 657-676.

"AC Hopping Conductivity in Degenerate Systems" Butcher P N and Hayden K J 1977 Proc. 7th Int. Conf. on Amorphous and Liquid Semiconductors, edited by W E Spear (Edinburgh: The University) p 234.

"Conductivities, Drift and Diffusion in Amorphous Semiconductors" Butcher P N, Clark J D, Hayden K J and McInnes J A 1978. To be published in the Proceedings of the 14th International Conference on the Physics of Semiconductors.

"Analysis of Hopping Conduction in Impurity Bands in Inversion Layers"

Hayden K J and Butcher P N 1978. Accepted for publication in Phil. Mag.

Abstract

This work develops the semiclassical theory of electrical conduction due to electrons in localized states, and compares the resultant formulae with a variety of experimental data.

We begin by using the equivalent electrical network, derived from the phenomenological rate equations, to deduce the dc conductivity of a number of model systems. Percolation arguments are used to derive both the exponent and the prefactor when the dc conductivity is written in the form $\sigma = \sigma_0 \exp [-s_p]$.

In particular, we derive formulae for the cases when the energies of the electron states are distributed over a very narrow range, a very wide range and an intermediate range. In the first two cases the formulae are in excellent agreement with computer generated data obtained by numerical solutions of Kirchhoff's equations for the equivalent network.

Experimental data obtained from studies of a number of systems are analysed, namely, impurity conduction in crystalline germanium and amorphous silicon, the conductivity of evaporated films of amorphous germanium and finally the conductivity due to electrons in an inversion layer formed in a metal-oxide-silicon-field-effect-transistor. In all cases very good agreement is found between experiment and theory.

Formulae are also derived for the ac conductivity. Comparison of these formulae with computer data again shows good agreement between theory and experiment. We show how detailed considerations indicate that the ac data obtained from evaporated films of amorphous germanium cannot be due to hopping at the Fermi level, as is normally assumed.

In conclusion, this work develops the simple hopping theory which adequately describes experimental data obtained from a variety of systems. Various problems are isolated; which relate to the model adopted rather than any approximation inherent in the deduction of the analytical formulae.

CHAPTER 1 - INTRODUCTION

The theoretical and experimental understanding of electron transport in systems consisting of a regular array of atoms has, for many years, received much attention in solid state physics. For such systems the electron states are extended throughout the array and the concept of a k-space is both fundamental and well defined. Electron transport processes, such as band conduction in crystals, can then be described in terms of transitions in k-space. In contrast an electron which is localized in real space, carries no current - the expectation value of the electron velocity is zero. Transport processes involving localized states are therefore determined by transitions of electrons from full states to neighbouring empty states. Since this basic process changes the position of the electron in real space, it is called a "hop", and localized state transport is therefore referred to as "hopping" transport. In this work we investigate one particular transport coefficient, the electrical conductivity σ .

The hopping mechanism was first proposed by Conwell (1956) and Mott (1956) to explain the dc electrical conductivity of compensated crystalline semiconductors cooled to liquid helium temperatures so as to suppress band conduction. For the next decade, the dc behaviour in this regime was the subject of extensive experimental investigations (Fritzsche and Lark-Horowitz 1954; Keyes and Sladek 1956; Fritzsche 1958, 1959, 1960; Fritzsche and Cuevas 1960; Atkins, Donovan and Walmsey 1960; Miller and Abrahams 1960). At these temperatures the hopping conductivity obeys an activation law, and the conductivity may be written as $\sigma = \sigma_p \exp(-\epsilon_3/k_B T)$, where ϵ_3 is the activation energy associated with the hopping processes. Experimental studies of the dc conductivity of n-type germanium at temperatures considerably below liquid helium, have been made recently by Allen and Adkins (1974).

The observed behaviour is different to that observed at liquid helium temperatures; the conductivity may be written as $\sigma = \sigma_p \exp \left[-(T_0/T)^{1/4} \right]$, where T_0 is a characteristic temperature.

Interest in hopping conductivity waned in the decade 1960-1970 but has increased greatly again in recent years due to an expansion of research into the physical properties of amorphous semiconductors and the behaviour of electrons in the inversion layer of metal-oxide-silicon-field-effect-transistor (MOSFET) devices. In both these cases, as we outline below, some of the electron states are localized. A hopping mechanism is therefore to be expected for transport processes involving these states. The observed experimental temperature dependence of the dc hopping conductivity of amorphous semiconductors falls broadly into two categories: either $\exp \left[-\epsilon/k_B T \right]$ where ϵ is an activation energy or $\exp \left[-(T_0/T)^{1/4} \right]$ where T_0 is a characteristic temperature. The $T^{1/4}$ behaviour was first found by Clark (1967) in evaporated germanium films and has been confirmed experimentally by many authors (Walley and Jonscher 1968; Chopra and Bahl 1970; Hauser and Staudinger 1973; Arizumi, Yoshida, Baba, Shimakawa and Nitta 1974; Agarwal, Gutta and Narasimhan 1975; Gilbert and Adkins 1976). The first theoretical derivation of the $T^{1/4}$ law is due to Mott (1969). Many authors have also derived the $T^{1/4}$ law using a variety of approaches (Ambegaokar, Halperin and Langer 1971; Pollak 1972; Butcher 1976a, b). In contrast to the $T^{1/4}$ behaviour found in evaporated films of amorphous germanium, Abkowitz, Le Comber and Spear (1976) find that amorphous germanium films produced by glow discharge exhibit a simple activated type temperature dependence. Activated behaviour is also found by many authors for chalcogenide glasses (Mott and Davis 1971; Nunoshita, Arai, Taneki and Hamakawa 1973).

Recently Spear and co-workers have succeeded in doping amorphous

silicon with phosphorus (Le Comber, Jones and Spear 1977). The resulting impurity states are localized and the observed conductivity due to these states has the same behaviour as impurity conduction in crystalline semiconductors.

Under certain experimental conditions hopping conduction can be observed in inversion layers in MOSFET devices. We outline the reasons for the presence of localized states in these devices below. The first suggestion that the data may be interpreted on the basis of hopping conduction was made by Mott (1973), and Stern (1974). Experimental observations have been made by many authors (Pepper, Pollit, Adkins and Oakley 1974; Pepper, Pollit and Adkins 1974; Pepper 1977; Harstein, Ning and Fowler 1976; Pollit 1977). Recently, hopping conduction due to impurity electrons has been reported in these devices (Harstein and Fowler 1975 a, b, 1976). An extensive review of transport processes in MOSFETS can be found in the paper by Mott, Pepper, Pollit, Wallis and Adkins (1975).

We see that the systems of interest fall into three main categories: impurity conduction, conduction in amorphous semiconductors, and the conductivity due to localized electrons in inversion layers. The first of these systems, namely conducting electrons in localized impurity states, is the best understood (for an extensive review see Shklovskii 1973). Figure 1 shows just such a system. It is a schematic representation of an n-type semiconductor in which the doping levels are low enough for all the impurity states to be localized. At very low temperatures most of the electrons are frozen out of the conduction band and we assume all the acceptor levels are full. Since the material is n-type there are more donors than acceptors, which implies that some of the donor levels are empty and some are full. Transport may therefore proceed through the donor levels by the hopping process indicated in the Figure.

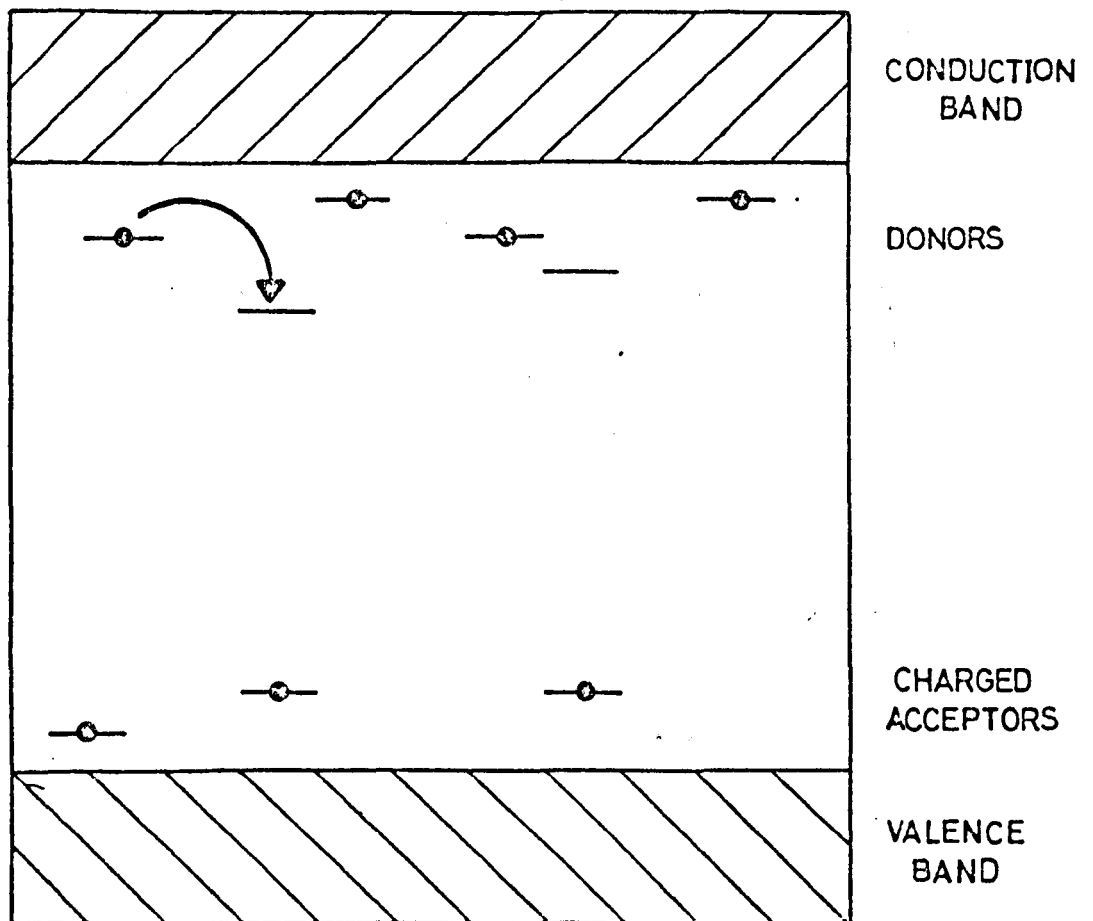


FIGURE 1 Schematic diagram of impurity conduction in an n-type crystalline semiconductor. Occupied sites are indicated by a dot. The arrow indicates a "hop".

Whilst the primary function of the acceptors is to ensure that some of the donor levels are empty, the fact that there are ionized donors and acceptors present distributed randomly throughout the crystal means that the donor levels are randomized due to the Coulomb field produced by these centres, as indicated in the diagram. The hops are therefore necessarily inelastic and must be phonon assisted. As we see later, the quantity $\Delta/k_B T$, where Δ is some average energy separation of the states, is crucial in determining the temperature dependence of the dc conductivity.

In analysing the conductivity data of amorphous semiconductors we are not in quite as good a position as in the impurity conduction case. While most authors would argue that at least some of the electron states in these disordered materials are localized, there has been no satisfactory description of these states in real materials. Anderson (1958), in a classic paper, shows how localized states arise as a direct consequence of the random nature of the system (in this case potential randomness). It is not at all clear, however, how to carry Anderson's arguments over to the amorphous semiconductor case. Many attempts have been made to solve Schrodinger's equations for a random array of scatterers directly on the computer (Thouless 1977; Thouless and Licciardello 1977). The results of these works appear to show that the introduction of disorder localizes at least some of the electron states. In particular, the energy of the electron states is critical in determining whether a state is localized or not. This idea was first mooted by Mott (1969) to explain data obtained from conductivity measurements in amorphous semiconductors. He postulated that, because of the randomness of these materials, electron states at the valence and conduction band extrema would be localized. Separating the localized and non-localized regimes is the 'mobility edge' positioned at an energy ϵ_v and ϵ_c in the valence and conduction band

respectively. This idea is shown schematically in Figure 2.

Electrons with energies lying between ϵ_v and ϵ_c are said to be in the 'mobility gap'. Also situated within the mobility gap are electron states associated with defects such as impurities, as illustrated in Figure 2. With this type of structure, the position of the Fermi level together with the magnitude of the density of states at the Fermi level are crucial in determining the behaviour of transport properties. For example, if the Fermi level lies in the localized states in the conduction band tail, then at high temperatures the dominant contribution to the conductivity may arise from activation to the mobility edge and then conduction in extended states. At lower temperatures hopping in the localized states may be the dominant process. Postulating a low density of states at the Fermi level also leads to an activated type conduction process (Mott and Davis 1971). The problem of the position of the Fermi level and electron statistics is discussed by many authors (Street and Mott 1975; Yoffa and Adler 1977; Okamoto and Hamakawa 1977).

Finally, we come to the last of the systems of interest in the present work, namely the inversion layer. In Figure 3 we show a schematic representation of the energy level diagram of a p-type semiconductor when it is incorporated in the basic form for a MOSFET, namely a metal-dielectric-semiconductor-capacitor structure. Application of a gate voltage to the metal changes the charge distribution at the semiconductor surface. Bending the bands sufficiently induces a layer at the surface in which the majority carrier is the minority carrier in the bulk. This condition is referred to as inversion. Schrieffer (1957) pointed out that, if the field was sufficiently strong, then a one-dimensional surface potential well is formed with a dimension smaller than the electron wavelength. Under these conditions, the electron wavefunction goes to zero outside the

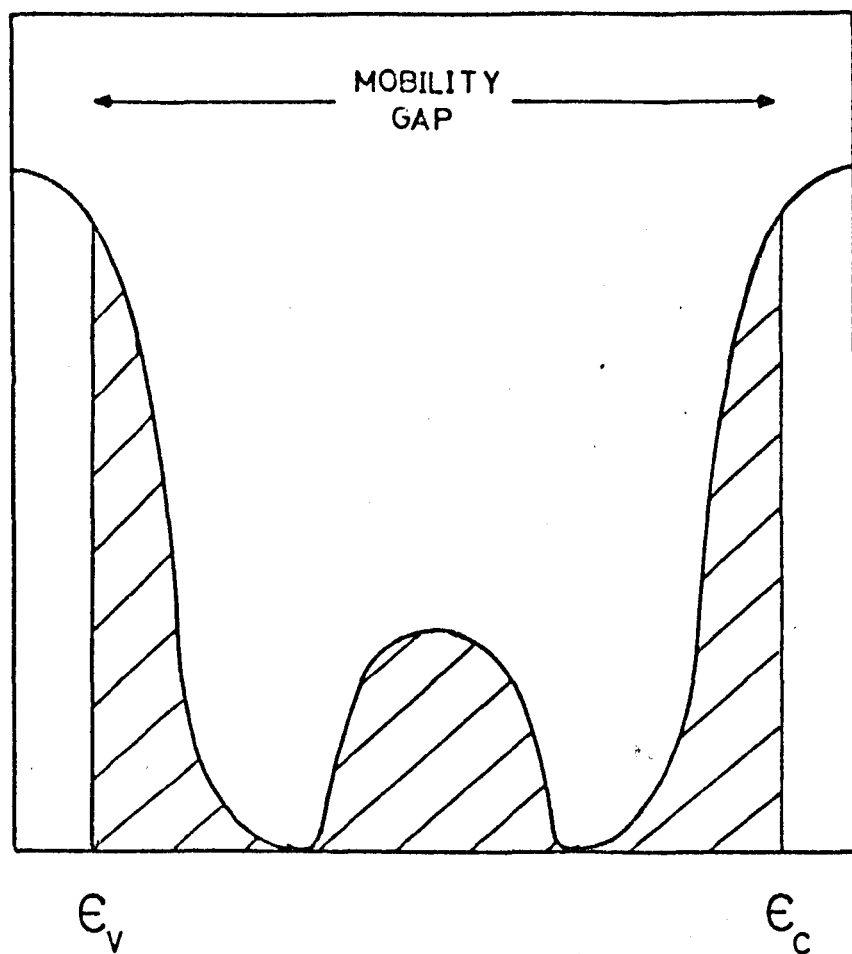


FIGURE 2 Schematic diagram of the density of states in an amorphous semiconductor. ϵ_c and ϵ_v refer to the mobility edges in the valence and conduction bands respectively. Localized states are shown shaded

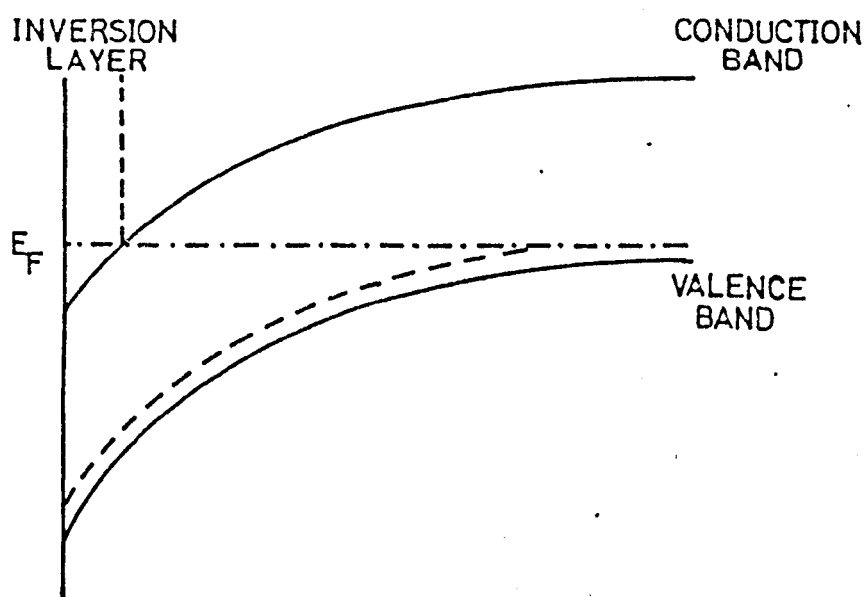


FIGURE 3 Schematic diagram illustrating the formation of an inversion layer in a p-type semiconductor. The dashed line represents the acceptor levels. The dash-dot line is the Fermi level.

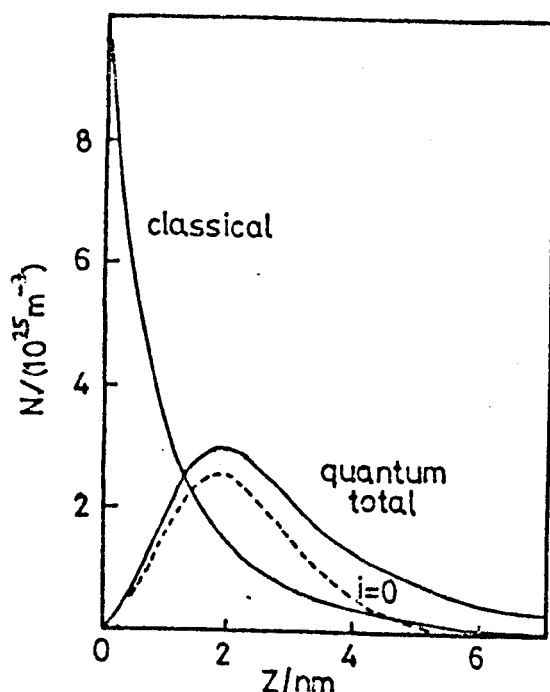


FIGURE 4 Classical and quantum mechanical inversion layers, showing charge densities for a Si(100) surface with electron concentration equal to 10^{16} m^{-2} . $T = 150 \text{ K}$. $N_A = 1.5 \times 10^{22} \text{ m}^{-3}$. $i = 0$ refers to the sub-band, the total charge distribution indicates the population of higher sub-bands. From Stern (1974)

potential well. In Figure 4 we show the results of a calculation by Stern (1972, 1974), who calculates the wavefunction by solving Schrodinger and Poisson equations in a self-consistent manner. We see, therefore, that the electron states are quantised in a direction perpendicular to the surface. Parallel to the surface the electrons behave normally. Such a situation is called a surface sub-band. This band behaves as a two-dimensional system. Thus any random fluctuations in the potential seen by the electron, arising for example, from defects in the SiO_2 layer will induce localization in a direction parallel to the interface. The conduction band in the inversion layer, therefore, will have localized tail states at its extremity as in the three-dimensional case. The addition of Na^+ ions into the SiO_2 leads to the formation of localized states associated with these Na^+ ions (Fowler and Harstein 1977). These states, which are called impurity states, form a band below the localized tail states. We see, therefore, that the band structure for the inversion layer electrons is the two-dimensional analogue of Figure 2. In Figure 5, we show just such a band structure. As in the amorphous material, the dominant transport process depends on the position of the Fermi level. However, an important property of MOSFET devices is the ease with which the Fermi level may be moved. By moving the Fermi level through the impurity band, localized states at the conduction band edge, mobility edge and into the extended states regime a variety of the transport mechanisms of a two-dimensional system may be investigated. In particular, we are interested in the two cases of the Fermi level lying in the tail states and in the band of impurity states.

All the experimental systems outlined above give data which may be analysed using formulae developed in a variety of ways. Unfortunately, some of the system parameters, except for one or two isolated cases, are not known and detailed investigation of the derived

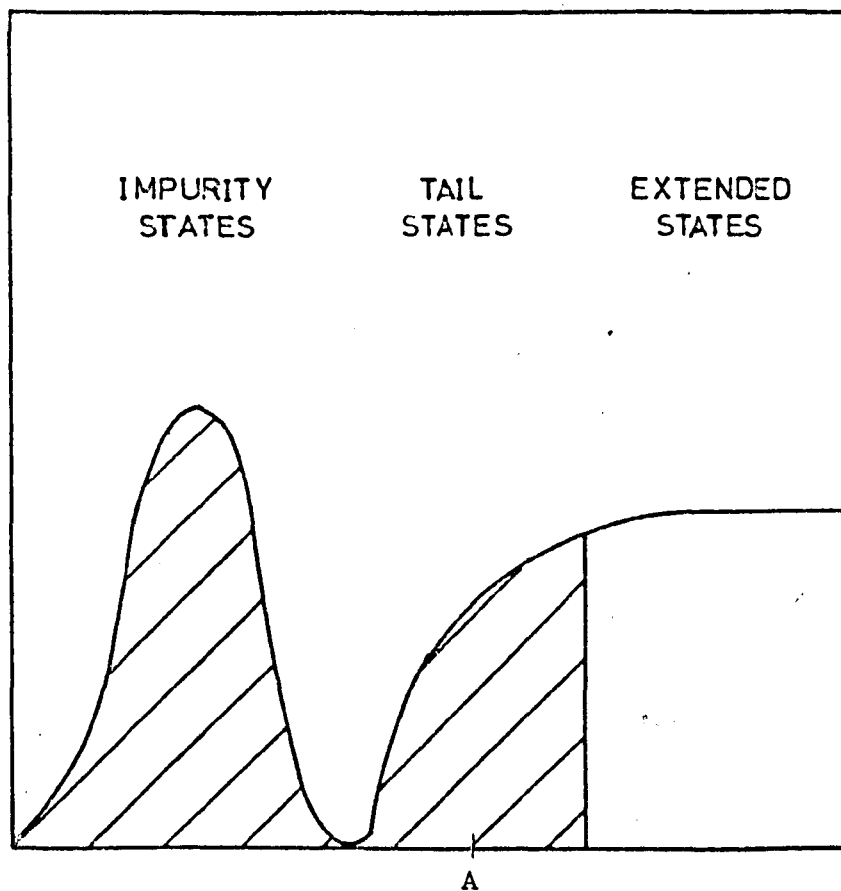


FIGURE 5 Schematic diagram showing the density of states in an inversion layer. Localized states are shown shaded.

formulae is difficult. With the advent of large storage computers, however, this problem may be overcome. As shown later, computer simulation of the hopping process is conceptually simple, albeit that large computers are necessary. We will therefore be interested in comparing our theoretical predictions with well defined computer generated data given by a variety of authors (Pike and Seager 1974; Seager and Pike 1974; Mashke, Overhoff and Thomas 1974; Butcher, Hayden and McInnes 1977; Butcher and McInnes 1978; McInnes and Butcher 1978).

Our primary interest here is with the dc conductivity of hopping systems. We shall, however, be interested in some aspects of the ac conductivity due to localized states. The first experimental and theoretical work on ac hopping conductivity was carried out by Pollak and Geballe (1961) who investigated the conductivity of compensated crystalline n-type silicon. Golin (1963) obtained similar results for p-type germanium. In both cases the observed frequency dependence of the ac conductivity is ω^s where $s \sim 0.8$. This type of frequency dependence has also been seen in amorphous materials by a variety of authors (Gilbert and Adkins 1976; Chopra and Bahl 1970; Arizumi et al 1974; Hauser and Staudinger 1973; Agarwal et al 1975). The data are usually interpreted on the basis of the Austin-Mott formula (Austin and Mott 1969), which predicts an $\omega^{0.8}$ frequency dependence. Recently, there has been considerable discussion concerning the different values for some system parameters deduced from the ac and dc data (Abkowitz, Le Comber and Spear 1976; Butcher and Hayden 1977).

The plan of the thesis is as follows. In Chapter 2 we introduce the semiclassical formalism for the conductivity due to localized electrons, and derive a formal expression of the ac conductivity from

the rate equations. We show how this approach fails to account for the dc conductivity. Chapter 3 deals with the derivation of the dc conductivity. In Chapter 4 the general expressions derived for the dc conductivity are applied to the simple case of non-degenerate hopping in narrow energy bands. The resulting formulae are then compared with computer generated and experimental data. In Chapter 5 we derive formulae applicable to degenerate hopping in very wide energy bands. The results are again compared with data obtained from computers and experiments. Chapter 6 deals with the analysis of inversion layer data obtained from the studies of impurity bands whose width lies between the limiting cases of very wide and very narrow bandwidths. We briefly review alternative dc formulae in Chapter 7. The ac conductivity is derived in Chapter 8 and the resultant formulae are compared with computational and experimental data. We also show in this chapter why the interpretation of the experimental ac data must be viewed with caution. Finally, Chapter 9 contains a general discussion of the work presented in the preceding chapters in the context of hopping conductivity in general.

CHAPTER 2 - SEMICLASSICAL FORMALISM

§2.1 Linearized Rate Equations

Since the pioneering paper of Miller and Abrahams (1960) very nearly all the theory of hopping conductivity has been based on the phenomenological rate equations for ac and dc conductivity (Brenig et al. 1971, Butcher 1972, 1973, 1974). A derivation of the rate equations from more fundamental principles has recently been published by Barker (1977). He shows that the rate equations are derivable from Kubo's formula (Kubo 1957) which is an exact expression for the ac and dc conductivities of any system. Other authors (Capek 1972, 1973, 1975; Capek, Koc and Zamek 1975) disagree. This debate rests on sophisticated quantum transport arguments, a regime not covered in this work. We shall, however, show in later sections computational results which indicate that Barker's conclusion is correct, and that the rate equations accurately describe transport due to electrons in localized states. We will therefore introduce the rate equations in an intuitive manner, but with the understanding that they may be derived rigorously. We follow the formalism introduced by Butcher (1976a). Consider a finite array of N_s sites in a macroscopic volume Ω and suppose each site may be occupied by only one electron. We label the sites by an integer m and write f_m for the probability that site m is occupied by an electron of either spin orientation. To determine f_m we use the rate equations

$$\frac{df_m}{dt} = \sum_n [f_n(1 - f_m)R_{nm} - f_m(1 - f_n)R_{mn}] \quad (2.1.1)$$

where R_{mn} is the transition rate from an occupied site m to an empty site n . When the electrons are in thermal equilibrium at temperature T , the quantity f_m reduces to the Fermi-Dirac function

$$f_m^0 = (\exp[\beta(\epsilon_m - \zeta^*)] + 1)^{-1} \quad (2.1.2)$$

where ϵ_m is the energy of an electron on site m and $\beta = (k_B T)^{-1}$.

In eqn. (2.1.2) $\zeta^* = \zeta + k_B T \ln 2$, where ζ is the chemical potential.

The $k_B T \ln 2$ term arises from the spin degeneracy of the state

(Blakemore 1967). This distinction between ζ and ζ^* will not be made explicit except in those cases when the $k_B T \ln 2$ term is important.

In thermal equilibrium detailed balance ensures that each term in the right-hand side of eqn. (2.1.1) vanishes separately. It follows from eqn. (2.1.2) that the transition rates R_{mn}^0 in thermal equilibrium satisfy the detailed balance relation

$$\frac{R_{mn}^0}{R_{nm}^0} = \exp[\beta(\epsilon_m - \epsilon_n)] \quad (2.1.3)$$

When a weak potential field is applied we write U_m for the potential at site m and suppose that R_{mn} satisfies eqn. (2.1.3) with $\epsilon_m - \epsilon_n$ replaced by $(\epsilon_m + U_m) - (\epsilon_n + U_n)$. Then, to first order in U_m and U_n we have

$$\frac{R_{mn}}{R_{nm}} = [R_{mn}^0 / R_{nm}^0] [1 + \beta(U_m - U_n)] \quad (2.1.4)$$

In the presence of the applied potential f_m suffers a perturbation f_m^1 . By substituting $f_m = f_m^0 + f_m^1$ in eqn. (2.1.1) and using eqn. (2.1.3), we find that f_m^1 is given to first order by the linearized rate equations

$$\frac{df_m^1}{dt} = \sum_n [f_n^1 R_{nm}^e - f_m^1 R_{mn}^e] + \beta \sum_n [F_n U_n R_{nm}^e - F_m U_m R_{mn}^e] \quad (2.1.5)$$

where

$$R_{mn}^e = \Gamma_{mn} / F_m \quad (2.1.6)$$

with
$$\Gamma_{mn} = f_m^0(1 - f_n^0)R_{mn}^0 \quad (2.1.7)$$

and
$$F_m = f_m^0(1 - f_m^0) \\ = -k_B T df_m^0 / dE_m \quad (2.1.8)$$

The formal solution of eqns. (2.1.5) is facilitated by the introduction of matrix notation. We write \underline{f}^1 and \underline{U} for row matrices whose m th columns are f_m^1 and U_m respectively and define a diagonal square matrix \underline{F} whose (mn) th element is F_m . Finally, we define a relaxation matrix \underline{R} whose (mn) th element is given by

$$R_{mn} = R_m^e \delta_{mn} - R_{mn}^e \quad (2.1.9)$$

where

$$R_m^e = \sum_n R_{mn}^e \quad (2.1.10)$$

In eqns. (2.1.9) and (2.1.10) R_{mn}^e vanishes when $m = n$ and δ_{mn} is the Kronecker- δ -symbol. With this notation eqns. (2.1.5) become

$$\frac{d\underline{f}^1}{dt} = -\underline{f}^1 \underline{R} - \beta \underline{U} \underline{F} \underline{R} \quad (2.1.11)$$

§2.2 Formal Expression For AC Conductivity

In order to derive an expression for the ac conductivity at frequency ω , we suppose that $U(\underline{r}, t)$ is the potential due to a uniform electric field E applied in the x -direction and having a sinusoidal time factor $\exp[-i\omega t]$. All the systems we consider are isotropic and the direction of the x -axis is arbitrary. Then $U(\underline{r}, t) = eEx \exp[-i\omega t]$ and $\underline{U} = eEx \exp[i\omega t]$ where \underline{x} is a row matrix whose m th column is x_m . Moreover $\underline{f}^1(t) = \underline{f}^1(0) \exp[i\omega t]$ and eqn. (2.1.11) reduces to

$$\underline{f}^1(0)(R - i\omega) = -\beta e E \underline{x} F R \quad (2.2.1)$$

The formal solution of eqn. (2.2.1) is

$$\underline{f}^1(0) = -\beta e E \underline{x} F R G \quad (2.2.2)$$

where the matrix G is defined by

$$(R - i\omega)G = 1 \quad (2.2.3)$$

The induced dipole moment in the x-direction is

$$P_x(t) = -e\Omega^{-1} \underline{f}^1(t) \underline{\tilde{x}} \quad (2.2.4)$$

where the tilde indicates the transpose of a matrix. The x-component of the current density is $-i\omega P_x(t)$ and the conductivity at frequency ω is therefore

$$\begin{aligned} \sigma(\omega) &= \frac{-i\omega P_x(t)}{E \exp[-i\omega t]} \\ &= -i\omega e^2 \Omega^{-1} \underline{x} F R G \underline{x} \end{aligned} \quad (2.2.5)$$

It is constructive to put eqn. (2.2.5) in another form. By using the relations

$$R G = 1 + i\omega G \quad (2.2.6)$$

$$1 + i\omega G_{mn} = -i\omega \sum_{n \neq m} G_{mn} \quad (2.2.7)$$

$$F_m G_{mn} = F_n G_{nm} \quad (2.2.8)$$

we may eliminate the diagonal elements of G from eqn. (2.2.5) when we write out the matrix products in full. We then obtain

$$\sigma(\omega) = \omega^2 e^2 \beta \Omega^{-1} \sum_{mn} F_m G_{mn} x_m (x_n - x_m) \quad (2.2.9)$$

The algebra is completed by symmetrising the summand in eqn. (2.2.9) and using eqn. (2.2.8). Thus we obtain the final result

$$\sigma(\omega) = -\frac{1}{2} \omega^2 e^2 \beta \Omega^{-1} \sum_{mn} F_m G_{mn} (x_m - x_n)^2 \quad (2.2.10)$$

Eqn. (2.2.10) is the fundamental equation governing the frequency dependent conductivity. We shall use it in later chapters to calculate $\sigma(\omega)$ for a variety of systems. Our primary concern, however, is with the dc conductivity, and we therefore turn our attention to the behaviour of (2.2.10) in the limit $\omega \rightarrow 0$.

§2.3 The DC Limit

To investigate the behaviour of eqn. (2.2.10) in the limit $\omega \rightarrow 0$, we need to discuss the frequency dependence of G_{mn} . We may derive a Dyson expansion for G from eqn. (2.2.3) by splitting R into a diagonal part R^d and an off diagonal part $-R^1$. On iterating we have

$$G = G^0 + G^0 R^1 G^0 + G^0 R^1 G^0 R^1 G^0 \dots \quad (2.3.1)$$

where

$$G^0 = (R^d - i\omega)^{-1} \quad (2.3.2)$$

is diagonal. Furthermore we see from eqn. (2.1.9) that $R_{mn}^d = R_m^e$ and $R_{mn}^1 = R_{mn}^e$. Hence

$$G_{mn} = G_{mn}^0 \delta_{mn} + G_{mn}^0 [R_{mn}^e + \sum_p R_{mp}^e G_{pp}^0 R_{pn}^e \dots] G_{nn}^0 \quad (2.3.3)$$

where

$$G_{mm}^0 = [R_m^e - i\omega]^{-1} \quad (2.3.4)$$

In the limit $\omega \rightarrow 0$, $G_{mn}^0 \rightarrow [R_m^e]^{-1}$ and we see from eqn. (2.2.10) therefore that $\sigma(\omega) \rightarrow 0$. Thus for any finite sized cluster $\sigma(0)$ is zero. We see here a very basic problem in the study of the dc conductivity of hopping systems. To obtain a non-zero contribution to $\sigma(\omega)$ in the limit $\omega \rightarrow 0$, one needs to consider an infinite sized system. The summation involved in (2.3.3) is then impossible to carry out for a random array of sites. Whilst the determination of G_{mn} is, in principle, possible for a finite sized system the result yields a zero value for $\sigma(0)$. In other words: this approach yields only the steady state polarization in the system under consideration.

We therefore see that a determination of $\sigma(0)$ relies on some suitable approximation to the summation for G_{mn} in the case of an infinite sized system. One such approximation is that made by Scher and Lax (1973) who obtain a non-zero dc conductivity. Butcher (1974) has shown that their model is equivalent to supposing that after each hop, all sites except the one presently occupied are re-randomized. This method has limited applicability to real hopping systems because difficult hops which are avoided in the fixed site case become significant when the sites are re-randomized. We conclude, therefore, that a more fruitful approach to the dc conductivity problem is that adopted by Miller and Abrahams (1960). They show that there exists an equivalent network problem and indicate the method of solution.

CHAPTER 3 - THE DC CONDUCTIVITY

§3.1 Equivalent Conductance Network

We have seen in the preceding chapter that the dc conductivity cannot be calculated from the formal expression for the ac conductivity in the limit $\omega \rightarrow 0$. We may, however, reformulate the problem as an electrical network problem, as first shown by Miller and Abrahams (1960). We begin by considering eqn. (2.1.5). By redefining $f_m = f_m^0 + \beta F_m \phi_m$ we may determine ϕ_m from the linearised rate equations

$$F_m \frac{d\phi_m}{dt} = \sum_n \beta \Gamma_{mn} [(\phi_n + U_n) - (\phi_m + U_m)] \quad (3.1.1)$$

Eqns. (2.1.5) and (3.1.1) differ only in notation. If we now multiply by $-e$ and write $V_m = -(\phi_m + U_m)e^{-1}$, $C_m = e^2 \beta F_m$ and

$$g_{mn} = e^2 \beta \Gamma_{mn} \quad (3.1.2)$$

eqn. (3.1.1) becomes

$$C_m \frac{d}{dt} [V_m + e^{-1} U_m] = \sum_n g_{mn} (V_n - V_m) \quad (3.1.3)$$

Now let us consider an electrical network having nodes which coincide with the electron sites. Suppose that each node is connected to ground by a series combination of a voltage generator $e^{-1} U_m$ and a capacitance C_m . Finally, suppose that a conductance g_{mn} connects nodes m and n . Writing V_m for the voltage at node m we find that Kirchhoff's equations for the network are precisely (3.1.3). This equivalent network is shown in Figure 6. It is now a simple problem to determine $\sigma_1(\omega)$, the real part of the conductivity of the network. The Joule heat dissipated in a volume Ω is $\frac{1}{2} \sigma_1(\omega) E^2 \Omega$ and this must equal the sum of the powers $\frac{1}{2} g_{mn} |V_m - V_n|^2$ dissipated in the individual conductances in Ω . Thus we obtain

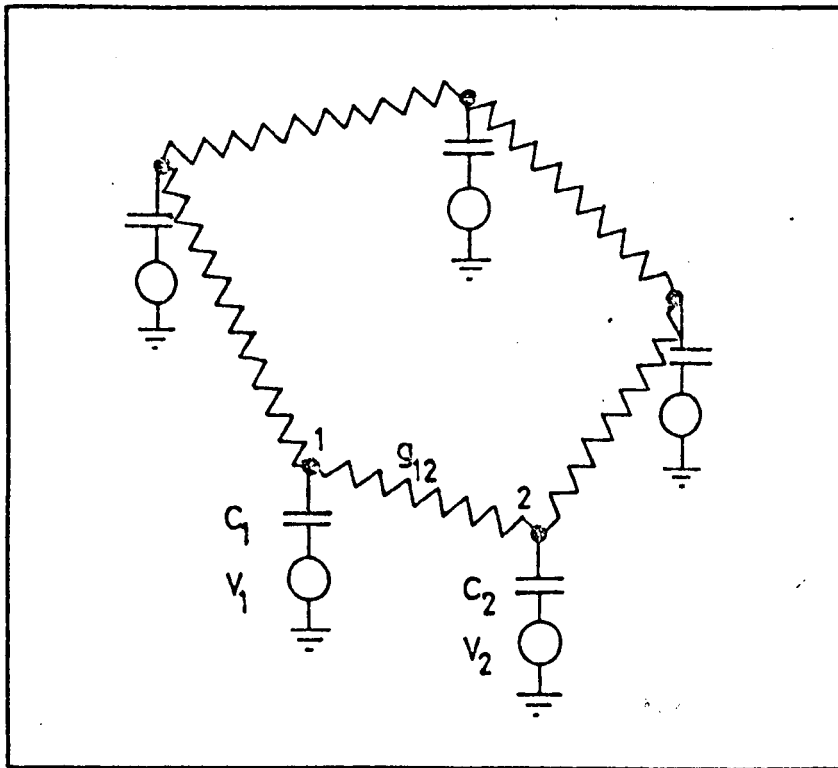


FIGURE 6 The equivalent network for five sites. Some of the conductances have been omitted for clarity. C_1 and V_1 refer to the capacitance and voltage generator associated with site 1 respectively.

$$\sigma_1(\omega) = \frac{1}{2} E^{-2} \Omega^{-1} \sum_{mn} g_{mn} |V_{mn}|^2 \quad (3.1.4)$$

where $V_{mn} \equiv V_m - V_n$. In (3.1.4), the summation is over all the sites in Ω and the factor $\frac{1}{2}$ prevents double counting. Eqn. (3.1.4) is conceptually simpler than (2.2.10). The evaluation of $\sigma_1(\omega)$ only requires a knowledge of the voltage drop across each conductance - a quantity which is easier to approximate than G_{mn} .

Equation (3.1.4) is the basis of our subsequent discussion. It is therefore of interest to derive it in a more formal way. Consider a box of length L and cross-sectional area A . We may define the current density across a plane at point x by summing the individual currents carried in each conductance g_{mn} where $x_m < x$ and $x_n > x$.

Thus

$$J(x) = \frac{1}{A} \sum_{mn} g_{mn} (V_m - V_n) \theta(x - x_m) \theta(x_n - x) \quad (3.1.5)$$

where $\theta(y)$ is the unit step function. We may now obtain an average value for $J(x)$ by integrating along the length of the box and dividing by L . Therefore

$$\begin{aligned} \langle J(x) \rangle &= \frac{1}{A} \sum_{mn} g_{mn} (V_m - V_n) \int \frac{\theta(x - x_m) \theta(x_n - x) dx}{L} \\ &= \frac{1}{2\Omega} \sum_{mn} g_{mn} (V_m - V_n) (x_n - x_m) \end{aligned} \quad (3.1.6)$$

Finally, since $\sigma_1(\omega) = \langle J \rangle / E$

$$\sigma_1(\omega) = \frac{1}{2\Omega E} \sum_{mn} g_{mn} (V_m - V_n) (x_n - x_m) \quad (3.1.7)$$

Now consider eqn. (3.1.3). If we multiply each side by x_m and sum over m we obtain, by symmetrising the right-hand side,

$$i\omega \sum_m C_m V_m x_m + C_m e^{-1} U_m x_m = \frac{1}{2} \sum_{mn} g_{mn} (V_n - V_m)(x_m - x_n) \quad (3.1.8)$$

Similarly by multiplying (3.1.3) by V_m^* we may write

$$i\omega \sum_m C_m V_m V_m^* + e^{-1} U_m C_m V_m^* = \frac{1}{2} \sum_{mn} g_{mn} |V_m - V_n|^2 \quad (3.1.9)$$

According to eqn. (3.1.7) the real part of the left-hand side of eqn. (3.1.8) is $\sigma_1(\omega)$. Obviously, from eqn. (3.1.8) therefore

$$\sigma_1(\omega) = \frac{-i\omega}{\Omega E} \sum_m C_m V_m x_m \quad (3.1.10)$$

Similarly, using eqns. (3.1.4) and (3.1.9)

$$\sigma_1(\omega) = \frac{i\omega}{\Omega E^2} \sum_m e^{-1} U_m C_m V_m^* \quad (3.1.11)$$

Since $U_m = eEx_m$ eqns. (3.1.10) and (3.1.11) are identical and we see how the expression (3.1.4) for the real part of the conductivity is related to the rate equations.

Eqn. (3.1.4) is valid for all frequencies. The equivalent electrical network analogue of the hopping problem is not, however, the most fruitful approach to the study of ac conductivity. As we show in Chapter 8, eqn. (2.2.10) is a more convenient starting point in this case. In contrast, studies of the dc conductivity are almost entirely based on the network model. Since $\omega = 0$ we may eliminate the capacitances and voltage generators from the network to obtain the random resistance network model (RRNM). The voltage drop V_{mn} is then real and we may write

$$\sigma = \frac{1}{2} E^{-2} \Omega^{-1} \sum_{mn} g_{mn} V_{mn}^2 \quad (3.1.12)$$

where we have used the simpler notation $\sigma \equiv \sigma_1(0)$. An analytical solution of the summation involved in eqn. (3.1.12) is obviously not possible for a realistic number of sites. We therefore approximate the summation in the manner described in the next section.

§3.2 Formal Expression of the DC Conductivity

When Ω is sufficiently large σ is independent of the particular configuration of the hopping system. The term "sufficiently large" means that the system is approaching the thermodynamics limit i.e. $N_s \rightarrow \infty$, $\Omega \rightarrow \infty$, $N_s/\Omega = \text{a constant}$. In this case we can confine our attention to the configuration average of eqn. (3.1.12). In the thermodynamic limit the configuration averaged conductivity $\langle \sigma \rangle$ is equal to the actual conductivity of almost any realization of the system. Certain configurations (notably a regular array of sites) can give infinite conductivities, but the measure of such systems goes to zero in the limit $N_s \rightarrow \infty$, and so we need not concern ourselves with these extraordinary contributions to $\langle \sigma \rangle$. To evaluate the average we suppose that the sites are independently and uniformly distributed over the volume Ω . We also suppose that ϵ_m is independently distributed with a probability density $\rho(\epsilon_m)n_s^{-1}$, where $\rho(\epsilon)$ is the density of states and n_s is the site density. Finally, we suppose that g_{mn} depends only on the intersite separation $r \equiv r_{mn}$ and the energies ϵ_m and ϵ_n . The configuration average of eqn. (3.1.12) then yields

$$\begin{aligned} \langle \sigma \rangle &= \frac{1}{2} E^{-2} \Omega^{-1} (n_s \Omega)^2 \int \frac{\rho(\epsilon_1) d\epsilon_1}{n_s} \int \frac{\rho(\epsilon_2) d\epsilon_2}{n_s} \int g_{12}^2 \langle V_{12}^2 \rangle \frac{4\pi r^2 dr}{\Omega} \\ &= 2\pi E^{-2} \int \rho(\epsilon_1) d\epsilon_1 \int \rho(\epsilon_2) d\epsilon_2 \int g_{12}^2 \langle V_{12}^2 \rangle r^2 dr \end{aligned} \quad (3.2.1)$$

where $\langle V_{12}^2 \rangle'$ is the average of V_{12}^2 over all stochastic variables except ϵ_1 , ϵ_2 and r .

In all the hopping systems of interest the dependence of g_{12} on ϵ_1 , ϵ_2 and r is dominated by exponential factors. It is therefore convenient to write

$$g_{12} = g_0 \exp[-s(\epsilon_1, \epsilon_2, r)] \quad (3.2.2)$$

where g_0 is a constant and the entire functional dependence of g_{12} is subsumed in the exponent $s(\epsilon_1, \epsilon_2, r)$. As we show in Section 3.3, providing $\exp[-s]$ is rapidly varying in comparison with any other factors involved, the integrand in (3.2.1) has a sharp peak at $s(\epsilon_1, \epsilon_2, r) = s_p$. The suggestion that the integrand is sharply peaked was originally made by Ambegaokar, Halperin and Langer (1971). They were the first authors to use the concept of "percolation" in the study of dc hopping conductivity. In Section 3.3, we will show why the RRNM shows percolative behaviour and how s_p is determined by a classical percolation criterion. The quantity s_p is called the "critical percolation exponent" and is defined as the least value of s_0 for which the conductances with $s(\epsilon_1, \epsilon_2, r) < s_0$ form a connected infinite cluster. With this idea in mind we may find a simple approximation to $\langle V_{12}^2 \rangle'$. When $s(\epsilon_1, \epsilon_2, r) > s_p$ we are concerned with a low conductance having a finite probability of belonging to an infinite cluster of conductances with the same or larger values. It follows that $\langle V_{12}^2 \rangle'$ is dominated by the boundary condition that a uniform macroscopic electric field with magnitude E be present in the system. When r is very large $\langle V_{12}^2 \rangle' = E^2 r^2 / 3$. On the other hand when $s < s_p$ we are concerned with a high conductance having zero probability of belonging to an infinite cluster of conductances with the same or larger magnitudes. The conductance must therefore belong to an

isolated cluster of high conductances and the current through it is determined by what is fed into the cluster from outside. We write I^2 for the mean square current flowing through g_{12} . Then $\langle V_{12}^2 \rangle' = I^2/g_{12}^2$. We use this form for all $s < s_p$ and choose I^2 to be a function of ϵ_1 and ϵ_2 such that $I^2/g_{12}^2 = E^2 r^2/3$ on the critical percolation surface. Thus $I^2 = g_o^2 \exp(-2s_p) E^2 r_p^2/3$ where r_p is given by

$$s(\epsilon_1, \epsilon_2, r_p) = s_p \quad (3.2.3)$$

When these approximations to $\langle V_{12}^2 \rangle'$ are substituted into eqn.

(3.2.1) we obtain the desired form for the dc hopping conductivity

$$\langle \sigma \rangle = \sigma_p \exp[-s_p] \quad (3.2.4)$$

where the prefactor σ_p is given by

$$\sigma_p = g_o \frac{2\pi}{3} \int_{-\infty}^{\infty} \rho(\epsilon_1) d\epsilon_1 \int_{-\infty}^{\infty} \rho(\epsilon_2) d\epsilon_2 \int_{-\infty}^{\infty} r^2 r_a^2 e^{-|s-s_p|} dr \quad (3.2.5)$$

with $r_a = r$ for $s > s_p$ and $r_a = r_p$ for $s < s_p$.

The fact that the conductivity may be written in the form of eqn. (3.2.4) may be deduced from experimental data. The exponent s_p is the crucial term in determining the dependence of $\langle \sigma \rangle$ on the system parameters. As we shall see in late chapters, the effect of the prefactor, σ_p , is qualitatively small, but is obviously important in determining the absolute magnitude of the conductivity. Experimentally, however, the important quantity is the logarithmic conductivity. For this reason the prefactor has not received as much attention in the literature as the exponent. Our derivation of σ_p is necessarily crude, but two points are worth noting. Firstly, our choice of $\langle V_{12}^2 \rangle'$, while being somewhat arbitrary, only affects

the prefactor. Secondly, the three-dimensional integral involved in evaluating σ_p must necessarily entail approximating the integrand if analytical results are desired.

We see from eqns. (3.2.4) and (3.2.5) that the evaluation of $\langle\sigma\rangle$ relies on the determination of s_p - a crucial quantity in the study of hopping conductivity. We have hinted that s_p is determined by a percolation argument, and in the next section turn our attention to this assumption.

§3.3 The Percolation Aspect of Hopping Conduction

In this section we turn our attention to the calculation of s_p . Various approaches to the problem have been made (for a brief review see Chapter 7). The most fruitful of these is the method originally introduced by Ambegaokar et al (1971), based on a percolation argument. The use of classical percolation theory in the semiclassical formalism of hopping conductivity is not an obvious one, and for this reason it will be discussed in some detail.

We begin with a very brief review of classical percolation, and then show how considerations of the hopping problem give arguments formally equivalent to those of percolation. A full account of classical percolation theory is contained in a review by Shante and Kirkpatrick (1971). The purpose of percolation theory is to determine how a given set of sites, regularly or randomly positioned in some space, is interconnected. We suppose this set is infinite in one or more dimensions. To determine how these sites are connected we need the "bonding criterion" which specifies whether any two sites are connected (this criterion could involve more than two sites in general). The bonding criterion is a function of one or more "bonding parameters". Two sites belong to the same "cluster" if there is an

unbroken sequence of bonds from the first site to the second. For a given set of sites, percolation theory attempts to determine the distribution of cluster sizes as a function of the bonding criterion. In particular, as we see below, one would like to find the bonding criterion for which clusters of infinite size first form. It is convenient to divide the solution of the percolation problem into two main categories (which are related), namely, site percolation and bond percolation. In the site percolation problem all sites within same radius R of another site are bonded to this site. The percolation problem is to find the critical radius R_c at which an infinite cluster of connected sites is formed. In the bond percolation problem a bond between any two sites is said to be present if the "bonding parameter" B_p is less than some value B_p^0 . The percolation problem is to find the critical value of the parameter B_p^0 (defined as B_p^c) for which the connected sites just form an infinite cluster. We will find that the problem of interest in the study of hopping conduction is the bond percolation problem. We note in passing that the n -dimensional bond percolation problem may be viewed as a site percolation problem in an $n + 1$ dimensional space (Pike and Seager 1974). In all cases the results of computer studies show that various system parameters depend primarily on the dimensionality of the system (Shante and Kirkpatrick 1971). One such parameter is the average number of bonds per site at the percolation threshold, N_p .

With these ideas in mind, we turn our attention to the problem of calculating s_p . If we presuppose that the RRNM may be solved using percolation techniques, we may identify the bonding parameter B_p with the quantity s , and the quantity B_p^c with s_p . It is then a trivial problem to calculate the average number of bonds (or conductances) per

site with $s < s_p$ and equate this to N_p . Since N_p is known from computer studies we will then obtain an equation for s_p . We therefore need to show that the RRNM is formally equivalent to a percolation problem. To do this let us consider the integrand in eqn. (3.2.1). For small s we are concerned with high conductances which dissipate very little power. For $s \rightarrow \infty$ we are concerned with infinite conductances which again dissipate no power. The integrand therefore has at least one maximum at some value of $s \equiv s_c$. Two questions remain to be answered: firstly, is the integrand strongly peaked at $s = s_c$, and secondly, how do we identify s_c ? Consider an arbitrary conductance, C , in the network (Figure 7). If C is very much larger than the surrounding conductances (Figure 7a) then the power dissipated is small and we may effectively put the conductance equal to infinity. On the other hand if C is very much smaller than the neighbouring conductances, (Figure 7b), more power will be dissipated in the "by-pass" chains C_B and we may put this conductance equal to zero. If we therefore consider the complete resistance network, we may remove conductances with $s > s_0$ (where s_0 is arbitrary) since these are "by-passed" by high conductance chains. We can then lower the value of s_0 until we cannot by-pass the lowest conductances in the network. We call this value s_p . Thus s_p is the least value of s_0 for which the conductances with $s < s_0$ form a connected infinite cluster. We may therefore determine s_p from a percolation argument. Our approximation to the mean square voltage drop $\langle V_{12}^2 \rangle'$, and the exponential nature of g_{12} mean that the integrand in (3.2.1) decays exponentially above and below $s = s_p$. We conclude, therefore, that the assumptions made about the integrand in eqn. (3.2.1), namely that $g_{12} \langle V_{12}^2 \rangle'$ is peaked at $s = s_p$, and that s_p may be determined from a percolation argument, are valid.

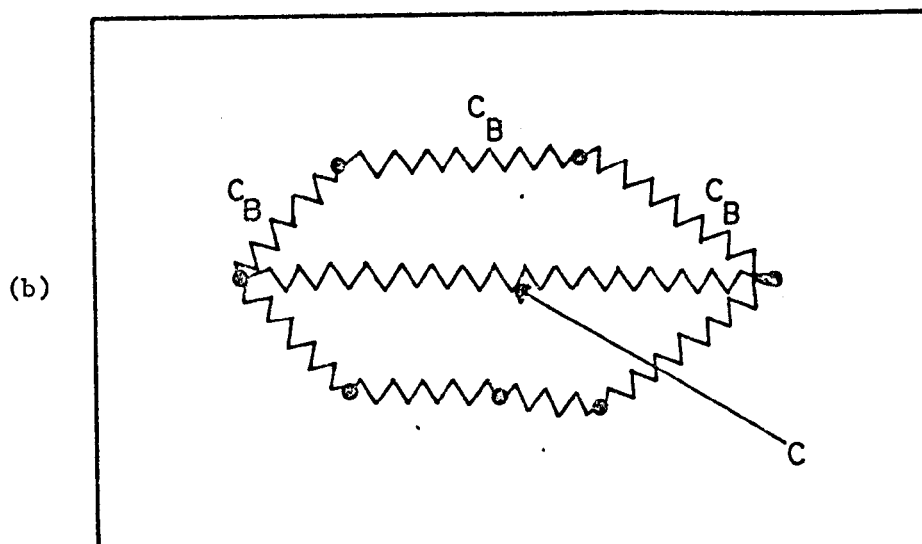
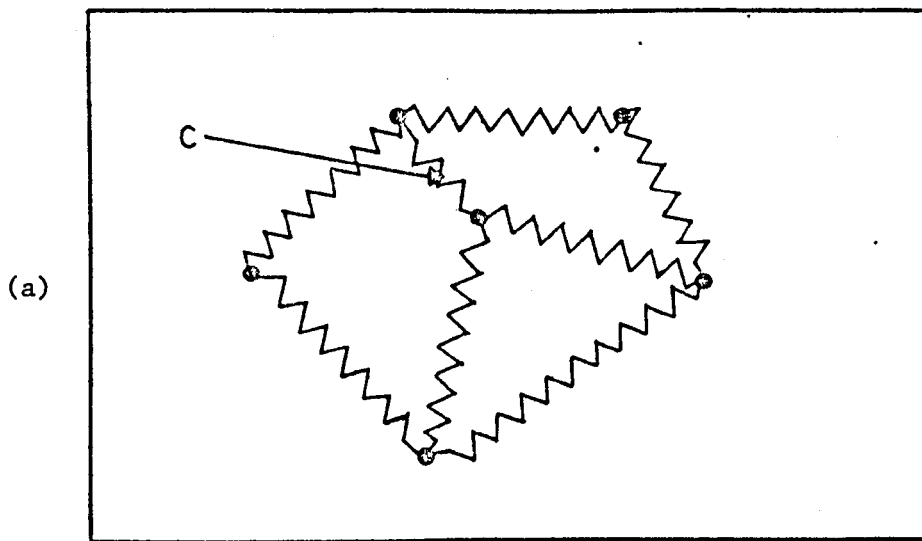


FIGURE 7 Limiting conductances in the equivalent conductance network. In (a) the conductance C is very large and is a "short circuit". In (b) the conductance C is very small and can be bypassed by chains of conductances C_B .

We may readily obtain an approximate formula for s_p . As discussed above, and in more detail in Shante and Kirkpatrick 1971, the average number N_p of bonds per site at the percolation threshold is determined primarily by the dimensionality of the percolation problem. Pike and Seager (1974) have determined N_p by collapsing randomly located spheres. They find that $N_p = 4.5, 2.7$ and 2.1 in 2, 3 and 4 spatial dimensions respectively. Kurkijarvi (1974) finds $N_p = 2.8$ in 3 dimensions from a study of random conductance networks. The dimensionality of the percolation problem is defined by the number of independent random variables required to characterise a site. When all sites have the same energy, the correct value of N_p to use is that corresponding to the number of spatial dimensions. The introduction of site energies increases the dimensionality of the percolation problem - we may treat the energy as a fourth dimension. The energy independent case is a site percolation problem in 2 or 3 dimensions. Pike and Seager show how the introduction of an energy into the exponent can be viewed as giving rise to a 2 or 3 dimensional bond percolation or a 3 or 4 dimensional site percolation system (corresponding to 2 or 3 spatial dimensions respectively). A full discussion concerning the appropriate values for N_p may be found in Chapter 9.

It is now a simple matter to find an expression for the average number of conductances with $s < s_p$ per site at the percolation threshold. The average number of conductances per unit volume with $s < s_p$ is B

where

$$2B = \int_{s < s_p} \rho(\epsilon_1) d\epsilon_1 \int \rho(\epsilon_2) d\epsilon_2 \int 4\pi r^2 dr \quad (3.3.1)$$

in which the factor of 2 prevents double counting. The range of integration is over all values of ϵ_1, ϵ_2 and r such that $s < s_p$.

Similarly the average number of sites per unit volume which have a non-zero probability of belonging to the infinite cluster is

$$S = \int_{s < s_p} \rho(\epsilon_1) d\epsilon_1 \quad (3.3.2)$$

The integration in eqn. (3.3.2) runs over the values of ϵ_1 for which the inequality $s(\epsilon_1, \epsilon_2, r) < s_p$ can be satisfied for some choice of ϵ_2 and r . Sites with energies outside this range cannot possibly belong to the cluster and may be said to be automatically isolated. Since each conductance is connected to two sites the desired equation for s_p is

$$\frac{2B}{S} = N_p \quad (3.3.3)$$

Eqns. (3.3.1), (3.3.2) and (3.3.3) are the final expressions used to evaluate s_p .

§3.4 The High Frequency and the High Density Limit

Before moving on to evaluate $\sigma(0)$ for a variety of models, we wish to discuss two limits where exact results are easily obtained, namely, the high frequency and the high density limits. We see from eqn. (2.3.4) that when $\omega \rightarrow \infty$, $G_{mn}^0 \rightarrow -(i\omega)^{-1}$. Using this result and eqns. (2.3.3) and (2.2.10) we may readily deduce

$$\sigma_1(\infty) = \frac{1}{2} e^2 \beta \Omega^{-1} \sum_{mn} \Gamma_{mn} (x_m - x_n)^2 \quad (3.4.1)$$

where $\sigma_1(\infty)$ is the real part of the conductivity in the limit $\omega \rightarrow \infty$.

We note that eqn. (3.4.1) may be derived from (3.1.4) since in the limit $\omega \rightarrow \infty$, $V_m \rightarrow -Ex_m$. Brenig et al (1971) show that $\sigma_1(\omega)$ is a monotonic increasing function of ω . Hence $\sigma_1(\infty) \geq \sigma_1(0)$. In highly random systems $\sigma_1(\infty) \gg \sigma_1(0)$ (Butcher and Morys 1973; Mott and Davis 1971; Butcher 1976). The equality $\sigma_1(\infty) = \sigma_1(0)$

can only be valid in special circumstances because it implies that $\sigma_1(\omega)$ is independent of ω . Now consider a random system, and allow the spatial density of sites to approach infinity. In this high density or continuum limit, $V_{mn} = -E(x_m - x_n)$ for all ω so that $\sigma_1(\omega) \equiv \sigma_1(\infty)$. Hence $\sigma_1(0) = \sigma_1(\infty)$ in a high density system. Substituting $V_m = ex_m$ into (3.2.1) gives

$$\langle \sigma_1(\infty) \rangle = 2\pi \int \rho(\epsilon_1) d\epsilon_1 \int \rho(\epsilon_2) d\epsilon_2 \int g_{12}(x_m - x_n)^2 r^2 dr \quad (3.4.2)$$

We see that this result can be obtained from eqns. (3.2.4) and (3.2.5) by putting $s_p = 0$.

CHAPTER 4 - NON-DEGENERATE HOPPING IN VERY NARROW ENERGY BANDS

§4.1 Analytical Formulae

In this chapter we evaluate the expressions for s_p and σ_p for a particularly simple model in which all the energies of the localised states are very nearly the same. The theoretical predictions are compared with experimental and computational data.

To proceed we need an expression for the thermal equilibrium hopping rate R_{12}^0 . A discussion of the transition rates, which are fundamental to the study of hopping conductivity, may be found in Appendix 3. We find when $\epsilon_2 > \epsilon_1$

$$R_{12}^0 = R_0 \exp[-p(r)] \frac{\beta(\epsilon_2 - \epsilon_1)}{\exp[\beta(\epsilon_2 - \epsilon_1)] - 1} \quad (4.1.1)$$

where

$$p(r) = 2\alpha r - \nu \ln \alpha r \quad (4.1.2)$$

R_0 is a hop rate characteristic of the system under consideration. The exponential term involving the site separation r , arises from the overlap of the localized states, where the decay constant is α . The parameter ν arises from consideration of the overlap integral (Miller and Abrahams 1960). When the conduction band has n ellipsoidal valleys with ellipticity parameter $\eta = (m_l/m_t) - 1$, they find that $\nu = 2$ when $\eta = 0$ and $\nu = 3/2$ when $\eta \gg 1$. Finally, the energy dependent contribution arises from the Bose-Einstein distribution of phonons involved in the inelastic transition.

When eqn. (4.1.1) is substituted into (3.1.2) we find that g_{12} takes the form (3.2.2) with

$$g_0 = e^2 \beta R_0 \quad (4.1.3)$$

and

$$s(\epsilon_1, \epsilon_2, r) = p(r) + q(\epsilon_1, \epsilon_2) \quad (4.1.4)$$

where

$$\begin{aligned} q(\epsilon_1, \epsilon_2) = & \ln[4 \cosh \frac{1}{2}\beta\epsilon_1 \cosh \frac{1}{2}\beta\epsilon_2 \sinh \frac{1}{2}\beta(\epsilon_1 - \epsilon_2)] \\ & - \ln[\frac{1}{2}\beta(\epsilon_1 - \epsilon_2)] \end{aligned} \quad (4.1.5)$$

in which the energies are measured from the chemical potential plus $k_B T \ln 2$.

We now suppose that the density of states is a sharply peaked function with a width much less than $k_B T$. In this case the hops are nearly elastic and $q(\epsilon_1, \epsilon_2)$ in eqn. (4.1.5) may be treated as a constant. To be specific we suppose that the Fermi level lies well away from the energy band. Then $\exp[-q(\epsilon_1, \epsilon_2)] = 2 \exp[-\beta\epsilon_3]$ where ϵ_3 is the conventional notation for the activation energy from the chemical potential to the energy band and the factor of 2 arises from the spin degeneracy term, $k_B T \ln 2$. Since $q(\epsilon_1, \epsilon_2)$ is not a stochastic variable in the model under discussion it is convenient to absorb it in the characteristic conductance g_0 . We therefore replace g_0 by

$$g_a = g_0^2 \exp[-\beta\epsilon_3] \quad (4.1.6)$$

We may then replace $q(\epsilon_1, \epsilon_2)$ by 0 in eqn. (4.1.5) and s then reduces simply to $p(r)$.

To calculate s_p we replace $\rho(\epsilon)$ by $n_s \delta(\epsilon - \epsilon_B)$ in (3.3.1) and (3.3.2), where n_s is the site density and ϵ_B is the energy at the centre of the band. Then eqn. (3.3.1) gives $2B = n_s^2 4\pi(r_p^3 - r_p'^3)$ where r_p and r_p' are respectively the larger and smaller of the two roots of the equation

$$s_p = p(r_p) \quad (4.1.7)$$

When $v = 0$ $r_p' = 0$, and we may verify that for all values of v of interest to us ($v \leq 2$) r_p' remains negligible compared to r_p .

Eqn. (3.3.1) for S gives $S = n_s$ since no sites are automatically isolated. Hence, using eqn. (3.3.3),

$$n_s \frac{4\pi}{3} r_p^3 = N_p \quad (4.1.8)$$

To calculate σ_p from eqn. (3.2.5) we replace g_o by g_a , the densities of states by δ -functions and s by $p(r)$. To evaluate the remaining integral over r we suppose that n_s is small. Then s_p and r_p are large and the dominant contribution to the integral comes from the neighbourhood of r_p . We therefore approximate r_a^2 by r_p^4 and $p(r)$ by $p(r_p) + p'(r_p)(r - r_p)$ and extend the lower limit of integration to $-\infty$. We then obtain the low density approximation

$$\sigma_p = g_a \frac{4\pi}{3} r_p^4 / p'(r_p) \quad (4.1.9)$$

where $p'(r_p) = 2\alpha - v/r_p \approx 2\alpha$ at low densities. We see from (4.1.2) and (4.1.7) that $\exp[-s_p] = (\alpha r_p)^v \exp[-2\alpha r_p]$. The slowly-varying quantity $(\alpha r_p)^v$ is best taken out of the exponential and absorbed in the conductivity prefactor. Then the final low-density formulae for $\langle \sigma \rangle$ obtained from (3.2.4), (4.1.8) and (4.1.9) is

$$\langle \sigma \rangle = \frac{3N_p^2}{8\pi} (g_a \alpha) (\alpha r_p)^{v-2} \exp[-2\alpha r_p] \quad (4.1.10)$$

where

$$r_p = (3N_p / 4\pi n_s)^{1/3} \quad (4.1.11)$$

In applying eqn. (4.1.10) to the interpretation of experimental data it is convenient to write

$$\sigma_v = \langle \sigma \rangle \exp[\beta \epsilon_3] (\alpha n_s^{-1/3})^{2-v} \quad (4.1.12)$$

Since g_a contains the activation factor $\exp[-\beta\epsilon_3]$, we see that a plot of $\log \sigma_v$ against $\alpha n_s^{-1/3}$ should be a straight line.

§4.2 Comparison with Computer Data

The formulae developed in the previous section are applicable to the analysis of activated hopping, observed in a variety of low density systems. Before we analyse experimental data, however, we wish to investigate the validity of the approximations used to evaluate the expressions for $\langle \sigma \rangle$. A number of authors have evaluated eqn. (3.1.4) using a computer (Seager and Pike 1974; Butcher, Hayden and McInnes 1977; Butcher and McInnes 1978). The general method is to distribute a number of sites randomly in a two- or three-dimensional space. The resulting conductances in the RRNM can be calculated using eqn. (3.2.2). The quantity g_0 is an arbitrary scaling factor in the system. The voltages V_{mn} are then minimized, subject to the boundary condition that a voltage is applied across the system. The conductivity is then evaluated using eqn. (3.1.4). We refer to conductivities determined in this way as 'computer generated data'.

We begin by comparing with the three-dimensional data of Seager and Pike (1974). The straight line in Figure 8 shows $\log \sigma_{3/2}$ calculated from eqn. (4.1.12) with $N_p = 2.7$ for the parameter values $v = 3/2$, $g_a = .145\Omega^{-1}$ and $\alpha^{-1} = 1.5\text{nm}$. The dots are derived from Figure 4 of Seager and Pike. They were calculated by numerical solution of Kirchhoff's equations for a random conductance network having the above parameter values. It should be noted in this connection that in eqn. (1) of Seager and Pike (1974): $G_0 = 0.145(\alpha r)^{3/2}\Omega^{-1}$ (private communication). The agreement between our simple analytical formula and the computed points is remarkably good. It should be emphasised that no parameters

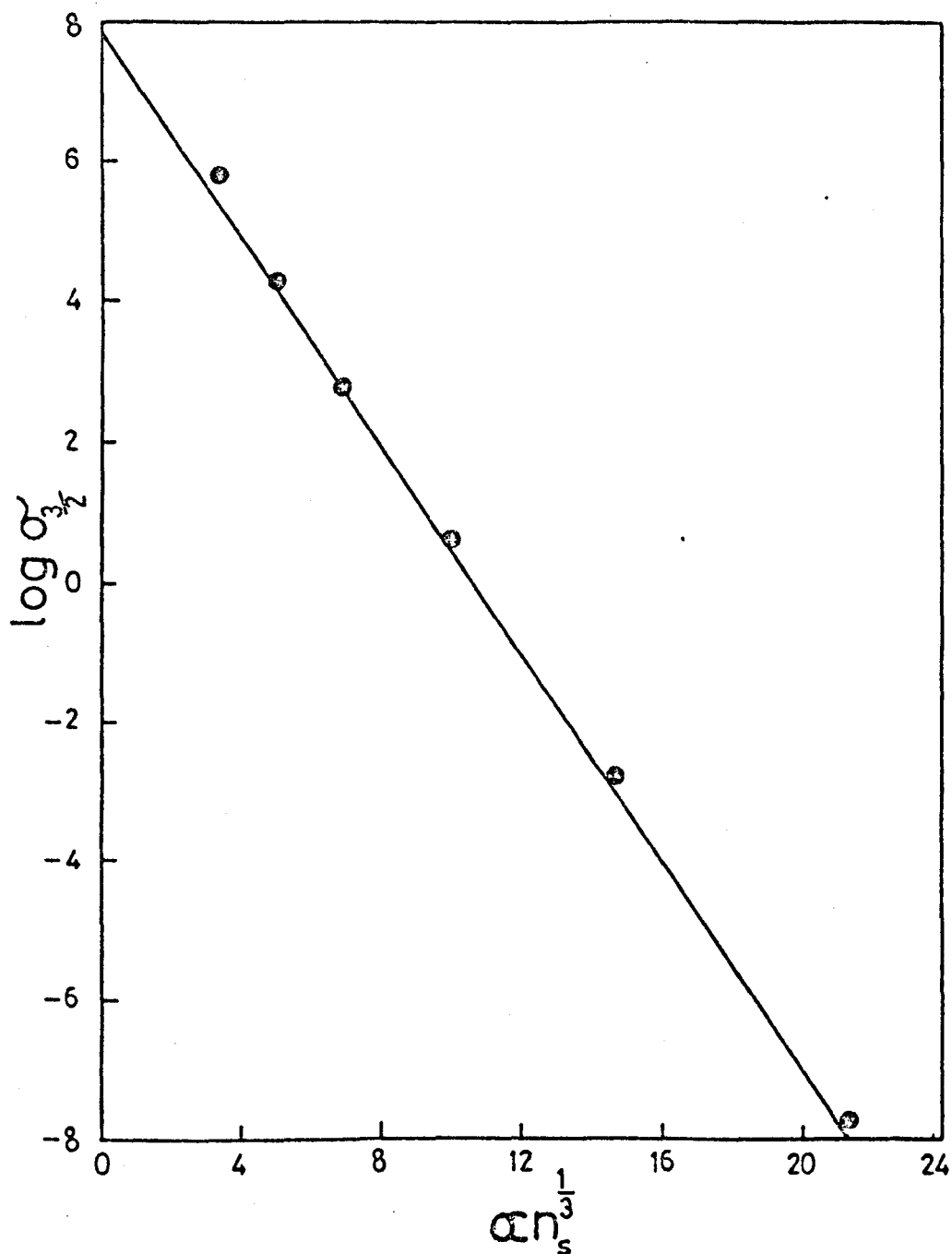


FIGURE 8 Plot of $\log \sigma_{3/2}$ against $\alpha n_s^{-1/3}$, where $\sigma_{3/2} = \langle \sigma \rangle \exp(\beta \epsilon_3) (\alpha n_s)^{1/2}$ with $\langle \sigma \rangle$ in $\Omega^{-1} \text{m}^{-1}$. Dots: derived from Figure 4 of Seager and Pike (1974). Straight line: calculated from (4.1.12) with $N_p = 2.7$, $\nu = 3/2$, $\alpha^{-1} = 1.5 \text{ nm}$ and $g_a = 0.145 \Omega^{-1}$.

have been adjusted. Further tests of the theory using computational data have recently been undertaken (Butcher, Hayden and McInnes 1977; Butcher and McInnes 1978). This work investigates the accuracy of the analytical formula in 2- and 3-dimensions and for high, intermediate and low site densities. In all cases the model is simplified by dropping the $(\alpha r)^V$ factor from the conductances. The conductivity is given by eqns. (3.2.4) and (3.2.5) where $s_p = 2\alpha r_p$ and

$$r_p = \left(\frac{3N_p}{4n_s} \right)^{1/3} \quad (4.2.1)$$

The evaluation of the integral involved in the prefactor is elementary but tedious and we find that (Butcher and McInnes 1978)

$$\sigma_p = (g_a \alpha) \frac{\pi}{6} \left[\frac{3N_p}{4\pi R_p^3} \right]^2 H \quad (4.2.2)$$

where $R_p = \alpha r_p$ and

$$H = 3 + 6R_p + 7R_p^2 + 2R_p^3 + 4R_p^4 - R_p^2 \exp[-2R_p] \quad (4.2.3)$$

For low densities ($n_s \rightarrow 0$) $H \rightarrow 4R_p^4$ while for high densities ($n_s \rightarrow \infty$) $H \rightarrow 3$ and $\exp[-2R_p] \approx 1$. The points in Figure 9 show conductivities calculated by numerical solution of Kirchhoff's equations (Butcher and McInnes 1978). The full curve is calculated from eqns. (4.2.1) and (4.2.2) with $N_p = 2.7$. The upper and lower dashed curves show the high and low density approximations respectively. The full curve is in excellent agreement with the calculated points over the full range of $\alpha n_s^{-1/3}$ considered. This is sufficient to cover the region exhibiting high density behaviour ($\alpha n_s^{-1/3} < 1.5$), low density behaviour ($\alpha n_s^{-1/3} > 3.5$) and the transition region between these two régimes. The lowest four computed points appear to be falling off rather less steeply than the analytical curve which suggests that N_p should be

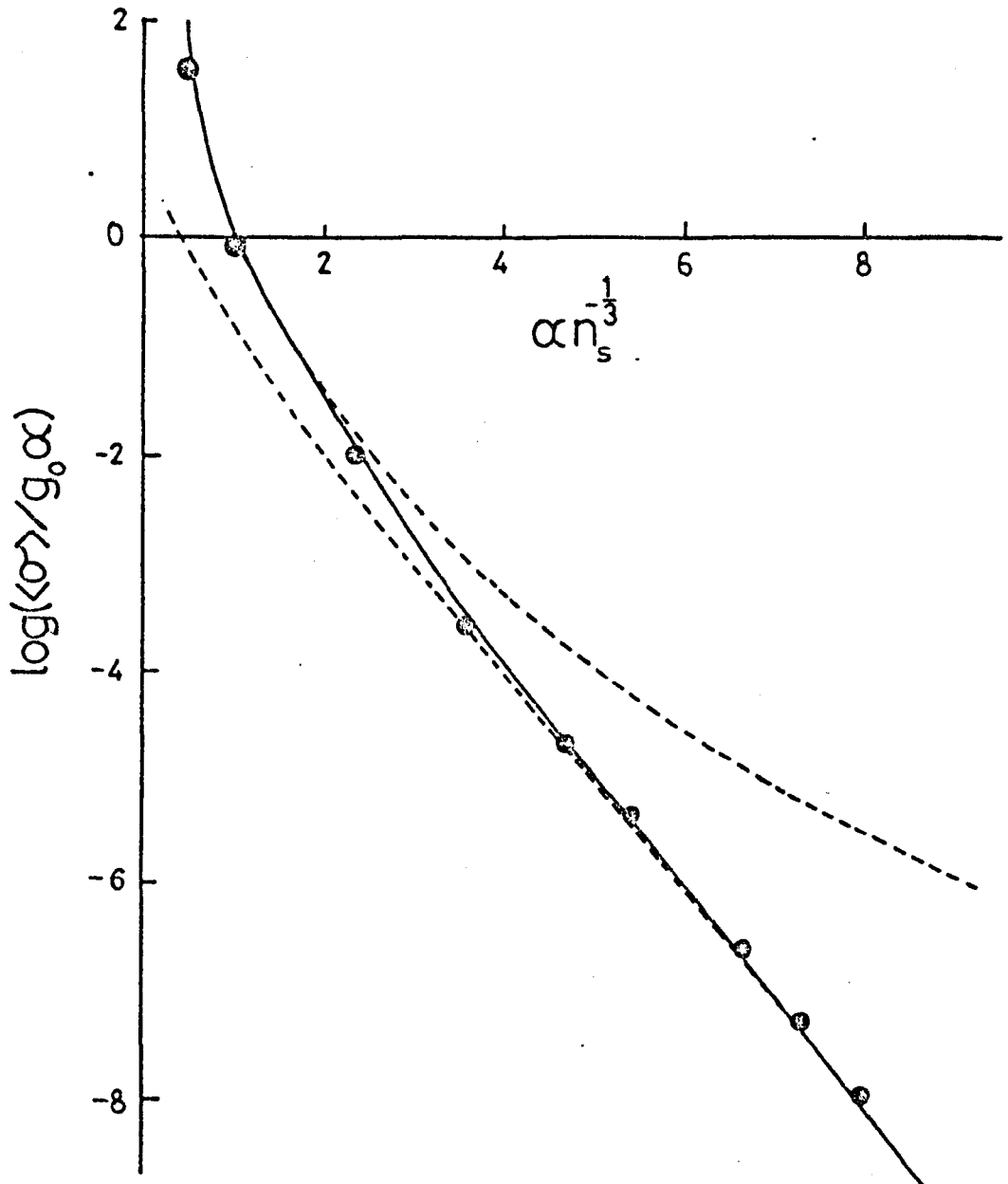


FIGURE 9 Plot of $\log(\langle\sigma\rangle/g_0\alpha)$ against $\alpha n_s^{-1/3}$ for a three-dimensional system with $\nu = 0$. Dots: computed from Kirchhoff's equations. Full curve: calculated from (4.2.1) and (4.2.2) with $N_p = 2.7$. Upper dashed curve: high density approximation. Lower dashed curve: low density approximation. From Butcher and McInnes 1978.

reduced by about 10%. A full discussion of the appropriate values of N_p is to be found in Chapter 9 and will not be discussed in detail here.

Computational studies have also been made for a two-dimensional system. The analytical formula for this model is obtained from (3.2.4) and (3.2.5) by setting $\rho(\epsilon) = \delta(\epsilon - \epsilon_B)n_s$, $s = 2\alpha r$ and replacing $2\pi r^2/3$ by $\pi r/2$. Without any further approximations we find that

$$\sigma = e^{-s_p} \frac{\pi}{2} g_o n_s^2 \int_0^\infty r r_a e^{-|2\alpha r - s_p|} dr \quad (4.2.4)$$

The integral in eqn. (4.2.4) is elementary. Moreover, s_p is determined by the two-dimensional analogue of eqn. (4.1.8) for this model, namely: $s_p = 2\alpha r_p$ and $n_s \pi r_p^2 = N_p$. The classical percolation calculations of Pike and Seager (1974) give $N_p = 4.49$. Thus we obtain the full curve in Figure 10 which is in excellent agreement with the computed points for all values of $\alpha n_s^{-1/2}$ investigated. The upper dashed curve in Figure 10 is the high density approximation $\langle \sigma \rangle = 3\pi g_o n_s^2 / 16\alpha^4$ obtained by setting $s_p = 0$ in (4.2.4). We see that it is valid for $\alpha n_s^{-1/2} < 1$. The lower dashed curve in Figure 10 is the low density approximation

$$\langle \sigma \rangle = \pi g_o n_s^2 (r_p^3 / 2\alpha) \exp[-2\alpha r_p] \quad (4.2.5)$$

obtained from eqn. (4.2.4) by putting $r r_a^2 = r_p^3$ and extending the lower limit of integration to $-\infty$. We see that it is a very good approximation for $\alpha n_s^{-1/2} > 2.5$. The agreement with the computed points may be improved still further by decreasing N_p slightly. A least squares fit to the lowest five points gives $N_p = 4.30 \pm .07$.

We see from a comparison with computer data that the approximate theory given in Section (4.1) is surprisingly accurate. We therefore

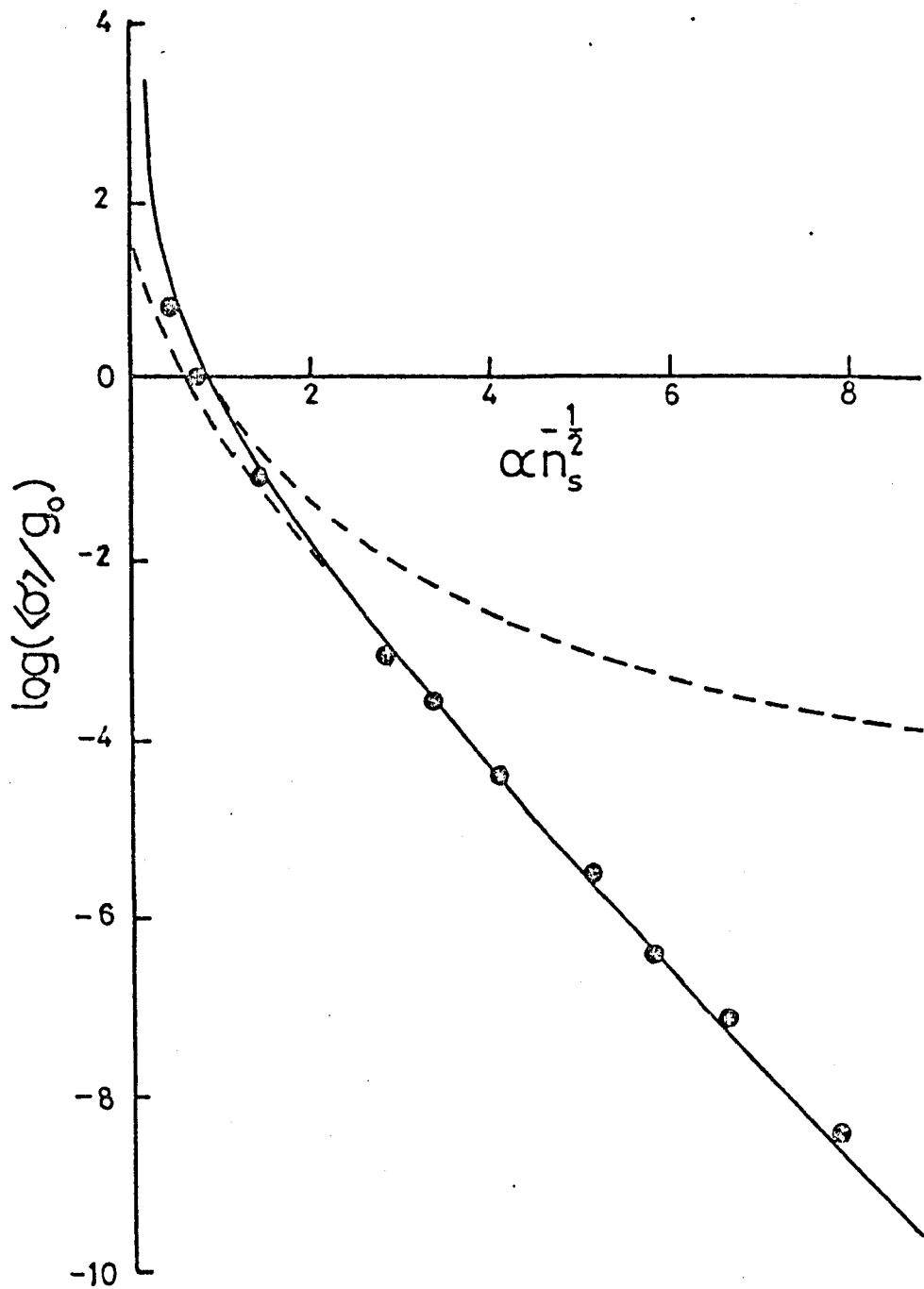


FIGURE 10 Plot of $\log(\langle \sigma \rangle / g_0)$ against $\alpha n_s^{-1/2}$ for a two-dimensional system with $\nu = 0$. Dots: computed from Kirchhoff's equations. Full line: calculated from (4.2.4). Upper dashed line: high density approximation. Lower dashed line: low density approximation.

feel justified in applying the formulae developed above to cases where our knowledge of the system and the system parameters is not so well advanced. This we do in the next section.

§4.3 Comparison of the Analytical Formulae with Data for Three-Dimensional Systems

In this section we wish to use the formulae developed in 2.1. to analyse experimental data. In particular, the formulae should be applicable to the case of impurity conduction in crystalline semiconductors. As outlined in the introduction, at sufficiently low temperatures, the predominant transport process in this system is hopping conduction due to the localised impurity states. If we assume that the bandwidth of the impurity band is much less than $k_B T$, then the formulae developed in this chapter may be used to analyse the data.

The characteristic hop rate R_o has been calculated by Miller and Abrahams (1960) for impurity conduction in crystalline semiconductors. They find that for a semiconductor whose conduction band has n minima

$$R_o = \frac{E_1^2 k_B T}{\pi \rho_o v_s^5 h^4} \left(\frac{e^2 \alpha}{6 \pi \epsilon \epsilon_o} \right)^2 \frac{1}{n} \left(\frac{\pi}{4 \eta} \right)^{2-\nu} \quad (4.3.1)$$

where E_1 , ρ_o , v_s are the deformation potential, density and velocity of sound respectively.

The continuous straight line in Figure 11 shows $\log \sigma_{3/2}$ calculated from eqn. (4.1.12) with $N_p = 2.7$ and parameter values appropriate to n-type germanium. Thus we take $\nu = 3/2$, $\alpha^{-1} = 7 \text{ nm}$ and calculate $g_a \exp[\beta \epsilon_3] = 2g_o$ from (4.3.1) and (4.1.3) with $E_1 = 11.4 \text{ eV}$,

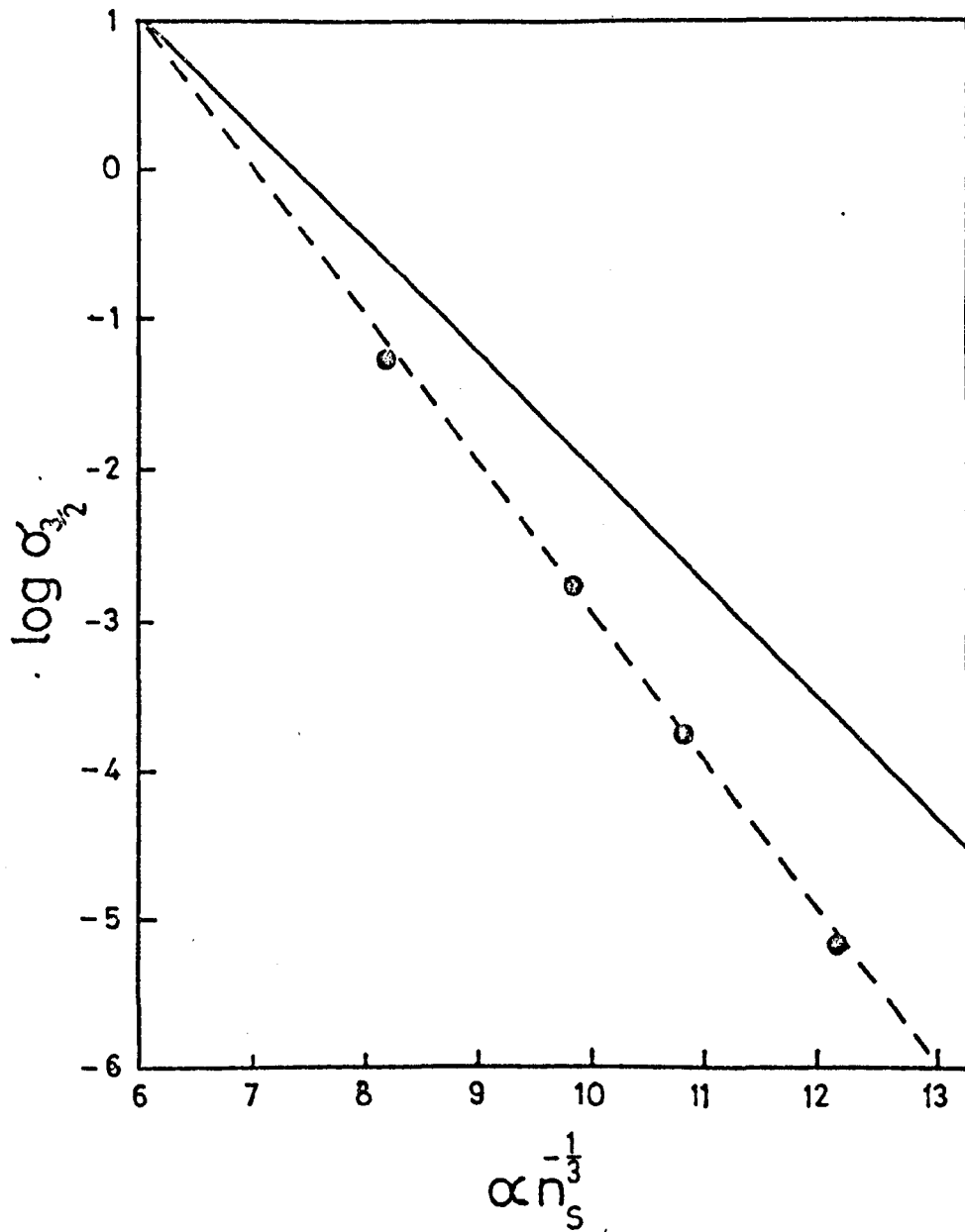


FIGURE 11 Plot of $\log \sigma_{3/2}$ against $\alpha n_s^{-1/3}$ where $\sigma_{3/2} = \langle \sigma \rangle \exp(\beta \epsilon_3) (\alpha n_s^{-1/3})^{1/2}$ with $\langle \sigma \rangle$ in $\Omega^{-1} \text{m}^{-1}$. Dots: data for n-type germanium from Fritzsche (1958). Full line: calculated from (4.1.12) with $N_p = 2.7$ and parameter values appropriate to n-type germanium.

$v_s = 4.92 \times 10^3 \text{ ms}^{-1}$, $\rho_o = 5.5 \times 10^3 \text{ kgm}^{-3}$, $\epsilon = 15.8$, $\eta = 18.8$ and $n = 4$ (Miller and Abrahams 1960). The dots in Figure 11 are calculated from (4.1.12) using the experimental data on n_s , $\langle \sigma \rangle$ and ϵ_3 reported by Fritzsche (1958) for antimony doped germanium at 2.5 K. The compensation ratio for all samples is less than 0.06. By confining our attention to samples with donor concentrations less than $8.5 \times 10^{21} \text{ m}^{-3}$ we may expect the observed conductivity to be dominated by a non-degenerate distribution of holes hopping in a narrow band of completely localized states (Shklovskii 1973). The dashed line through the experimental points is within about an order of magnitude of the continuous theoretical line, but has a considerably steeper slope. This discrepancy is hard to understand because the magnitude of the theoretical slope is $0.868 (3N_p/4\alpha)^{1/3}$ which contains no adjustable parameters.

In Figure 12 we make a similar comparison of the theoretical predictions with experimental data for gallium doped germanium at 1.25 K reported by Fritzsche and Cuevas (1960). Since there are no published theoretical expressions for the thermal equilibrium hopping rate between acceptors we use (4.1.1), (4.1.2) and (4.3.1) with $n = 1$ and $\nu = 2$. The continuous straight line in Figure 12 shows $\log \sigma_2$ calculated from eqn. (4.1.12) with $N = 2.7$, $\alpha^{-1} = 8.7 \text{ nm}$ (Kohn 1957) and $E_1 = 3.1 \text{ eV}$. The value assumed for E_1 is 2/3 of that given by Reggiani (1976) because Reggiani and co-workers use a deformation potential 3/2 larger than Miller and Abrahams (Costato et al 1974). The dashed straight line through the experimental points has a slope close to the theoretical value and an intercept which is only an order of magnitude below that predicted. The agreement is surprisingly good. Our treatment of the hopping rate in p-type material has been superficial and we have not adjusted any parameters. The acceptor density in the experimental samples is

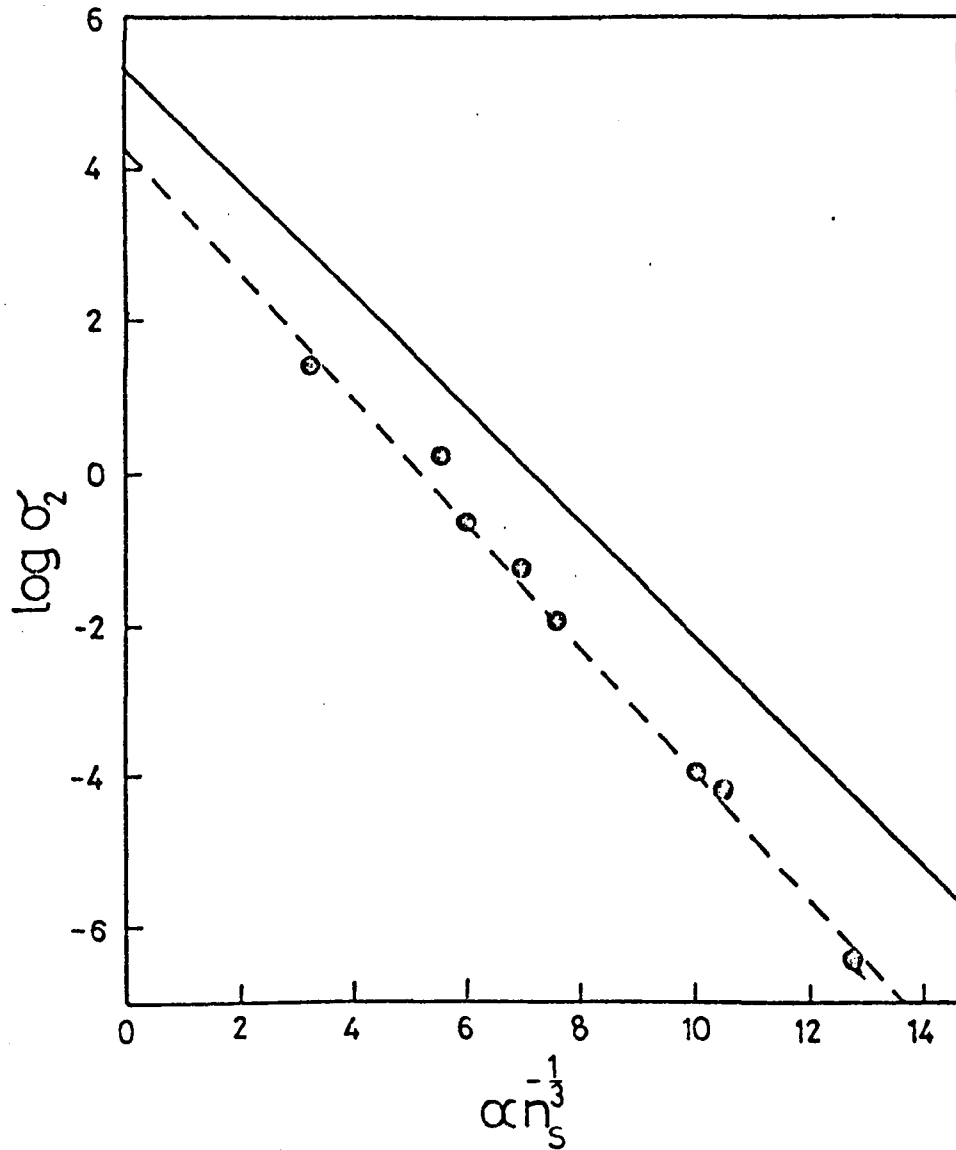


FIGURE 12 Plot of $\log \sigma_2$ against $\alpha n_s^{-1/3}$ where $\sigma_2 = \langle \sigma \rangle \exp(\beta \epsilon_3)$ with $\langle \sigma \rangle = \Omega^{-1} \text{m}^{-1}$. Dots: data for p-type germanium taken from Fritzsche and Cuevas (1960). Full line: calculated from (4.1.12) and $N_p = 2.7$ and parameter values appropriate to p-type germanium.

small enough to ensure complete localization. However, the compensation ratio means that our assumption that the impurity bandwidth is negligible is a poor one.

Finally in this section we discuss some more recent experimental data. Le Comber, Jones and Spear (1977) have recently succeeded in doping amorphous silicon with phosphorus. In Figure 13 we show the experimentally determined values of hopping conductivity as functions of doping concentration. In this system we do not know α , the decay constant of the localized wave function, or g_0 , the characteristic conductance in the equivalent random resistance model. We therefore proceed by fitting a straight line to the experimental points, and deduce α and g_0 from the slope and intercept respectively. The full line in Figure 13 is such a fit. From it we deduce $\alpha^{-1} = 1.7$ nm. This value for α is a reasonable one, but there have been no theoretical or experimental values quoted for amorphous silicon. However, for the case of phosphorus in crystalline silicon, $\alpha^{-1} = 2.1$ nm. The value of g_0 obtained is 0.7 mS, but again there are no published theoretical or experimental values for amorphous silicon. We may, however, make an order of magnitude estimate as follows: we use the parameter values appropriate to crystalline silicon to determine R_0 using eqn. (4.3.1), and hence g_0 from (4.1.3). It does not seem appropriate to carry over concepts such as number of band minima and ellipticity to the amorphous case. We therefore assume the conduction band has one spherically symmetric conduction band and use parameter values $E_1 = 6$ eV, $\alpha^{-1} = 2.1$ nm, $\epsilon = 11.7$, $\rho_0 = 2.3 \times 10^4$ kgm⁻³, $v_s = 9 \times 10^3$ ms⁻¹, $n = 1$, $\nu = 2$. With these values we obtain $g_0 = 1.3$ mS, which is very close to the values of 0.7 mS deduced from the data.

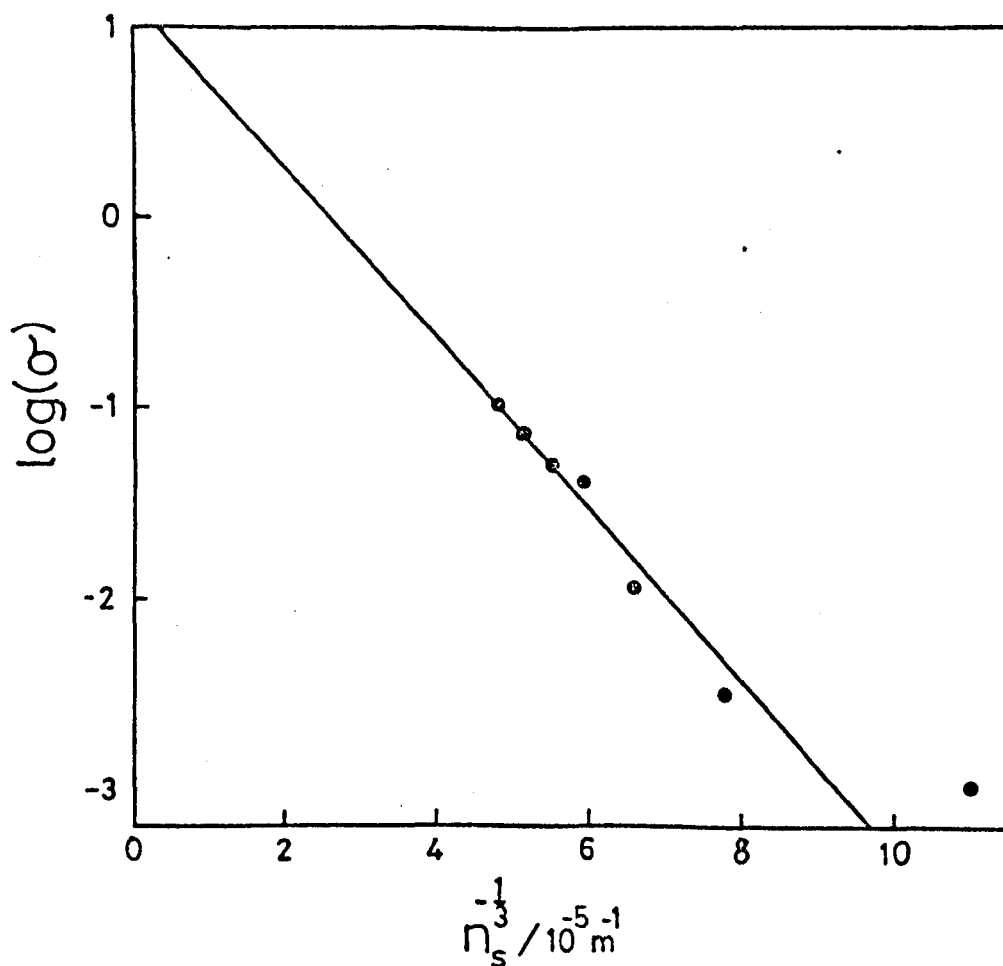


FIGURE 13 Plot of $\log \langle \sigma \rangle$ against $n_s^{-1/3}$ with σ in $\Omega^{-1} \text{ m}^{-1}$,

The dots are experimental values found by Le Comber, Jones and Spear (1977) for phosphorus doped amorphous silicon. The full line is a best straight line fit to these points.

§4.4 Discussion

In this chapter we have developed the general formulae given in Chapter 3 for the simple case where the resistances in the RRNM depend only on the site separation. The resulting formulae are then particularly simple. Our results are compared with alternative formulae in Chapter 7. Detailed comparison with computer generated data in Section 4.2 shows that the methods of approximation involved in the derivation of the analytical formulae are valid. The model of non-degenerate hopping in a narrow energy band is a very crude one for the interpretation of activated hopping data obtained from the study of impurity conduction in crystalline and amorphous semiconductors. Nevertheless, the agreement between the analytical formulae and the experimental data in the case of crystalline germanium is reasonably good. One might hope to remove the discrepancies by closer attention to the detailed assumptions made in the calculations concerning the statistics, transition rates, densities of states and parameter values. The application of the formulae to the analysis of impurity conduction in amorphous silicon yields values of α and g_0 which are close to the crystalline values.

CHAPTER 5 - DEGENERATE HOPPING IN VERY WIDE ENERGY BANDS

§5.1 Formulae for Hopping in Wide Bands

In the previous chapter we developed approximate analytical formulae for the dc hopping conductivity of systems in which the energies of the localized electrons are distributed over a very small range. In this case the integrals are easy to evaluate. We now wish to turn our attention to the more interesting case of degenerate hopping in a wide band of localized states. The integrals are then more complicated but an approximate analytical evaluation of them is still possible. We shall be interested in both two- and three-dimensional systems. The derivation of the relevant formula in this chapter is for three-dimensions unless otherwise indicated.

The behaviour of $\langle \sigma \rangle$ depends on the form of the density of states. To be definite and to keep the analysis as simple as possible, we suppose that $\rho(\epsilon)$ has a constant value ρ_F . Then $\rho(\epsilon_1)$ and $\rho(\epsilon_2)$ may be taken outside the integrals involved in eqns. (3.2.5), (3.3.1), (3.3.2). The evaluation of 2B in eqn. (3.3.1) is facilitated by introducing $q = q(\epsilon_1, \epsilon_2)$ as a new variable of integration. Let us write $A(q)$ for the area of the (ϵ_1, ϵ_2) -plane for which $q(\epsilon_1, \epsilon_2) < q$. We see from eqn. (4.1.5) that $q(\epsilon_1, \epsilon_2)$ has a minimum value of $\ln 4$ which henceforth we denote by q_m . Thus $A(q) = 0$ for $q < q_m$. Moreover we see from (4.1.4) that $s < s_p$ implies that $r'_p < r < r_p$ where r_p and r'_p are respectively the larger and smaller roots of the equation $p(r) + q_m = s_p$ i.e.

$$p(r'_p) + q_m = p(r_p) + q_m = s_p \quad (5.1.1)$$

It follows that eqn. (3.3.1) may be written in the form

$$\begin{aligned}
2B &= 4\pi\rho_F^2 \int_{r_p}^{r_p} r^2 A[s_p - p(r)] dr \\
&= \frac{4\pi}{3} \rho_F^2 \int_{r_p}^{r_p} r^3 A'[s_p - p(r)] (2\alpha - vr^{-1}) dr
\end{aligned} \tag{5.1.2}$$

In the second line we have integrated by parts and used (4.1.2).

We may use the same approach to simplify eqn. (3.2.5) for σ_p . For low temperatures and densities the dominant contribution to the integral comes from the neighbourhood of the critical percolation surface $s = s_p$. We may, therefore, approximate r_a by r throughout the integrand. When $q = q(\epsilon_1, \epsilon_2)$ is introduced as a new variable of integration, we note that the area of the (ϵ_1, ϵ_2) -plane between the contours $q(x, y) = q$ and $q(x, y) = q + dq$ is $A'(q)dq$. Hence

$$\sigma_p = g_o \frac{2\pi}{3} \rho_F^2 \int_0^\infty r^4 dr \int_{q_m}^\infty A'(q) \exp[-|s_p - q - p(r)|] dq \tag{5.1.3}$$

Now, the exponential in eqn. (5.1.3) reaches its maximum value of unity when $q = s_p - p(r)$. Moreover, we see from eqn. (5.1.1), that $s_p - p(r) > q_m$ provided that $r_p' < r < r_p$. We ignore contributions to the integral from values of r outside this range and approximate the contribution from values of r in this range by putting $q = s_p - p(r)$ in $A'(q)$ and extending the lower limit of the q -integration to $-\infty$.

Thus we obtain

$$\sigma_p = g_o \frac{4\pi}{3} \rho_F^2 \int_{r_p}^{r_p} r^4 A'[s_p - p(r)] dr \tag{5.1.4}$$

To complete the evaluation of the integrals (5.1.2) and (5.1.4) we must approximate $A(q)$. A preliminary study of the integrals shows

that we are primarily concerned with large values of q at low densities and low temperatures. For this case we find, by considering eqn. (4.1.5), that a crude approximation to the contour $q(\epsilon_1, \epsilon_2) = q$ is provided by the polygon of straight lines drawn in Figure 14. We have given the coordinates of three points in the diagram. The remaining points follow from the obvious symmetry of the polygon. The dashed polygon in Figure 14 shows the cruder approximation to the contour which is obtained when $q(\epsilon_1, \epsilon_2)$ is replaced by $\frac{1}{2}(|\epsilon_1| + |\epsilon_2| + |\epsilon_1 - \epsilon_2|)$ as is frequently done to simplify the integrals arising in hopping conductivity problems (Ambegaokar et al 1971, Butcher and Morys 1973, Butcher 1976 a, b). Neglecting contributions from the small shaded triangles we have

$$A(q) = (k_B T)^2 [3q^2 + 4q \ln q] \quad (5.1.5)$$

where the term involving $3q^2$ is the contribution from within the dashed polygon.

When eqn. (5.1.5) is substituted into (5.1.2) and (5.1.4) we find that the integrals are, with one exception, elementary. An adequate approximation to this exception is easily obtained. The final expressions are unwieldy and have been relegated to Appendix 1. The terms involving r_p' are always negligible in the cases we consider. Consequently, the integrals in (5.1.2) and (5.1.4) may be written in the forms $(k_B T)^2 \alpha^{-3} J(R_p)$ and $(k_B T)^2 \alpha^{-5} K(R_p)$ respectively, where $R_p \equiv \alpha r_p$ and $J(R_p)$ and $K(R_p)$ have the non-dimensional forms given in Appendix 1. It is also convenient to write

$$R_{po} \equiv \alpha r_{po} = \left(\frac{5N_p \alpha^2}{2\pi \rho_F k_B T} \right)^{\frac{1}{2}} \quad (5.1.6)$$

the significance of which is discussed below. Then eqns. (5.1.2) and (5.1.4) become

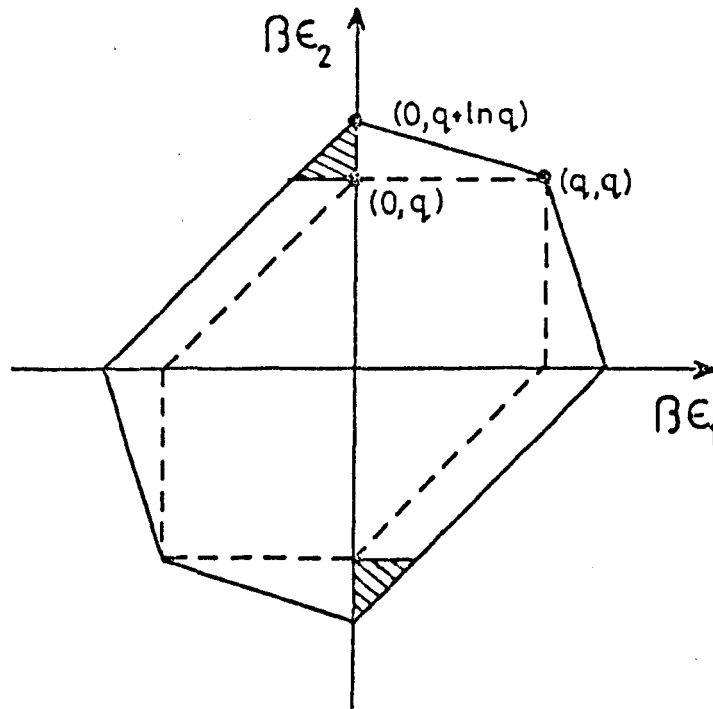


FIGURE 14 Schematic diagram of the contours $q(\epsilon_1, \epsilon_2) = q$. The polygon of full lines is the approximation used in the present analysis. Polygon of dashed lines is the approximation used in previous analyses. The shaded triangles are omitted in calculating $A(q)$.

$$2B = \frac{10N}{3R_{po}^4} (\rho_F k_B T) J(R_p) \quad (5.1.7)$$

and

$$\sigma_p = \frac{25N^2}{3 R_{po}^8} g_o \alpha K(R_p) \quad (5.1.8)$$

The calculations are completed by considering the integral S' in (3.3.2). Using (4.1.4) we see that $s < s_p$ implies that $q(\epsilon_1, \epsilon_2) < s_p - p_m$ where $p_m = v \ln(2\alpha/v)$ is the minimum value of $p(r)$ derived from eqn. (4.1.2). Inspection of the polygon of full lines in Figure 14 shows that we must therefore keep $|\epsilon_1| < k_B T |s_p - p_m - \ln(s_p - p_m)|$ to avoid automatic isolation of site number 1. Hence (3.3.2) reduces to

$$S' = 2\rho_F k_B T [s_p - p_m - \ln(s_p - p_m)] \quad (5.1.9)$$

and eqn. (3.3.3) for s_p becomes

$$\frac{3}{5} R_{po}^4 = \frac{J(R_p)}{s_p - p_m - \ln(s_p - p_m)} \quad (5.1.10)$$

where we have used (5.1.7). We may also express s_p in terms of $R_p \equiv \alpha r_p$ in (5.1.10). We use (4.1.2) and (5.1.1) to obtain the equation

$$s_p = 2R_p - v \ln R_p + q_m \quad (5.1.11)$$

We have now assembled all the equations required for the calculation of $\langle \sigma \rangle$. The direct route to the calculation would be to fix R_{po} , solve (5.1.10) and (5.1.11) for s_p and R_p and evaluate σ_p from (5.1.8). Fortunately this complicated procedure may be avoided by using a different route. We fix R_p , calculate s_p from (5.1.11), R_{po} from (5.1.10) and then evaluate σ_p using (5.1.8). There are no equations to be solved, only explicit expressions to be evaluated. The end result is the same: $\langle \sigma \rangle$ as a function of R_{po} .

The physical significance of R_{po} is easily found. We see from eqn. (5.1.11) that R_p is the maximum possible hopping range on the critical percolation surface in units of α^{-1} . R_{po} is the same quantity for the simpler case when $v = 0$ and $q(\epsilon_1, \epsilon_2) = \frac{1}{2}\beta[|\epsilon_1| + |\epsilon_2| + |\epsilon_1 - \epsilon_2|]$. To verify this we note that $p_m = q_m = 0$ and $s_p = 2R_p$ from equation (5.1.11). Moreover the logarithmic term is missing from (5.1.5) and inspection of the equations in Appendix 1 shows $J(R_p)$ reduces to $6R_p^5/5$. Hence eqn. (5.1.10) yields $R_p = R_{po}$.

The equations describing a two-dimensional system are readily found. We find that $4\pi r^3/3$ is replaced by πr^2 in (5.1.2) and $4\pi r^4/3$ is replaced by πr^3 in (5.1.4). Moreover, the integrals involved in these equations may be written in the forms $(k_B T)^2 \alpha^{-2} J(R_p)$ and $(k_B T)^2 \alpha^{-4} K(R_p)$, respectively where $J(R_p)$ and $K(R_p)$ have the non-dimensional forms given in Appendix 1. In the case when $v = 0$ and $q(\epsilon_1, \epsilon_2) = \frac{1}{2}\beta[|\epsilon_1| + |\epsilon_2| + |\epsilon_1 - \epsilon_2|]$, the maximum hopping range on the critical percolation surface reduces to

$$R_{po} = \left(\frac{2N_p \alpha^2}{\pi \rho_F k_B T} \right)^{1/3} \quad (5.1.12)$$

Consequently, in eqns. (5.1.7) and (5.1.8) the factors $10N_p/3R_{po}^4$ and $25N_p^2(g_o \alpha)/3\pi R_{po}^8$ are replaced by $2N_p/R_{po}^3$ and $4N_p^2 g_o / \pi R_{po}^6$ respectively. Eqns. (5.1.9) and (5.1.11) are unaltered and the factor of 3/5 in eqn. (5.1.10) is replaced by unity.

§5.2 Comparison with Computer Data

To assess the validity of the approximate formulae derived in Section 5.1 we compare the values of $\langle \sigma \rangle$ which they yield with values obtained by direct numerical solution of Kirchhoff's equations for a random resistance network. Two such numerical studies have

been performed: Seager and Pike (1974) and McInnes (Butcher, Hayden and McInnes 1977; Butcher and McInnes 1978; McInnes and Butcher 1978). We begin by considering the data of Seager and Pike (1974), who have made such calculations for models of the type described here in both two and three dimensions with $\nu = 3/2$, $\alpha^{-1} = 1.5 \text{ nm}$ and $g_0 = 581 \text{ mS}$. In Figure 15 we compare their computed points for a two-dimensional system with $\rho_F = 10^{18} \text{ m}^{-2} \text{ eV}^{-1}$ with the curve for the same system calculated from the analytical formulae with $N_p = 2.7$. The conductivity values published by Seager and Pike (1974) have been scaled up by a factor of $\sqrt{5} \times 10^{-5}$ to yield results measured in Siemens (Seager and Pike, private communication). The agreement is excellent over most of the temperature range. The falling away of the computed points at the high temperature end is due to the finite bandwidth assumed by Seager and Pike. The departures of the computed points from the analytical line at the low temperature end may reflect inaccuracies in the iterative technique used to solve Kirchhoff's equations which converges more slowly at low temperatures (McInnes, private communication).

To investigate these discrepancies McInnes and Butcher (1978) have repeated the calculation using many more sites. In Figure 16 we show the result of their calculations together with the theoretical prediction made using the analytical formulae with $\alpha^{-1} = 5 \text{ nm}$, $\rho_F = 10^{18} \text{ m}^{-2} \text{ eV}^{-1}$ in a bandwidth $W = 10 \text{ meV}$ symmetrically distributed about the Fermi level, and $N_p = 2.7$. The full line is the curve calculated from the analytical formulae. The points are those found computationally by McInnes and Butcher (1978). We see that at low temperatures the theoretical and computational points are in excellent agreement. At the high temperature end the effect of the finite bandwidth is clearly visible. For very high temperatures our formulae fail since the reduced bandwidth $W/k_B T \rightarrow 0$ in the computational work. In the infinite temperature limit, we therefore go over to the case

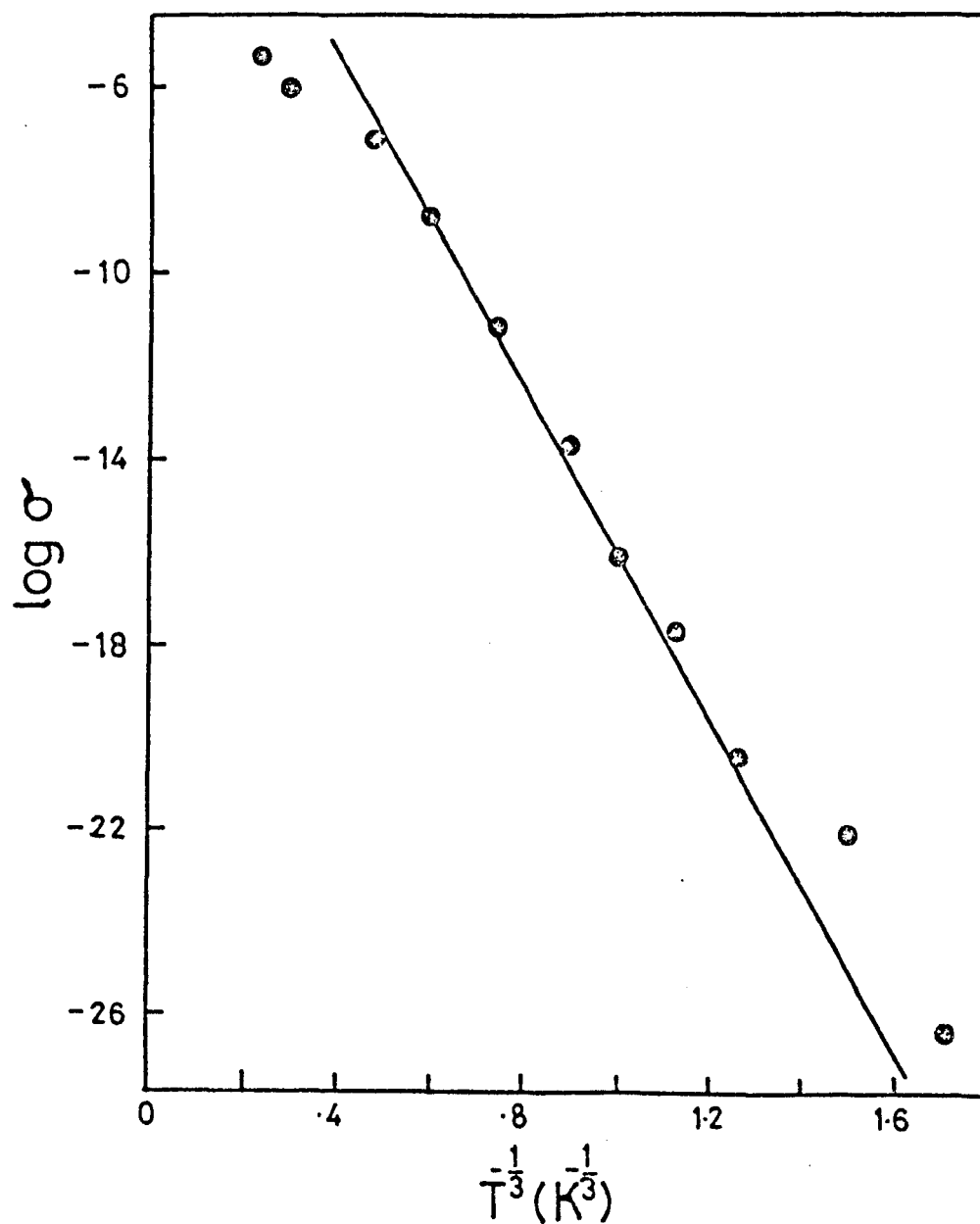


FIGURE 15 DC conductivity for a two-dimensional system with $\rho_F = 10^{18} \text{ m}^{-2} \text{ eV}^{-1}$. Dots: obtained from Figure 7 of Seager and Pike (1974). Continuous line: calculated from the analytical formulae for the same parameter values with $N_p = 2.7$.

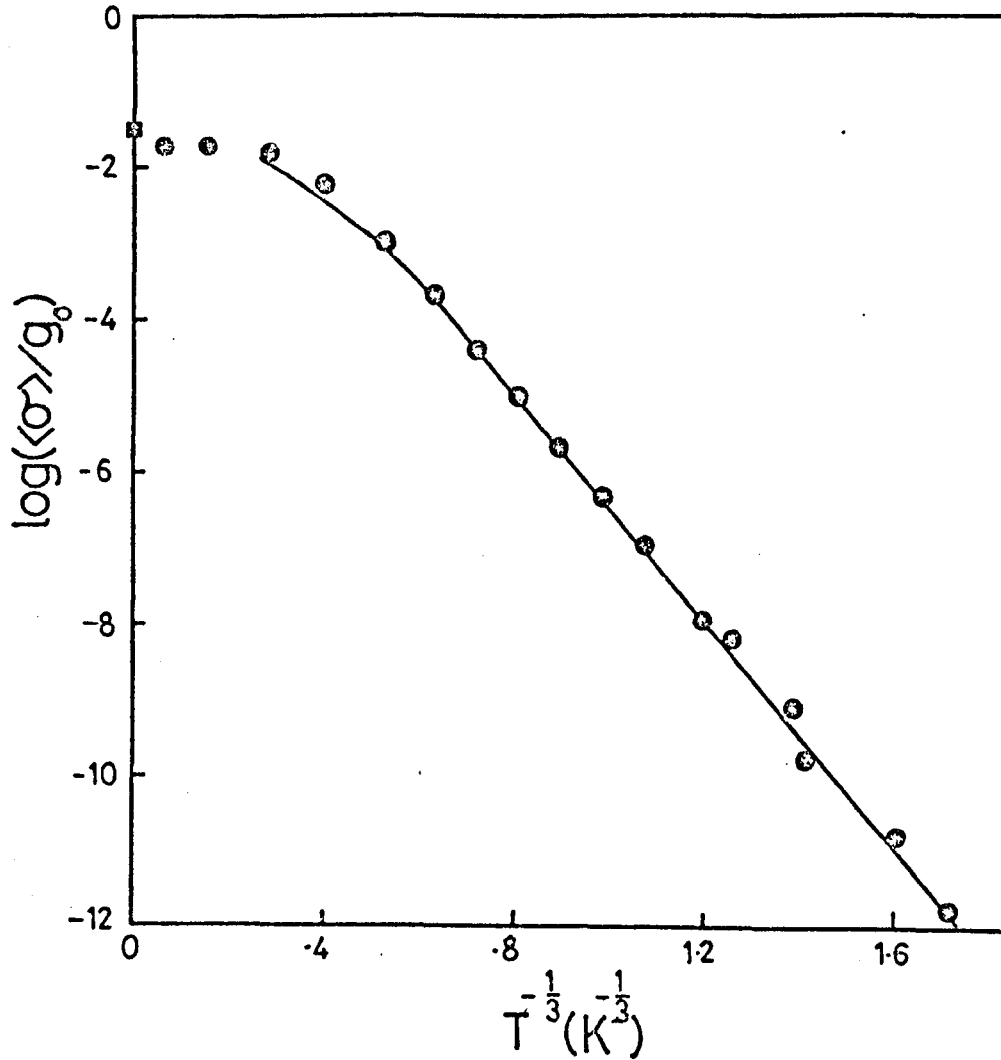


FIGURE 16 The dc conductivity for a two-dimensional system with $\rho_F = 10^{18} \text{ m}^{-2} \text{ eV}^{-1}$ and $\alpha^{-1} = 5 \text{ nm}$. The dots are the points found computationally by McInnes and Butcher (1978). The full line is the curve calculated from the analytical formulae with $N_p = 2.7$.

discussed in the previous chapter, namely hopping in a very narrow band. The theoretical prediction for the value of the conductivity obtained using these system parameters in the limit $T \rightarrow \infty$ is marked on the graph by a square. We see that the computer points tend very nearly to this point. We conclude therefore that the approximate formulae developed in the previous section accurately model the behaviour of $\langle \sigma \rangle$ in the two-dimensional case.

In Figure 17 we compare the computed points calculated by Seager and Pike (1974) for three-dimensional systems with $\rho_F = 10^{27}$, 10^{26} and $10^{25} \text{ m}^{-3} \text{ eV}^{-1}$ with the curves for the same system calculated from the analytical formulae with $N_p = 2.1$. The agreement is fair for $\rho_F = 10^{27} \text{ m}^{-3} \text{ eV}^{-1}$ and excellent for $\rho_F = 10^{26} \text{ m}^{-3} \text{ eV}^{-1}$ but the computed points for $\rho_F = 10^{25} \text{ m}^{-3} \text{ eV}^{-1}$ are about an order of magnitude above the analytical curve. This behaviour is surprising since the analysis in Section 5.1 is adapted to the low density case and the agreement with the computed points would be expected to improve as ρ_F decreases. To investigate whether this discrepancy is due to premature termination of the iterative solution of Kirchhoff's equations (McInnes, private communication), McInnes and Butcher (1978) have repeated the low density calculations using the same system parameters as Seager and Pike. The results are shown in Figure 18. The dots are the computational values found by McInnes and Butcher (1978), while the full line is the curve calculated from the analytical formulae. We see that throughout the temperature range the agreement is very good. For very high temperatures the computer points again tend to the narrow band limit indicated on the ordinate by a square.

§5.3 Universal Curves and Comparison with Experimental Data for Three-Dimensional Systems

The degree of agreement between the analytical formulae developed

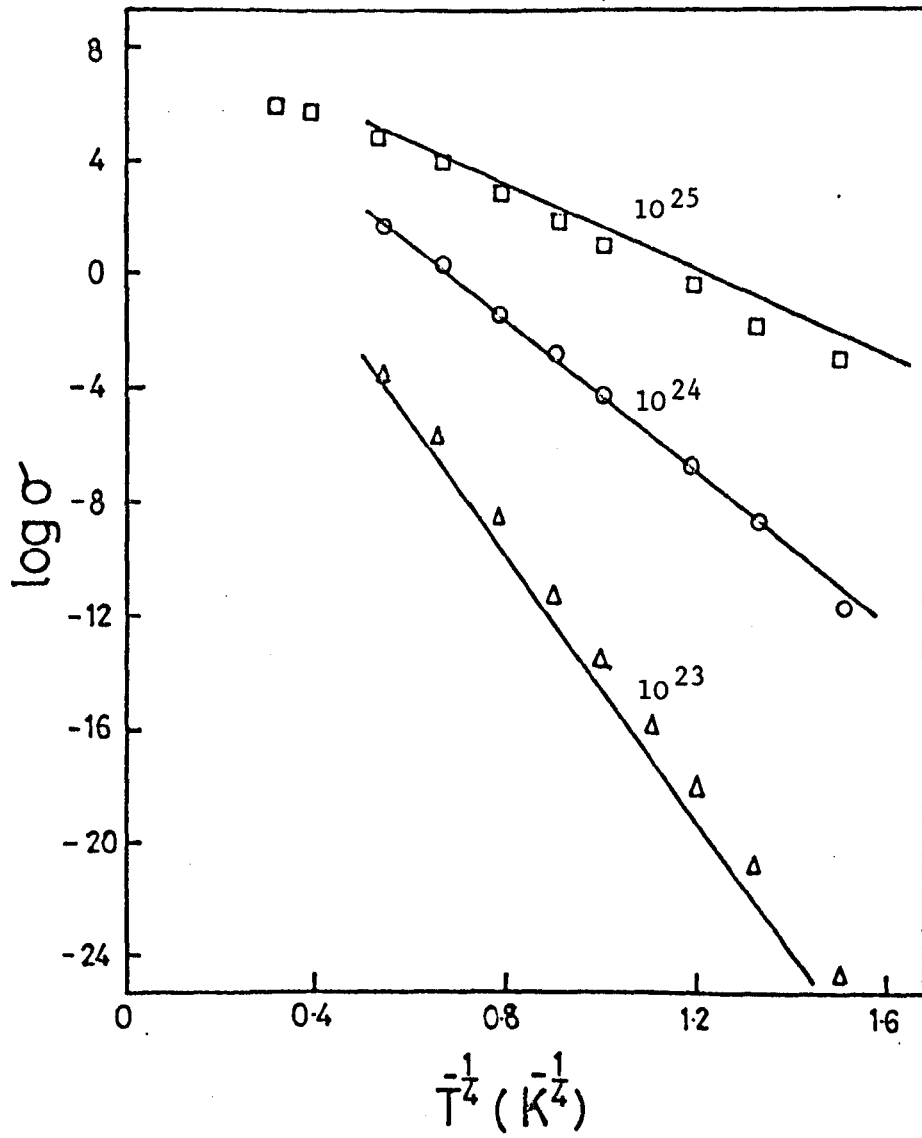


FIGURE 17 DC conductivity for a three-dimensional system for the values of ρ_F shown in $m^{-3} \text{ eV}^{-1}$. Points: from Figure 6 of Seager and Pike (1974). Continuous lines: calculated from the analytical formulae for the same parameter values with $N_p = 2.1$.

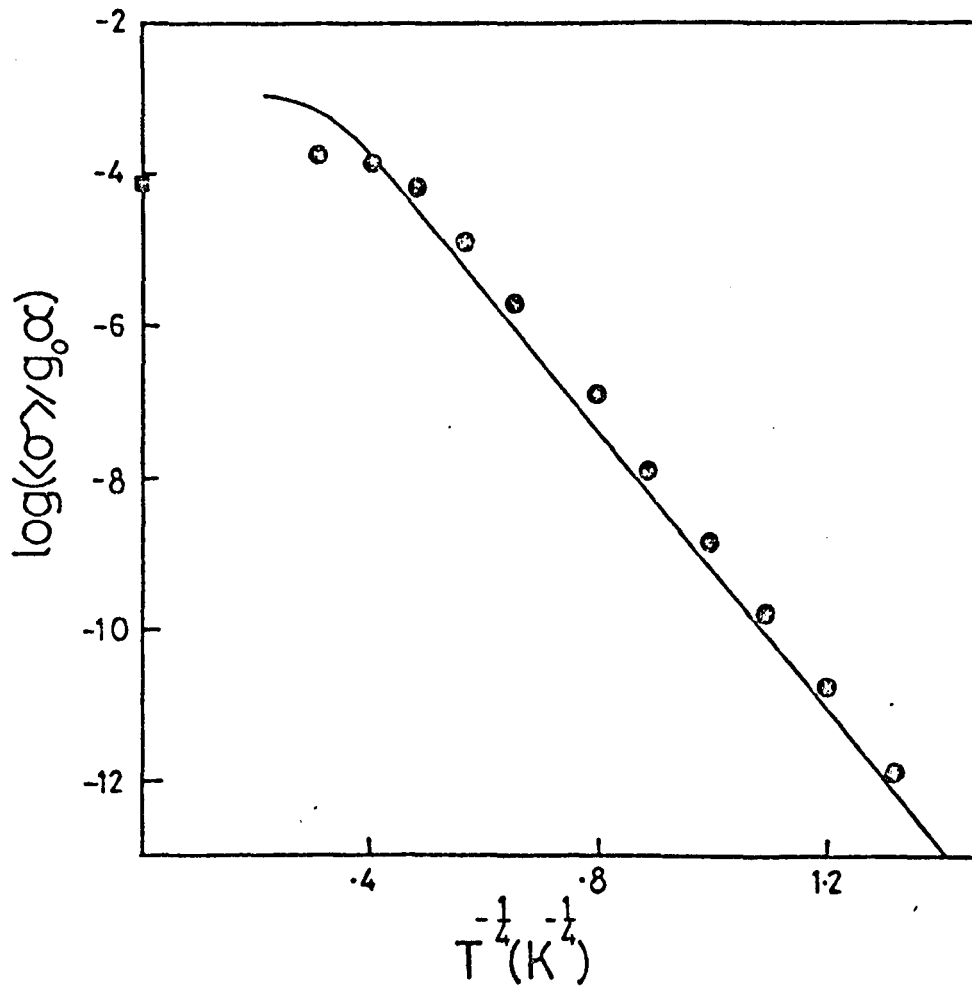


FIGURE 18 The dc conductivity of a three-dimensional system with $\rho_F = 10^{25} \text{ m}^{-3} \text{ eV}^{-1}$. Dots: values found computationally by McInnes and Butcher. Full lines: curve calculated from the analytical formulae with $N_p = 2.1$.

in this chapter and the computer data as shown in Section 5.2, enables one to analyse experimental data with some confidence. Before we turn our attention to this data, however, it is useful to discuss some general properties of the formulae developed above. For values of R_p in the experimentally accessible range (5 to 30), several of the terms contributing to $J(R_p)$ and $K(R_p)$ are of the same order of magnitude and no satisfactory approximation scheme suggests itself. Fortunately, when all the terms are retained, the relationship between R_p and R_{po} calculated from eqns. (5.1.10) and (5.1.11) has a very simple form. The result for $\nu = 2$ is shown in Figure 19.

For R_{po} in the range 10 to 30 we have $R_p = (0.98R_{po} - 1.16)$ to a good approximation. The constant term in this relation is particularly significant for the absolute magnitude of $\langle\sigma\rangle$ because, as is seen from eqn. (5.1.11) it appears doubled in the exponent s_p . For $R_{po} < 10$, R_p rises above the values predicted by this simple linear relationship, but the analytical formulae are also becoming inaccurate. The relationship between R_p and R_{po} for $\nu = 3/2$ and 0 in three dimensions and for $\nu = 0, 3/2$ and 2 in two dimensions is qualitatively the same. We show the corresponding values for M and C in Table 1, where M and C are defined by $R_p = MR_{po} + C$. In Figure 20, $\log \langle\sigma/\sigma_c\rangle$ is plotted against R_{po} for $\nu = 3/2$ (full curve labelled $\omega = 0$) and $\nu = 2$ (dashed curve labelled $\omega = 0$) where $\sigma_c = 5N_p^2 g_o \alpha / 6\pi$ is a convenient unit of conductivity. The curves are very nearly linear i.e. $\log \langle\sigma\rangle$ is approximately linear in $T^{-1/2}$ as we would expect (Ambegaokar et al 1971). The dotted curve labelled $\omega = 0$ shows $\log \langle\sigma/\sigma_c\rangle$ for $\nu = 2$ plotted against R_p instead of R_{po} . It serves to indicate the error involved in ignoring the differences between R_p and R_{po} which is about an order of magnitude. The dash-dot curve labelled $\omega = \infty$ in Figure 20 shows $\log (\langle\sigma(\infty)\rangle/\sigma_c)$

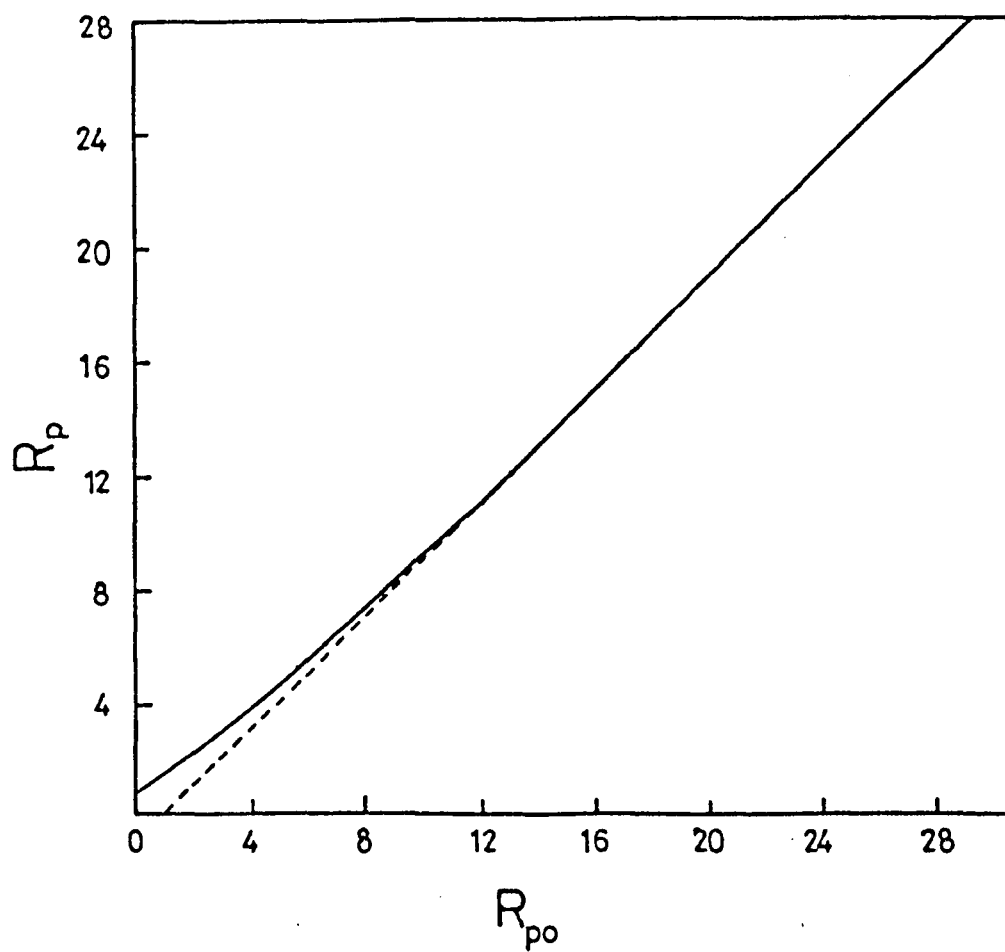


FIGURE 19 Plot of R_p against R_{po} for a three-dimensional model with $\nu = 3/2$.

DIMENSIONS	ν	M	C
3D	2	.98	-1.16
	3/2	.98	-1.19
	0	.99	- .96
2D	2	.98	-1.28
	3/2	.98	-1.26
	0	.99	-1.05

TABLE 1 Parameters in the approximate linear relationship

$$R_p = MR_{po} + C.$$

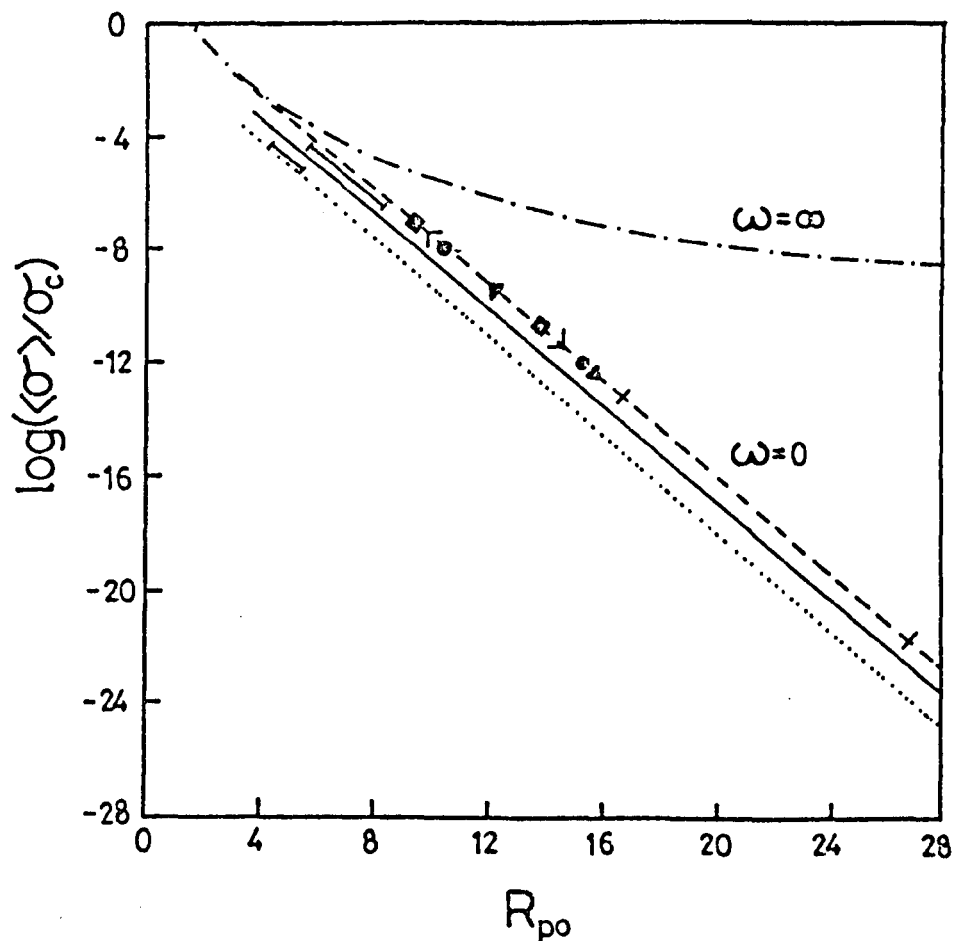


FIGURE 20 Plot of $\log(\langle\sigma\rangle/\sigma_0)$ against R_{p0} for a three-dimensional system where $\sigma_c = 5N_p^2 g_0 \alpha / 6\pi$, with $N_p = 2.1$. Full line: $\nu = 3/2$. Dashed line: $\nu = 2$. Dotted line: plot of $\log(\langle\sigma\rangle/\sigma_c)$ against R_p for $\nu = 3/2$. Dash-dot curve: plot of $\log(\langle\sigma_1(\infty)\rangle/\sigma_c)$ against R_{p0} for $\nu = 2$. The short straight lines show a fit of Allen and Adkins (1972) data to the theoretical $\nu = 3/2$ line. The symbols on the $\nu = 2$ theoretical line indicate the limit of the amorphous germanium data listed in Table 2.

for $\nu = 2$ as a function of R_{po} where $\sigma_1(\infty)$ is the limiting value of the real part of the ac conductivity when $\omega \rightarrow \infty$. We point out in Section 3.4 that $\sigma_1(\infty)$ may be calculated from eqns. (3.2.4) and (3.2.5) by setting s_p equal to the minimum value of s . The resulting integral is evaluated in Appendix 1. We find that

$$\frac{\langle \sigma_1(\infty) \rangle}{\sigma_c} = \frac{10\pi^2}{3} \frac{\Gamma(5 + \nu)}{2^{5+\nu}} R_{po}^{-8} \quad (5.3.1)$$

The numerical coefficient of R_{po}^{-8} in (5.3.1) is 185 for $\nu = 2$ (the case plotted) and 105 for $\nu = 3/2$. We see that the $\langle \sigma_1(\infty) \rangle$ curve touches the dashed dc curve for $\nu = 2$ at $R_{po} \sim 4$. This simple observation serves to enhance our confidence in the dc curves for values of R_{po} greater than 4 or 5. As discussed in Chapter 3, $\langle \sigma \rangle$ becomes identical to $\langle \sigma_1(\infty) \rangle$ in a high density (low R_{po}) system. Thus a complete plot of $\log (\langle \sigma \rangle / \sigma_c)$ for $\nu = 2$ valid for all R_{po} , would start on the dashed $\omega = 0$ curve for large values of R_{po} and go smoothly over to the dash-dot $\omega = \infty$ curve for $R_{po} < 4$.

The results presented in Figures 17 and 18 show that the analytic formula for $\langle \sigma \rangle$ provides a good approximation to the dc conductivity of a three-dimensional system in the $T^{-1/4}$ regime. It remains to test the model (and the rate equation formalism) against experimental data. Allen and Adkins (1972) have measured the dc conductivity of heavily doped n-type germanium crystals at temperatures low enough for $T^{-1/4}$ behaviour to be observed. If we ignore any effects due to the heavy doping, then all the parameters of the system, with the exception of ρ_F , may be identified with the well-known values for n-type germanium. We may also use the expression for the characteristic frequency R_o , calculated by Miller and Abrahams (1960) which is given by eqn. (4.3.1). Since R_o is proportional to T , the characteristic conductance $g_o \equiv e^2 \beta R_o$

is independent of T . We therefore use g_o rather than R_o when discussing $T^{\frac{1}{4}}$ data. Using the parameter values given in Chapter 4, it is found that $\nu = 3/2$, $\alpha^{-1} = 7 \text{ nm}$ and $g_o = 1.3 \text{ mS}$. The two straightline segments in Figure 20 show the data of Allen and Adkins (1972) for samples A2 (higher conductivity plot) and A3 (lower conductivity plot), plotted using these parameter values with $N_p = 2.1$ and $\rho_F = 2.9 \times 10^{26} \text{ m}^{-3} \text{ eV}^{-1}$ and $5.3 \times 10^{25} \text{ m}^{-3} \text{ eV}^{-1}$ respectively. These values of ρ_F were chosen so that the slopes of the experimental data lines are the same as the $\nu = 3/2$ theoretical line. The absolute locations of the experimental data lines of Figure 20 are then completely determined. We see that they lie about a factor of 4 on either side of the theoretical curve. In making this comparison between theory and experiment we have adjusted only one parameter: ρ_F . The numerical comparison becomes easier to make if we adjust both ρ_F and g_o so as to put both the experimental data lines precisely on the theoretical line. The values required to give this fit are shown in Table 2. The values of ρ_F differ little from those quoted above and the g_o values are about a factor of four above and below the predicted value of 1.3 mS .

We see that the experimental data for samples A2 and A3 lies at the extreme end of the region of R_{po} for which $T^{\frac{1}{4}}$ behaviour is expected. For lower values of R_{po} we would be concerned with a high density system for which $\langle \sigma \rangle$ is given more appropriately by eqn. (5.3.1). Allen and Adkins (1972) give data for another sample (A1) with a higher conductivity which apparently exhibited $T^{\frac{1}{4}}$ behaviour. It is not surprising that we were unable to achieve any satisfactory agreement between the data for this sample and the extrapolated low density theoretical curve for any value of ρ_F when $g_o \sim 1.3 \text{ mS}$. Adjustment of ρ_F to match the slope of the experimental data line and the low density theoretical curve places the experimental data line about 2






ρ_F ($m^{-3} eV^{-1}$)	g_o (mS)	Source	Sample identification
8.8×10^{23}	82	Agarwal, Gutta and Narasimhan (1975)	$T_A = 350^\circ C$ (lowest conductivity) 
1.7×10^{24}	89	Chopra and Bahl (1970)	Fig. 9 
2.3×10^{24}	0.53	Arizumi, Yoshida, Baba Shimakawa and Nitta (1974)	Fig. 1 annealed 
2.6×10^{23}	54	Hauser and Staudinger (1973)	Ge NO.7 annealed 
1.5×10^{24}	190	Gilbert and Adkins (1976)	Fig. 4 
5.4×10^{25}	5.4	Allen and Adkins (1972)	A3
3.1×10^{26}	0.3	Allen and Adkins (1972)	A2

TABLE 2 Values of ρ_F and g_o derived from three-dimensional experimental data. The first four cases are for evaporated films of amorphous germanium with $\nu = 2$. The last two cases are for n-type crystalline germanium with $\nu = \frac{3}{2}$.

orders of magnitude below the theory line. Allen and Adkins fit their data for all samples using a similar exponent to that used here and making a variety of assumptions about the prefactor, α^{-1} and the dielectric constant. Their best estimates of ρ_F for samples A2 and A3 are quite close to those in Table 2, but were obtained on the assumption that the dielectric constant is considerably enhanced over the value for pure germanium.

Extensive experimental studies of evaporated films of amorphous germanium show that the dc conductivity has a $T^{\frac{1}{4}}$ behaviour. This is usually interpreted as due to hopping between localized states induced by the randomness of the material. There is, however, very little understanding of the nature of these localized states. If we assume that they are hydrogen-like we may analyse the data on the basis of the model under discussion here, but our knowledge of the system parameters is necessarily uncertain. It is usually assumed that $\nu = 0$ in theoretical studies (Ambegaokar et al 1971; Butcher and Morys 1973; Butcher 1976 a, b). However, a factor of r^2 is to be expected from the overlap integrals involved in the transition rates, and so we assume that $\nu = 2$. In crystalline germanium we used $\nu = 3/2$. This departure from the basic $\nu = 2$ behaviour is due to the large ellipticity of the energy surfaces in the conduction band valleys. Because of the uncertainty surrounding the structure of amorphous germanium, this refinement seems inappropriate. For α^{-1} we take the value determined recently by Gilbert and Adkins (1976) from studies of hopping in both thick and thin films. The theory then contains two unknown parameters; ρ_F and g_0 . These may be adjusted so as to put any collection of $T^{\frac{1}{4}}$ data points on the $\nu = 2$ (dashed) curve in Figure 20 and we have done that for a variety of cases. The range of the data is indicated by marks on the curve and the values of ρ_F and g_0 used are given in Table 2.

The values of ρ_F are determined by the slope of a plot of $\log \sigma$ against T^{-1} . They differ from those of the original authors because of our use of $\alpha^{-1} = 1.4$ nm, $N_p = 2.1$ and $\nu = 2$. The values of g_0 are more interesting. With the exception of one very low value deduced from the data of Arizumi et al (1974), the g_0 values are of the order of 75 mS. No theoretical estimate of g_0 is available for amorphous germanium, but we may obtain an order of magnitude estimate as follows. We suppose that all the material parameters governing the characteristic hop rate R_0 are the same as the crystalline case with the exception of α^{-1} which is assigned the value 1.4 nm as for amorphous germanium. Furthermore, we suppose that the conduction band in the amorphous case consists of one spherically symmetric valley. Then eqns. (4.1.3) and (4.3.1) with $\nu = 2$ and $n = 1$ give $g_0 = 150$ mS which is the order of that observed.

§5.4 Universal Curves and Comparison with Experimental Data for Two-Dimensional Systems

We may readily use the formulae developed in Section 5.1 to describe degenerate hopping in two-dimensional systems for which the appropriate value of N_p is 2.7. The relationship between R_p and R_{po} remains linear with the parameters given in Table 1. In Figure 21 we show the two-dimensional universal curve (cf. the three-dimensional case). $\log(\langle \sigma \rangle / \sigma_c)$ is plotted against R_{po} for $\nu = 3/2$ (full curve labelled $\omega = 0$) and $\nu = 2$ (dashed curve labelled $\omega = 0$). For the two-dimensional case $\sigma_c = 3N_p^2 g_0 / 5\pi$ and R_{po} is given by (5.1.12). These dc curves are again nearly linear, implying that $\log \langle \sigma \rangle$ is approximately linear in $T^{-1/3}$ as one would expect in the two-dimensional case.

The dash-dot curve labelled $\omega = \infty$ in Figure 21 shows $\log(\langle \sigma_1(\infty) \rangle / \sigma_c)$ for $\nu = 2$ as a function of R_{po} where $\langle \sigma_1(\infty) \rangle$ is again the limiting value

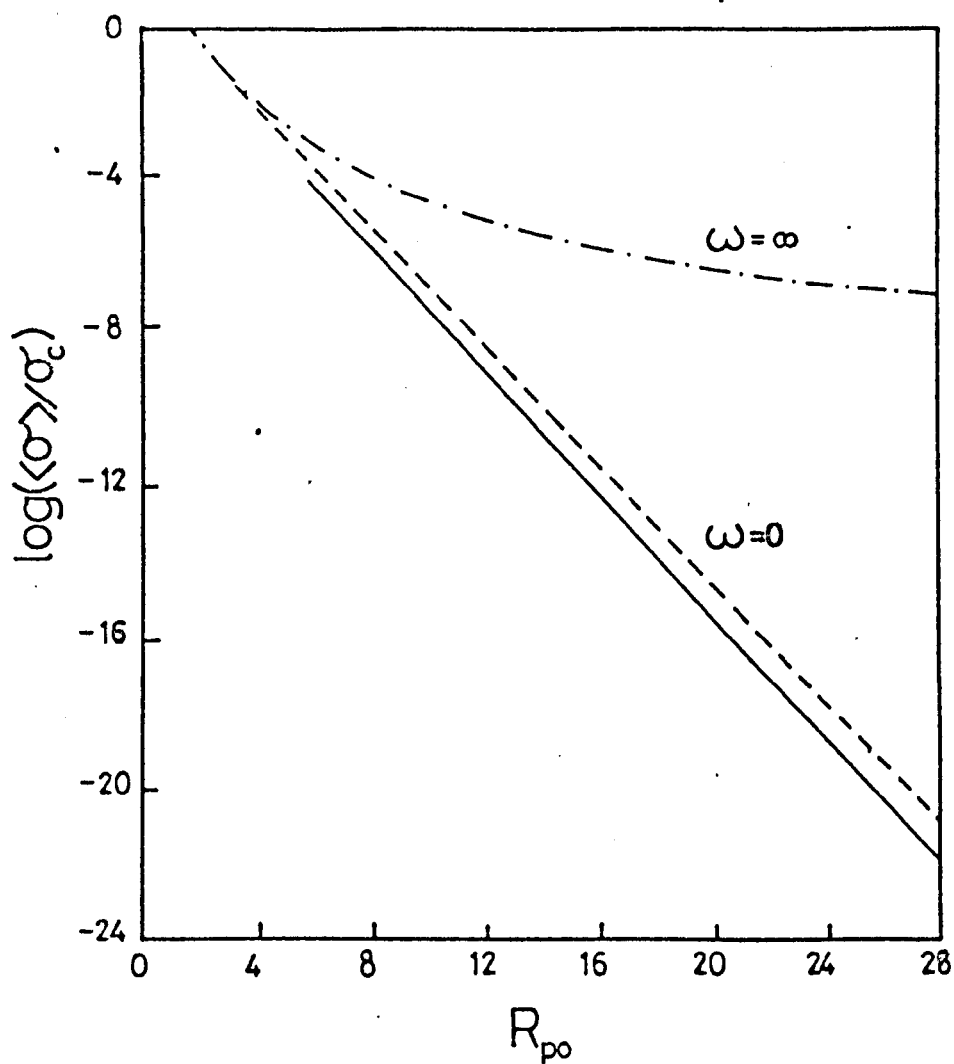


FIGURE 21 Plot of $\log (\langle \sigma \rangle / \sigma_c)$ against R_{po} for a two-dimensional system where $\sigma_c = 3N_p^2 g_o / 5\pi$ with $N_p = 2.7$. Full line: $\nu = 3/2$. Dashed line: $\nu = 2$. Dash-dot curve: plot of $\log (\langle \sigma(\infty) \rangle / \sigma_c)$ for $\nu = 2$.

of the real part of the conductivity when $\omega \rightarrow \infty$. In the two-dimensional case we find that

$$\frac{\langle \sigma_1(\infty) \rangle}{\sigma_c} = \frac{20\pi^2}{9} \frac{\Gamma(4 + \nu)}{2^{4+\nu}} R_{po}^{-6} \quad (5.4.1)$$

The numerical coefficient of R_{po}^{-6} in (5.4.1) is 41 for $\nu = 2$ (the case plotted) and 25 for $\nu = 3/2$. As we show in Section 3.4, $\langle \sigma \rangle = \langle \sigma_1(\infty) \rangle$ in a high density system. We see from Figure 21 that the transition between the low and high density regimes occurs when $R_{po} \sim 4$ in two dimensions as well as in three dimensions.

We are now in a position to analyse two-dimensional data. Until recently the only experimental two-dimensional studies involved thin film conduction in amorphous materials (see for example Hauser and Staudinger 1973). However, recent studies of inversion layers in metal-oxide-silicon field effect transistors (MOSFETS) have shown two-dimensional hopping conduction (Pepper, Pollit and Adkins 1974; Pepper, Pollit, Adkins and Oakley 1974). Experimentally at very low temperatures the conductivity exhibits $T^{-1/3}$ behaviour while at higher temperatures there is a transition to activated T^{-1} behaviour. We interpret this as follows. If the Fermi level is at a position such as A (see Figure 5) in the conduction bandtail below the mobility edge, then for low temperatures, typical states an energy $k_B T$ from the Fermi level lie well within the localized state region. At higher temperatures, activation to the mobility edge and then transport due to extended states becomes preferential. These are the two regions observed experimentally. The analytical formulae developed in this chapter can therefore be used to analyse the low temperature $T^{-1/3}$ data obtained experimentally.

In applying our analytical formulae to analyse this two-dimensional data

we are in much the same position as with the three-dimensional data for amorphous germanium in Section 5.3: most of the physical parameters of the system are unknown. Moreover, no detailed calculation of the two-dimensional hopping rates has been performed. We therefore again use the Miller and Abrahams type rate and put $\nu = 2$. For the two cases considered here, ρ_F has been measured experimentally (Pepper, private communication, Pollit 1976a, b) and so the unknown parameters reduce to α and g_0 which we adjust so that the data lies on the $\nu = 2$ line in Figure 21.

Conductivity data for an n-channel device were taken from Pollit (1976a). They correspond to a gate voltage of 0.8 V for which Pollit finds $\rho_F = 0.6 \times 10^{18} \text{ m}^{-2} \text{ eV}^{-1}$ (see also Pollit 1976b). The data fits the dashed theoretical curve between $R_{po} = 6$ and 9 when $\alpha^{-1} = 7.0 \text{ nm}$ and $g_0 = 3.0 \text{ mS}$. Conductivity data for a p-channel device were taken from the lowest curve given in Figure 20 of Mott et al (1975), for which $\rho_F = 1.8 \times 10^{18} \text{ m}^{-2} \text{ eV}^{-1}$ (Pepper, private communication). The data fits the dashed theoretical curve between $R_{po} = 4$ and 9 when $\alpha^{-1} = 5.5 \text{ nm}$ and $g_0 = 3.6 \times 10^{-3} \text{ mS}$. Our estimates of α^{-1} are about a factor of two larger than those deduced by the original authors because we use a different expression for the exponent, s_p , in $\langle \sigma \rangle$. There have been no theoretical calculations of hopping rates in inversion layers from which we can determine a theoretical value for g_0 . We note, however, that in Section 4.3 we calculated a value of 1.3 mS for three-dimensional hopping in crystalline silicon. The value of g_0 deduced here from the n-channel data is not very different from this while the value deduced from the p-channel data is three orders of magnitude smaller.

§5.5 Discussion

In this chapter we have developed formulae which are applicable to situations where the bandwidth of localized states is much wider

than the characteristic energy in the percolation path $s_p k_B T$. The agreement with computer data is remarkably good. It should be emphasized that no parameters have been adjusted in comparing the analytical results for $\langle \sigma \rangle$ with computer results. A general discussion of the comparison with computer data, both for the wide band and narrow band cases, can be found in Chapter 9.

The dash-dot curves labelled $\omega = \infty$ in Figures 20 and 21 show the behaviour of $\langle \sigma_1(\infty) \rangle$ for degenerate systems with $\nu = 2$ in three and two dimensions respectively. These curves also provide good approximations to $\langle \sigma \rangle$ for $R_{po} < 4$. For $R_{po} > 4$ the difference between these curves and the dashed curves labelled $\omega = 0$ gives the total increment of the ac conductivity between $\omega = 0$ and $\omega = \infty$ predicted by the rate equation formalism. The predicted increment is many orders of magnitude when R_{po} is large, but falls below $2\frac{1}{2}$ orders when $R_{po} < 10$. Further experimental studies of the ac conductivity of degenerate systems in this regime (e.g. heavily doped n-type crystalline germanium) would therefore be of considerable value.

The model we have assumed is well adapted to n-type crystalline germanium. This is confirmed by the good quantitative agreement between the theory and the experimental data of Allen and Adkins (1972) shown in Figure 20 and Table 2. The model is less well adapted to all the other systems for which we have compared the theory with experimental data. Our knowledge of the parameter values in these cases is insufficient to allow rigorous quantitative tests which might suggest modifications of the model. Agreement between theory and experiment can always be obtained by adjusting the parameters in the model instead of changing the model itself.

CHAPTER 6 - HOPPING IN ENERGY BANDS OF INTERMEDIATE WIDTH

§6.1 General Formulae

Chapters 4 and 5 have dealt with the dc conductivity of systems where the localized state energies are distributed over an extremely narrow and a very large bandwidth respectively. In this chapter we develop formulae applicable to the intermediate case of a finite bandwidth. In particular, we shall be interested in two-dimensional systems for which analytical results may be found, since we wish to compare the formulae with experimental data obtained from MOSFET devices.

To obtain relatively simple analytical formulae we adopt a model in which $\rho(\epsilon)$ is a constant ρ_F over a bandwidth W . Moreover we use the Miller and Abrahams type rates given in (4.1.1), and simplify s by putting $v = 0$. Finally, we approximate q by the more usual expression (Butcher 1976 a, b; Ambegaokar et al 1971) to obtain

$$s(\epsilon_1, \epsilon_2, r) = 2\alpha r + \frac{\beta}{2} \left[|\epsilon_1| + |\epsilon_2| + |\epsilon_1 - \epsilon_2| \right] \quad (6.1.1)$$

in which the energies are measured relative to the Fermi level plus $k_B T \ln 2$. Strictly speaking, we should retain this spin degeneracy term. However, because of the number of previous simplifying approximations and for simplicity, we shall ignore it. We see from eqns. (5.1.2) and (5.1.4) that the evaluation of s_p and σ_p only requires a knowledge of $A(q)$. For the case under discussion here the form of $A(q)$ is somewhat more complicated than that used in Chapter 5 since the bandwidth restriction alters the form of $A(q)$ depending on the relative sizes of q (and hence s_p) and W' , where $W' = W/2k_B T$. Moreover, $A(q)$ also depends on the position of the band of localized states relative to the Fermi level. We therefore relegate the actual calculation of $2B$, S and σ_p to Appendix 2. Furthermore, we shall only discuss in detail

the case in which the Fermi level lies in the centre of the band. The more general case of an off-centre Fermi level is dealt with in Appendix 2. The motivation for discussing the first case in detail is the existence of experimental data in which the Fermi level is in the centre of the band.

Three régimes are identifiable depending on the relative values of s_p and W' . When $0 < s_p < W'$, s_p reduces to

$$s_{po} = (16N_p^{(3)} \alpha^2 / \pi \rho_F k_B T)^{1/3} \quad (6.1.2)$$

The significance of the superscript on N_p is discussed below. This is the usual exponent associated with degenerate hopping in two dimensions (see eqn. (5.1.6)) and reflects the fact that the bandwidth is effectively infinite. Eqn. (6.1.2) is valid up to a temperature T' such that $s_p = W'$. In two dimensions we find

$$T' = \left(\frac{\pi \rho_F W^3}{128 N_p^{(3)} \alpha^2 k_B^2} \right)^{1/2} \quad (6.1.3)$$

Above this temperature eqn. (6.1.2) is no longer valid. We find instead polynomial equations for s_p when $s_p > W'$. Before solving these equations, however, a value must be given to the percolation parameter N_p . We know from Chapter 4 that for very narrow bands (i.e. $T \rightarrow \infty$) N_p is given by the two-dimensional value $N_p^{(2)} = 4.5$. In the case of very wide bands (i.e. $T \rightarrow 0$), N_p takes the effective three-dimensional value $N_p^{(3)} = 2.7$ as discussed in Chapter 5. There is no theoretical or computational work concerning the appropriate value of N_p as a function of the temperature and the bandwidth of the localised states. Various authors (Pike and Seager 1974; Pollak 1972; Shante 1978) have argued that N_p is temperature independent. Their arguments, however, are based on the assumption that the effective dimensionality of the

system does not alter over the temperature range under consideration.

In our case, we change from wide band hopping to narrow band hopping

as the temperature increases and so one may expect N_p to vary with

temperature. This point is discussed in more detail in Chapter 9. We

therefore adopt the following ansatz for the temperature dependence of

N_p . Below T' we put $N_p = N_p^{(3)}$. For $T > T'$ we write $N_p = N_p^{(3)} + \Delta N_p (T - T')/T$, where T' is given by eqn. (6.1.3) and $\Delta N_p = N_p^{(2)} - N_p^{(3)}$. The values

of s_p computed using this ansatz are shown in Figure 22. The

quantity $s_{p\infty}$ is a convenient normalizing factor and is the s_p

value obtained from eqns. (A2.1.4) and (A2.1.5) as $T \rightarrow \infty$, i.e. in

the limit $s_p \gg W'$. Thus

$$s_{p\infty} = \left(\frac{4N_p^{(2)} \alpha^2}{\pi n_s} \right)^{\frac{1}{2}} \quad (6.1.4)$$

where $n_s = \rho_F W$ is the spatial density of states. We note that this

is the expression derived in Chapter 4 for a two-dimensional narrow

band system. Curve A is a plot of $s_p/s_{p\infty}$ against a normalized reciprocal

temperature X (lower axis). Curve B is a plot of $s_p/s_{p\infty}$ against $X^{1/3}$

(upper axis). We find from curve A that, for $s_p/s_{p\infty} \leq 1.7$, s_p is well

approximated by the equation

$$s_p = \frac{W}{3k_B T} + s_{p\infty} \quad (6.1.5)$$

Since $\sigma = \sigma_p \exp(-s_p)$ we may identify the quantity $W/3$ as the activation

energy for the hopping process. At lower temperatures $s_p/s_{p\infty} > 1.7$

and the temperature dependence of s_p is slower than T^{-1} . This

transition occurs at the position marked by the horizontal dotted line.

Replotting $s_p/s_{p\infty}$ against $X^{1/3}$ (curve B) shows that s_p is now proportional

to $T^{-1/3}$. The dot shows the temperature T' . We note that in the linear

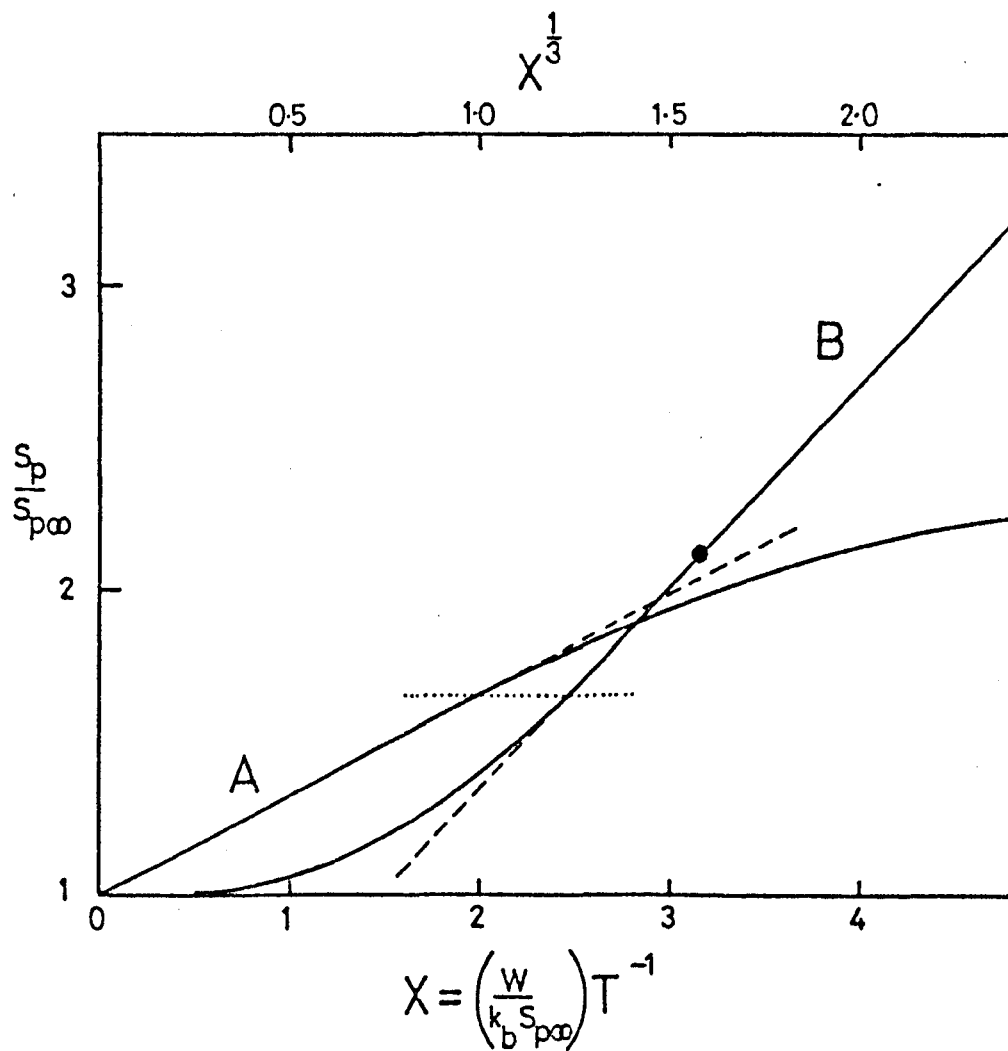


FIGURE 22 Plots of $s_p/s_{p\infty}$ against T^{-1} and $T^{-1/3}$ where T is in units of $W/k_b s_{p\infty}$. Here $s_{p\infty} = (4N_p^{(3)} \alpha^2 / \pi n_s)^{1/2}$. Curve A refers to the lower axis and curve B refers to the upper axis.

régime of curve B, s_p is given by eqn. (6.1.2). From Figure 22, one may readily deduce the transition temperature θ , at which variable range hopping goes over to activated hopping. The transition is abrupt and occurs at a temperature

$$\theta = \frac{W}{2k_B s_{p\infty}} \quad (6.1.6)$$

To achieve precision in the analysis of experimental data, this estimate of θ must be modified by considering the effect of the prefactor, as is done below. However, one may readily verify that $\theta \sim 3T'$ i.e. the transition to activated behaviour does not occur when $s_p = W$. This behaviour has been predicted on dimensional grounds by Pollak (1972). It serves to illustrate the point that the important energies in the percolation chain are somewhat less than $s_p k_B T$, a point discussed more fully in Chapter 9.

When $s_p > 2W'$, the polynomial equation for s_p is a quadratic and hence an analytical formula is easily obtained:

$$s_p = \frac{5W}{12k_B T} + \left(\frac{4\alpha^2 N_p}{\pi n_s} \right)^{\frac{1}{2}} \left[1 - \frac{5W^2 \pi n_s}{576 \alpha^2 (k_B T)^2 N_p} \right]^{\frac{1}{2}} \quad (6.1.7)$$

Eqn. (6.1.7) implies that $\epsilon = 5W/12$ (c.f. computer solution where $\epsilon = W/3$). There is, however, a correction factor due to the temperature dependence of N_p in eqn. (6.1.7). We put the quantity in the square bracket equal to unity, since the second term is necessarily less than $5/576$ when $s_p > 2W'$. Recognising that $N_p = N_p^{(2)} - \Delta N_p T'/T$, where T' is given by eqn. (6.1.3), we may expand $N_p^{\frac{1}{2}}$ to first order in terms involving T'^{-1} . We then obtain

$$s_p = \left(\frac{5}{12} - \frac{1}{2\sqrt{32}} \frac{\Delta N_p}{(N_p^{(2)} N_p^{(3)})^{\frac{1}{2}}} \right) \frac{W}{k_B T} + s_{p\infty} \quad (6.1.8)$$

The number in brackets is equal to .37 and we again regain an activation energy in the order of $W/3$.

Finally we discuss the effect of the conductivity prefactor on the calculated value of the transition temperature θ and the activation energy ϵ . As shown in detail in Appendix 2, the behaviour of the prefactor again depends on the relative values of s_p and W . The result of the calculation is shown in Figure 23 where we plot $\log(\sigma/\sigma_\infty)$ against T^{-1} . Here σ_∞ is the infinite temperature conductivity $\sigma_\infty = (\pi g_0 n_s^2 s_{p\infty}^3 / 16\alpha^4) \exp(-s_{p\infty})$ derived in Chapter 4, for very narrow bands. The two curves correspond to different site densities n_s . The bandwidth W , and the decay constant α were kept constant at .0045 eV and 3.1 nm respectively in the calculation. We see that the relationship between the activation energy ϵ and the bandwidth W , measured from the straight line section of the plot, is given by

$$\epsilon = .38W \quad (6.1.9)$$

which is only a little different from the result derived above from a consideration of s_p alone. The dots mark the transition temperatures θ for each curve. In Figure 24 we show how θ varies with $s_{p\infty}$ and the bandwidth, W , of localized states. For larger values of $s_{p\infty}$ the determination of θ becomes difficult because the transition is very slow, and so these values must be treated with caution.

Finally, we discuss the effect of the prefactor on the conductivity in the low temperature $T^{-1/3}$ régime. In Figure 25 we show a typical plot of $\log(\sigma/\sigma_\infty)$ against s_{po} for a particular choice of system parameters ($W = 4.5$ meV, $\rho_F = 1.73 \times 10^{18} \text{ m}^{-2} \text{ eV}^{-1}$, $\alpha = 3.1$ nm). The dot signifies the temperature θ , whilst the square signifies T' . We see that for temperatures lower than θ , $\log \sigma$ is proportional to $T^{-1/3}$. The effect of the prefactor, is to reduce T_0 slightly. This reduction is independent of the system parameters. In fact, in this region s_p is given by $s'_{po} = .97 s_{po}$, i.e.

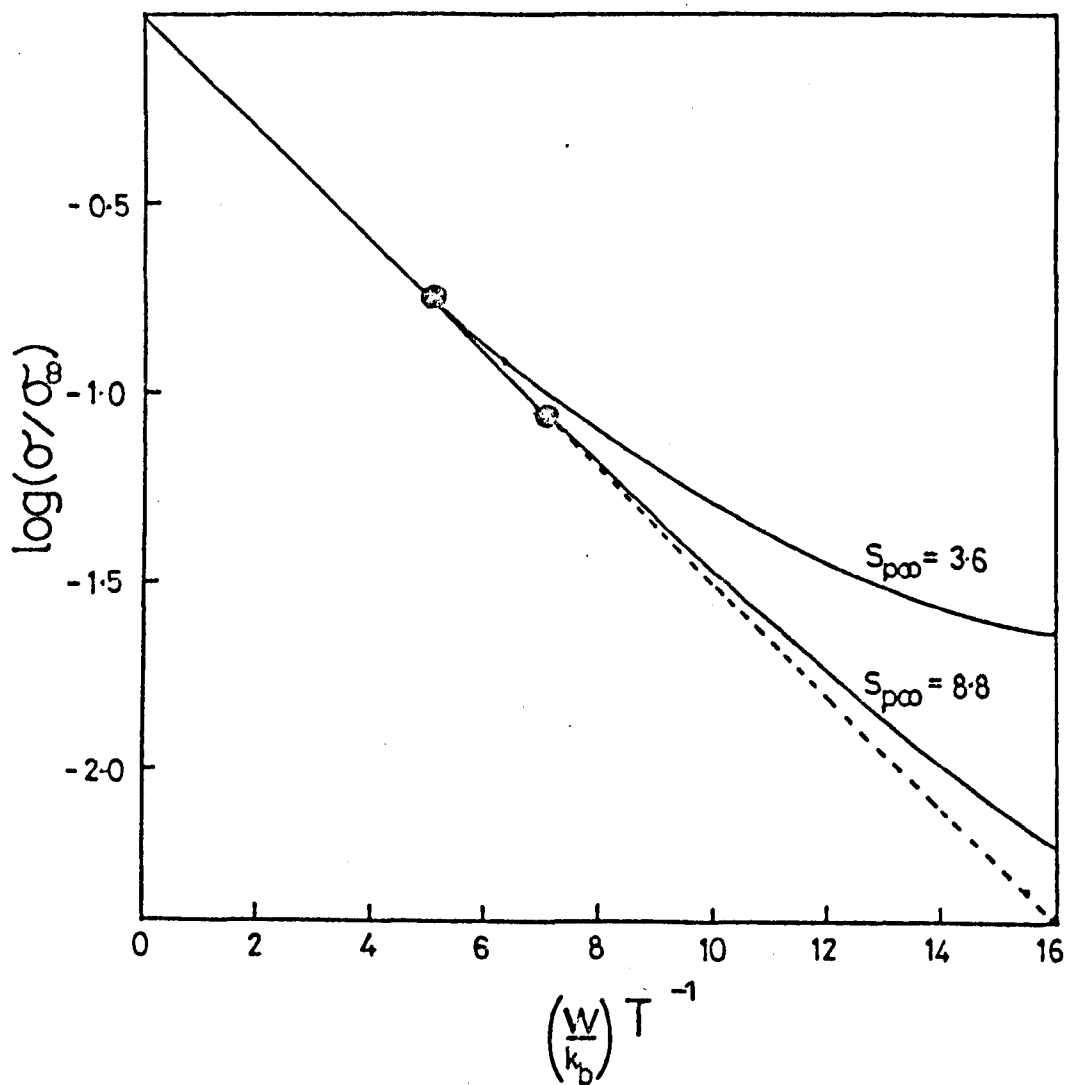


FIGURE 23 Plot of $\log (\sigma / \sigma_{\infty})$ against a normalized inverse temperature where $\sigma_{\infty} = (g_0 \pi n_s^2 s_{p\infty}^3 / 16 \alpha^4) \exp(-s_{p\infty})$. The dots indicate the transition temperature θ for two different values of the site density indicated by the $s_{p\infty}$ values.

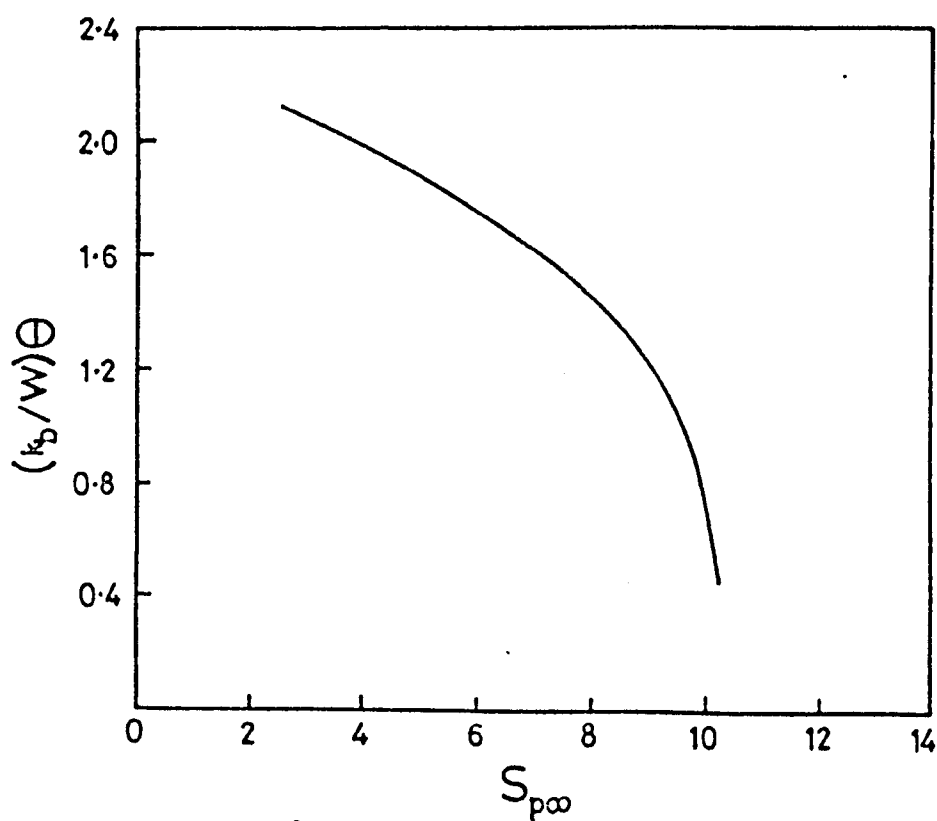


FIGURE 24 Plot of the normalized transition temperature θ against

$$s_{p\infty} = (4N_p^{(2)} \alpha^2 / \pi n_s)^{\frac{1}{2}}.$$

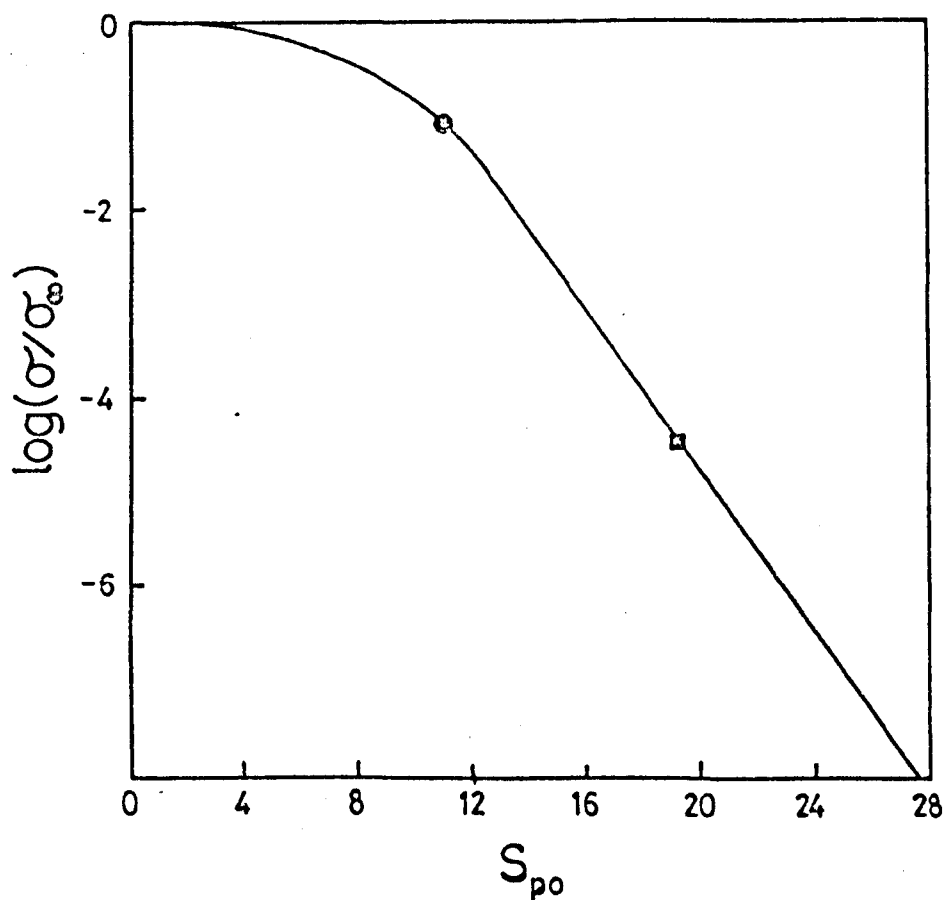


FIGURE 25 Typical plot of $\log(\sigma/\sigma_\infty)$ against $s_{po} = (16N_p^{(3)}\alpha^2/\pi\rho_F k_B T)^{1/3}$.

The square indicates the temperature T^1 , and the dot shows the transition temperature θ . The parameter values are $W = 4.5$ meV, $\rho_F = 1.73 \times 10^{18} \text{ m}^{-2} \text{ eV}^{-1}$ and $\alpha^{-1} = 3.1$ nm.

$$s_{po}' = \left(\frac{14.8 \alpha_N^2 (3)}{\pi \rho_F k_B T} \right)^{1/3} \quad (6.1.10)$$

The effect of the prefactor on the slope of the $T^{1/3}$ plot as shown in eqn. (6.1.10) is similar to that predicted in Chapter 5, and illustrated in Table 1. We are now in a position to analyse experimental data using the formulae developed above.

§6.2 Comparison with Experiment

Until recently experimental investigations of inversion layers (Pepper, Pollit and Adkins 1974; Pollit 1976; Mott et al 1975) concerned the localized states at the band extrema. The temperature dependence of $\log \langle \sigma \rangle$ shows $T^{-1/3}$ behaviour at sufficiently low temperatures with a transition to a T^{-1} law at higher temperatures. In this case, the activated behaviour is due to carrier activation at the Fermi level to the extended states at the mobility edge. Recently, however, data obtained from the study of impurity bands in inversion layers in silicon has been shown to exhibit three modes of conduction: activation to the mobility edge, 'nearest neighbour hopping' and 'variable range hopping' (Fowler and Harstein 1977). The last two terms were originally introduced by Mott to describe the narrow band and wide band régimes respectively. They are useful terms when describing hopping in a finite bandwidth of energies. For high temperatures (i.e. the narrow band case) preferential hops are to the nearest neighbour in real space. At lower temperatures more favoured hops are to sites close together in energy, and these are, generally speaking, not nearest neighbours. This régime may be referred to as variable range hopping.

The formulae developed in the previous sections adequately describe the transition between narrow band hopping and wide band hopping and may therefore be applied to the data of Fowler and Harstein (1977).

Firstly, let us consider the activated region (figures 4 and 6 of Fowler and Harstein). We see from eqns. (6.1.5) and (6.1.4) that a graph of $\log(\sigma)$ against $n_s^{-1/2}$ should yield a straight line from which a value of α , the decay constant, may be inferred. Figure 9 of Fowler and Harstein is such a plot. However, their expression for $s_{p\infty}$ differs from ours. They deduce $\alpha^{-1} = 1.3 \text{ nm}$, whereas, using eqn. (6.1.4) we deduce $\alpha^{-1} = 3.1 \text{ nm}$, which is considerably larger. The justification for using (6.1.4) is the agreement obtained with computer studies presented in Chapter 4. The values for the bandwidth W , obtained from eqn. (6.1.9), are approximately three times those of Fowler and Harstein who assume $W \sim \epsilon$. Consequently, their figure 8 is still valid if the ordinate is multiplied by $(.38)^{-1}$. Finally, the spatial density n_s can be inferred experimentally using substrate bias (Fowler and Harstein 1977; Harstein and Fowler 1975). Thus all the system parameters may be deduced from the activated conductivity data.

With these ideas in mind we turn our attention to figure 4 of Fowler and Harstein, where the conductivity of a sample with $n_s = 5.3 \times 10^{15} \text{ m}^{-2}$ is reported. By altering the substrate bias, the activation energy associated with nearest neighbour hopping may be varied since the substrate bias affects the bandwidth of localized states. The activation energy may be measured from the straight line section of the T^{-1} plot and a value for W , the bandwidth of localized states, deduced using eqn. (6.1.9). The only remaining parameter, g_0 , may be inferred from the infinite temperature intercept using the expression for the infinite temperature conductivity $\sigma_\infty = (g_0 \pi n_s^2 s_p^3 / 16 \alpha^4) \exp(-s_{p\infty})$. In Figure 26 we show a plot of $\log(\sigma)$ against T^{-1} . The dots are the experimental points obtained by Fowler and Harstein. The full lines are obtained from the theory using the system parameters deduced in the manner outlined above. The activation energies E_1 and E_3 are concerned with activation to the mobility edge, and nearest neighbours

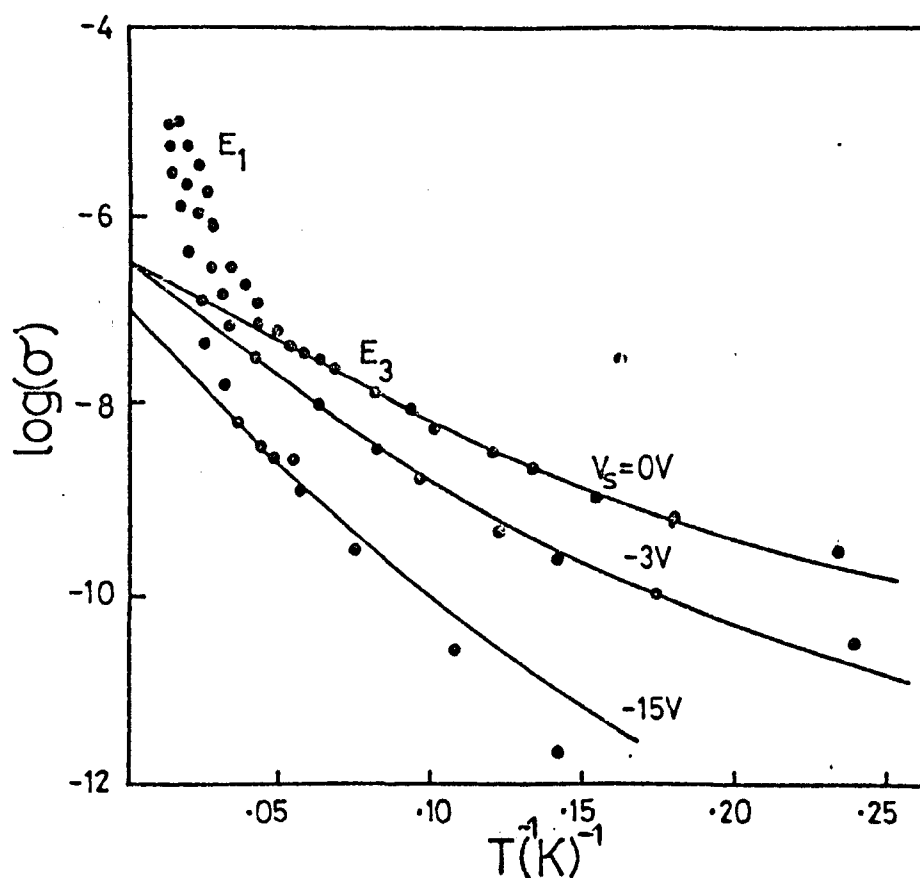


FIGURE 26 Plot of $\log(\sigma)$ against T^{-1} . The dots are the experimental points obtained by Fowler and Harstein (1977). The full lines are the theoretical curves obtained using the parameter values given in the text. V_s is the substrate bias.

hopping respectively. The bandwidths deduced from the straight line section (E_3), and using eqn. (6.1.9) are 8.7 meV, 11.8 meV and 17.1 meV for substrate bias of 0V, -3V and -15V respectively. We see that for substrate bias of 0V and -3V the behaviour of the conductivity is well fitted by the theory. However, for a substrate bias of magnitude 15V the theory predicts a $T^{-1/3}$ temperature dependence (due to the large bandwidth) whereas the observed temperature dependence appears to be closer to T^{-1} . This point is discussed below.

§6.3 Discussion

The main objective of the work described in this chapter has been to develop formulae which describe hopping conductivity in a two-dimensional band of states whose width is in the order of $s_p k_B T$ (the characteristic energy in the equivalent random resistance network). Impurity bands in inversion layers provide an easily controlled system against which to test the theoretical predictions. We see from Figure 27 that the theory predicts the behaviour of the conductivity quite accurately for low values of substrate bias (0 and -3 volts). For these two values the theoretical conductivities in the lowest temperature region appear to be slightly smaller than those observed experimentally. It is convenient to write the exponential part of the conductivity in this region in the form $\exp\left[-(T_0/T)^{1/3}\right]$. This discrepancy would then imply that our theoretical values for T_0 (2.5×10^4 K and 2.0×10^4 K) are slightly larger than the experimental values. Data on the conductivity of a single sample over a large temperature range would be helpful in comparing theoretical and experimental values of T_0 . The predicted transition temperatures of 7.5 K and 10 K for the two highest conductivity samples are in excellent agreement with those observed experimentally.

For a substrate bias of -15V the agreement is not good. The bandwidth deduced from the straight line section of the T^{-1} plot is

so large that the theory leads us to expect $T^{-1/3}$ variable range hopping over the whole of the low temperature régime. This lack of agreement may be due to a variety of factors. For large bandwidths our assumption of a rectangular band of states is not a good one. The quantitative changes that occur if a more realistic density of states profile is adopted may be calculated numerically. Furthermore, the effect of large substrate bias is to force the electrons closer to the Na^+ ions. One might then expect neighbouring states to have correlated energies and the theory developed here must be modified to take this into account.

The values of g_0 , deduced from the infinite temperature intercept, are 20 mS for the lowest two values of substrate bias and 6.7 mS for a substrate bias of -15 V. By using the expression $g_0 = e^2 \beta R_0$ we may readily obtain a value for the characteristic hopping rate R_0 . Over the temperature range of interest, $R_0 \sim 10^{13}$ Hz, which is in the order of that expected. A theoretical estimate of g_0 is possible by using eqn. (4.3.1). Using parameter values appropriate to n-type Si, namely $\epsilon = 11.7$, $E_1 = 6$ eV, $n = 6$, $\rho_0 = 2.33 \text{ gm cm}^{-3}$, $V_s = 9.0 \times 10^3 \text{ ms}^{-1}$, $\nu = 3/2$, $\eta = 3.8$, we obtain $g_0 = 0.6 \text{ mS}$ when $\alpha^{-1} = 31 \text{ \AA}$. This value is over an order below the experimental figure. A calculation of the transition rates between impurity states in inversion layers with due regard to the nature of the wavefunctions, dielectric effects of the SiO_2 layer, surface effects etc. would be very valuable in this context.

CHAPTER 7 - REVIEW OF ALTERNATIVE FORMULAE

§7.1 Introduction

In this section we review briefly alternative formulae for the dc conductivity derived in a variety of ways. Fundamentally, we may identify three main types of theory: single hop theories, those based on percolation arguments and those derived numerically. Single hop theories rely on the derivation of some particular average quantity related to a single hop. They are in principle open to the same criticism, namely, that the derivation of the dc conductivity relies on solving the problem of a random walk on a random lattice, and it is a feature of this type of problem that the solution cannot be expressed in terms of any quantity related to a single hop (Butcher 1976a, b). Formulae developed using percolation theory appear to have a more secure basis, but the uncertainty involved in determining the numerical coefficient involved in s_p , and the entire functional dependence of the prefactor, seems fundamental to any discussion of these theories. Finally, the numerical work has a variety of uses: the determination of parameters such as N_p , the derivation of functional dependencies such as the temperature dependence of the prefactor and investigations of the validity of analytical formulae. Sections 7.2 and 7.3 deal with alternative formulae for the exponent and prefactor respectively.

§7.2 Alternative Theories for the Exponent

Perhaps one of the best known examples of formulae which depend on the single hop approach is that due to Mott (1969), in which he originally predicted the $T^{\frac{1}{4}}$ law found in many materials. Mott uses the exponent $s = 2\alpha r + \beta\Delta$, where $\Delta \equiv |E_m - E_n|$. This exponent is minimized subject to the constraint $4\pi r^3 \rho_F \Delta / 3 = 1$. The minimum value

of s is

$$s_m = [(8\alpha)^3 / 9\pi\rho_F k_B T]^{1/4} \quad (7.2.1)$$

We may readily find s_p , in the manner shown in previous chapters, when $s = 2\alpha r + \beta\Delta$. In this case $s_p = [12N_p \alpha^3 / \pi\rho_F k_B T]^{1/4}$ which reduces to s_m if we put $N_p = 128/27$ (c.f. the value 2.1 which we use). The reasons for choosing this value for N_p have been outlined by Butcher (1976a). It arises because Mott's derivation of the exponent s_m is an approximate method of completing the integrals involved in the calculation of s_p .

The work of Scher and Lax (1973) may also be classified under the heading of single hop theories. Their analysis is quite general and the resultant formulae describe the frequency dependent conductivity as well as the dc case. Their model consists of a regular array of sites in which the probability of a hop between any two sites at time t after entering the first site, is specified by a waiting time distribution. The calculation is involved but a few points can be made. Butcher (1974) has shown that the same results can be obtained by considering a random array of sites and performing an approximate summation of the Dyson expansion for G_{mm} involved in eqn. (2.3.3), involving only the self-avoiding walks. Moreover, the approximate treatment provides the exact solution of a different problem. It yields the exact value of $\sigma(\omega)$ for a system such that the electron performs a random walk in which each site, other than the one currently occupied, is re-randomized immediately after every hop. The effect of this re-randomization is obviously large in certain situations, in particular, the dc limit. In the fixed site model, difficult hops can be avoided by considering other paths in the system (an argument which is the basis of the percolation solutions discussed in this work). In the Scher and Lax model, however, the particle has to make a difficult jump sooner or later, and the contribution of these types of transition

to $\sigma(\omega)$ is significant. They therefore predict a value for $\sigma(0)$ which is different from that given in previous chapters. These criticisms are similar to those raised by most authors about the work of Miller and Abrahams (1960), who calculate the resistance of the RRNM using non-percolative arguments (Shklovskii 1973). Indeed, there is a close similarity between the site density dependence of the exponent in the narrow band model predicted by both Scher and Lax, and Miller and Abrahams.

The fact that the dc conductivity may be written as $\sigma = \sigma_0 \exp[-s_p]$ is deducible from experimental data. There have been many theoretical derivations of s_p which rely on percolation theory (Ambegaokar et al 1971, Pollak 1972, Shklovskii 1973, Shante 1978). All the methods of approach are very similar to that outlined in previous chapters, with the exception of Pollak (1972) who uses a different averaging procedure to determine the number of bonds with $s < s_p$ at each site.

If we define the quantity

$$N(\epsilon_m, s_p) = \int_{s < s_p} \rho(\epsilon_n) d\epsilon_n \quad (7.2.2)$$

then we may rewrite eqns. (3.3.1) and (3.3.2) as

$$2B = \int \rho(\epsilon_m) N(\epsilon_m, s_p) d\epsilon_m \int 4\pi r^2 dr \quad (7.2.3)$$

and

$$S = N(\epsilon_m, s_p) \quad (7.2.4)$$

In contrast Pollak writes

$$2B^P = \int \rho(\epsilon_m) d\epsilon_m \int \rho(\epsilon_n) N(\epsilon_m, s_p) d\epsilon_n \int 4\pi r^2 dr \quad (7.2.5)$$

$$S^P = \int \rho(\epsilon_m) N(\epsilon_m, s_p) d\epsilon_m \int 4\pi r^2 dr \quad (7.2.6)$$

This more complicated weighting factor does not alter s_p qualitatively. Indeed, the change in the numerical coefficients involved is quite small and can be removed by altering the parameter N_p slightly. We conclude that all the percolation approaches give the same functional dependence for s_p , the only differences arising from numerical factors.

§7.3 Alternative Theories for the Prefactor

The fact that the prefactor has only a quantitative effect on the conductivity has meant that it has received considerably less attention than the exponent s_p . Furthermore, the testing of theoretical predictions against experimental data is difficult for two reasons. Firstly, the dependence of the prefactor on system parameters such as the temperature is not strong compared with the exponent. Secondly, the prefactor contains scaling factors such as g_0 which rely on a precise knowledge of the electron-phonon interaction. Of course, for comparison with computer data this scaling is irrelevant, but for the application of theoretical formulae to experimental data such as that obtained from amorphous germanium, the degree of uncertainty is large.

We begin by considering the narrow band model outlined in Chapter 4. We see from eqn. (4.1.10) that, for $v = 0$, we predict $\sigma_p = (3N_p^2/8\pi)g_0\alpha(ar_p)^{-2}$, where r_p is given by eqn. (4.1.11). Kirkijarvi (1974), using information gained from computer studies of percolation in finite clusters, deduces $\sigma_p\alpha(ar_p)^{-1.6 \pm .25}$. He does not obtain any estimate of the constant of proportionality. The value 1.6 is quite close to our value. Another prefactor has recently been predicted

by Skal and Shklovskii (1975) using a numerical approach based on the theory of chain lengths in the infinite cluster involved in percolation. They obtain, for the case when $\nu = 2$,

$$\sigma_p = \frac{8}{9} \left(\frac{4\pi}{3N_p} \right)^\delta (g_o^\alpha) (\alpha r_p)^\delta \quad (7.3.1)$$

where r_p is given by (4.1.11). The value of δ lies between 0 and 0.4. The case $\delta = 0$ gives a prefactor which is independent of r_p , as is the case with our formula when $\nu = 2$ (eqn. (4.1.10)). In this case the ratio of our prefactor to that of Skal and Shklovskii is .98, a difference which is undetectable in practice. Recently Kahlert and Landwehr (1976) have analysed data obtained from studies of impurity conduction in GaAs using Skal and Shklovskii's formulae. For this material $\nu = 2$, and so for the reasons outlined above we would also obtain the very good agreement between theory and experiment reported by these authors.

There have been a number of prefactor formulae predicted for the case of degenerate hopping in wide bands. Rather than discuss each case individually, we have tabulated the results in Table 3. Here, we give the complete expression for the conductivity, together with the basic theoretical approach. Generally speaking, the prefactors differ in their dependence on R_{po} , and on a trivial numerical factor. For convenience, we reproduce our expression derived in Chapter 6 for the case when $s = 2\alpha r + \frac{\beta}{2} \left[|\epsilon_1| + |\epsilon_2| + |\epsilon_1 - \epsilon_2| \right]$. The close agreement we obtain with computer data, illustrated in Figures 15 - 18, suggests that our formulae accurately describe degenerate hopping. Furthermore, Allen and Adkins (1972) were unable to fit their data with any of the expressions reproduced here, without assuming large changes in the dielectric constant.

PREFACTOR	EXPONENT	SOURCE	BASIS
$\frac{40}{3\pi} \frac{N_p^2 g_o^\alpha}{2 s_{po}}$	s_{po}	This work	Percolation
$\frac{3}{8\pi} \frac{1}{\sqrt{20N_p}} g_o^\alpha s_{po}^2$	$.9 s_{po}$	Mott 1969	Single Hop
$\frac{3\pi^2}{4} \left(\frac{8}{9}\right)^{\frac{1}{4}} (40N_p)^{\frac{1}{4}} \frac{g_o^\alpha}{s_{po}}$	$.9 s_{po}$	Mott 1972	Single Hop
$\frac{32\pi^2}{78} (g_o^\alpha) \left(\frac{\pi}{40N_p}\right)^{\frac{1}{4}} s_{po}$	$.8 s_{po}$	Pollak 1972	Percolation
$36\pi^3 (.022) (g_o^\alpha) s_{po}^{.35}$	s_{po}	Kirkpatrick 1973	Percolation

TABLE 3 Alternative theory for degenerate hopping in very wide bands. Here $s_{po} = 2 R_{po}$ where R_{po} is given by (5.1.6).

CHAPTER 8 - AC CONDUCTIVITY

§8.1 The Pair Approximation

In this chapter we derive approximate formulae for ac conductivity due to localized electrons. As we see from eqns. (2.2.10) and (2.3.3), for any non-zero frequency, $\langle \sigma(\omega) \rangle$ may be expanded in powers of n_s , the site density. For low densities ($n_s \rightarrow 0$) the dominant term is proportional to n_s^2 . It is easy to calculate and is known as the pair approximation.

The pair approximation is obtained by selecting the contributions to the Dyson expansion (2.3.3) with $n \neq m$, in which all the intermediate sites are either n or m . Thus

$$\begin{aligned} G_{mn}^P &= G_{mm}^O R_{mn}^e (1 + q_{mn} + q_{mn}^2 \dots) G_{nn}^O \\ &= G_{mm}^O R_{mn}^e G_{nn}^O (1 - q_{mn})^{-1} \end{aligned} \quad (8.1.1)$$

where $q_{mn} = G_{nn}^O R_{nm}^e G_{mm}^O R_{mn}^e$. To order n_s^2 in the final result we may identify R_m^e and R_n^e with R_{mn}^e and R_{nm}^e respectively in evaluating (8.1.1) with the aid of (2.3.4). Thus we obtain

$$G_{mn}^P = \frac{i R_{mn}^e \tau_{mn}}{\omega (1 - i \omega \tau_{mn})} \quad (8.1.2)$$

where the relaxation time τ_{mn} is given by

$$\tau_{mn}^{-1} = R_{mn}^e + R_{nm}^e \quad (8.1.3)$$

This expression may also be derived by inverting the 2×2 matrix which results from ignoring all the other sites except n and m . (Pollak and Geballe 1961).

Substituting G_{mn}^P into eqn. (2.2.10), we obtain the formal

system averaged result

$$\langle \sigma(\omega) \rangle = \frac{1}{2} e^2 \beta \Omega^{-1} (-i\omega) \sum_{mn} \left\langle \frac{F_{mn} R_{mn}^e}{1 - i\omega \tau_{mn}} (x_n - x_m)^2 \right\rangle \quad (8.1.4)$$

For the purposes of this work we are only interested in the real part of the ac conductivity $\langle \sigma_1^P(\omega) \rangle$. Therefore,

$$\langle \sigma_1^P(\omega) \rangle = \frac{1}{2} e^2 \beta \Omega^{-1} \omega^2 \sum_{mn} \left\langle \frac{\Gamma_{mn} \tau_{mn}^2}{1 + \omega^2 \tau_{mn}^2} (x_m - x_n)^2 \right\rangle \quad (8.1.5)$$

where we have used eqn. (2.1.6). If we now suppose that the energies ϵ_1 and ϵ_2 are distributed with a probability distribution $\rho(\epsilon_1)/n_s$ and $\rho(\epsilon_2)/n_s$ respectively, and the sites are randomly distributed over a volume Ω , we may write eqn. (8.1.5) in the form

$$\langle \sigma_1^P(\omega) \rangle = \frac{2\pi}{3} e^2 \beta \omega \int \rho(\epsilon_1) d\epsilon_1 \int \rho(\epsilon_2) d\epsilon_2 \int \tau_{12} \Gamma_{12} \frac{\omega \tau_{12}}{1 + \omega^2 \tau_{12}^2} r^4 dr \quad (8.1.6)$$

We note that eqn. (8.1.6) is easily derived from consideration of the equivalent network described in Section 3.1. If we put all the conductances except g_{12} equal to zero, then we may readily find the square voltage drop across V_{12} for the isolated RC circuit. In fact $|V_{12}^2| = (\omega \tau_{12})^2 / (1 + \omega^2 \tau_{12}^2)^2$. Noting that $g_{12} = e^2 \beta \Gamma_{12}$, we see that eqn. (3.2.1) becomes identical to (8.1.6). The factor $\omega \tau (1 + \omega^2 \tau^2)^{-1}$ is peaked on the "critical ac surface" $\omega \tau = 1$. With this idea in mind we may find a simple approximation to $\langle \sigma_1(\omega) \rangle$. Consideration of the integrands involved in (8.1.6) and (3.2.1) shows that the quantity $g_{12} \langle V_{12}^2 \rangle$ has two peaks - one on the critical percolation surface and one on the critical ac surface. We therefore suppose that the total conductivity at frequency ω is given by the sum of the contributions from each peak calculated separately or

$$\sigma(\omega) = \sigma(0) + \sigma_1^P(\omega) \quad (8.1.7)$$

§8.2 Comparison with Computer Data

We are now in a position to compare the simple formulae developed in the previous section with computer generated data. The only computational work is that carried out recently by McInnes (Butcher, Hayden, McInnes, Clark 1978). He solves Kirchhoff's equations for the equivalent network given in Section 3.1 and shown in Figure 6. The model adopted is a three-dimensional energy independent case outlined in Chapter 4, with $\nu = 3/2$. The dc contribution to $\langle \sigma_1(\omega) \rangle$ is then given by (4.1.10). The pair approximation contribution is then particularly simple:

$$\langle \sigma_1(\omega) \rangle = \frac{2\pi e^2}{3} \beta n_s^2 \int_0^{\omega\tau_{12}} \frac{\Gamma_{12}}{\Gamma_{12}} \frac{\omega\tau_{12}}{1 + \omega^2\tau_{12}^2} r^4 dr \quad (8.2.1)$$

The evaluation of the final integral in (8.2.1) is best performed numerically.

The comparison with the computer data is shown in Figure 27. The dots are the computational points. The full line is $\langle \sigma_1(\omega) \rangle$ calculated using eqns. (8.1.7), (4.1.10) and (8.2.1). The dotted lines are the ac and dc asymptotes. We see that the simple formulae are in good agreement with the computer points for all frequencies. The total span in conductivity is three orders, as one would expect for a value of $\alpha n_s^{-1/3} = 9$ from inspection of Figure 9. It would be helpful to have computational data for a lower density system, where the span in conductivity is greater, but unfortunately the convergence in the iterative procedure used to solve Kirchhoff's equations becomes too slow.

§8.3 Conductivity of Degenerate Systems

The comparison with computer data presented in the previous

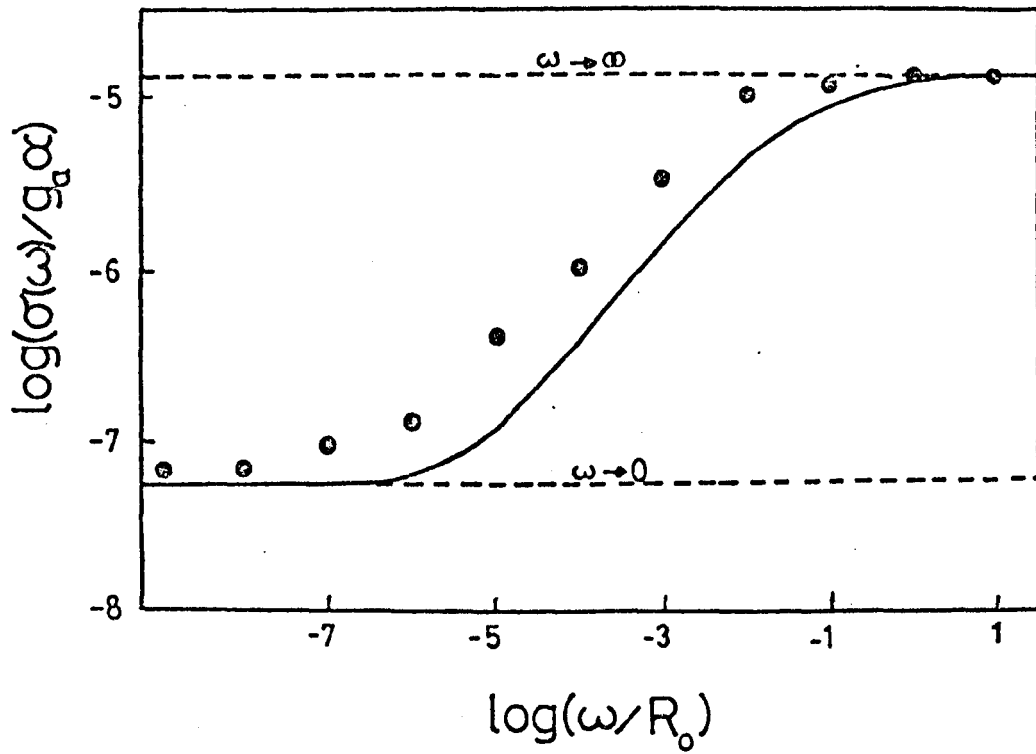


FIGURE 27 Plot of $\log (\sigma(\omega) / g_0 \alpha)$ against $\log (\omega / R_0)$. The dots are the computational points obtained by the solution of Kirchhoff's equations. The full line is the analytical curve obtained from (8.1.7), (4.1.10) and (8.2.1). The higher and lower dotted lines are the $\sigma(\infty)$ and $\sigma(0)$ asymptotes respectively.

section shows that our approximations to $\sigma(\omega)$ are valid for the simple case where all the energies of the sites are identical. We now wish to calculate the ac conductivity of a more realistic system, namely that of a degenerate system of localized electrons whose energies are distributed over a very large bandwidth. The model we shall adopt is that outlined in Chapter 5. Since we shall be interested in analysing amorphous germanium data we put $v = 2$. To evaluate the pair contribution to $\langle \sigma_1(\omega) \rangle$ we approximate the factor $\omega\tau(1 + \omega^2\tau^2)^{-1}$ in (8.1.6) by $(\pi/4\alpha)\delta(r - r_\omega)$ where r_ω is the solution of the equation $\omega\tau_{12} = 1$ for r . Using eqns. (2.1.6) and (8.1.3) we may therefore write (8.1.6) as

$$\langle \sigma_1^p(\omega) \rangle = \frac{\pi^2}{6\alpha^5} e^{2\beta\omega} \int \rho(\epsilon_1) d\epsilon_1 \int \rho(\epsilon_2) d\epsilon_2 F(\epsilon_1, \epsilon_2) R_\omega^4 \quad (8.3.1)$$

where $R_\omega = \alpha r_\omega$ and $F(\epsilon_1, \epsilon_2) = [F_1^{-1} + F_2^{-1}] = .25 \left[\cosh^2 \frac{\beta\epsilon_1}{2} + \cosh^2 \frac{\beta\epsilon_2}{2} \right]$. In (8.3.1) R_ω^4 is slowly varying in comparison with $F(\epsilon_1, \epsilon_2)$. We can therefore set $\epsilon_1 = \epsilon_2 = 0$ in R_ω and take it outside the integral.

Thus we obtain the Austin-Mott formula for the present model:

$$\langle \sigma_1^p(\omega) \rangle = (\pi^2 k_B T \rho_F^2 / 6\alpha^5) I \omega (R_\omega^0)^4 \quad (8.3.2)$$

where we have put $\rho(\epsilon)$ equal to a constant value ρ_F and

$$I = \left[e^{2\beta(k_B T)} \right]^{-1} \int d\epsilon_1 \int d\epsilon_2 F(\epsilon_1, \epsilon_2) = 3.66 \quad (8.3.3)$$

In eqn. (8.3.2) R_ω^0 denotes the value of R_ω when $\epsilon_1 = \epsilon_2 = 0$. It is obtained from the equation $\omega\tau = 1$, namely

$$\frac{\omega}{2R_\omega^0} = (R_\omega^0)^2 \exp(-2R_\omega^0) \quad (8.3.4)$$

It is convenient to write (8.3.2) in terms of the quantity

$$R_{po} = \left[5N_p \alpha^3 / 2\pi \rho_F k_B T \right]^{\frac{1}{4}}, \text{ whose significance is outlined in Chapter}$$

5. Then

$$\frac{\langle \sigma_1^P(\omega) \rangle}{\sigma_c} = \frac{5\pi}{2} I (R_\omega^0)^4 \left(\frac{\omega}{2R_o} \right) \frac{1}{R_{po}^8} \quad (8.3.5)$$

We see that $\langle \sigma_1^P(\omega) \rangle / \sigma_c$ has the same R_{po} dependence as $\langle \sigma(\infty) \rangle / \sigma_c = 10\pi^2 6! / 3.2^7 R_{po}^8$. Consequently plots of $\log(\langle \sigma_1^P(\omega) \rangle / \sigma_c)$ against R_p^0 for fixed ω have the same shape for all ω . In Figure 28 we show plots of $\log(\langle \sigma_1^P(\omega) \rangle / \sigma_c)$ against R_{po} . The dashed curve is the $\sigma(\infty)$ plot. The dotted lines are $\sigma_1^P(\omega)$ for the R_ω^0 values indicated. The corresponding values of $\omega/2R_o$ can be calculated from (8.3.4). The full line is the $\omega = 0$ line, derived in Chapter 5 (see Figure 20). We see that the ac and dc curves intersect at values of R_ω^0 such that R_ω^0 is very approximately equal to R_{po} . Thus, for fixed R_{po} , as ω increases from zero, the conductivity remains at the dc value until a frequency ω_c such that $R_{po} \sim R_\omega^0$. For frequencies in excess of ω_2 , we move vertically in Figure 28, up to the $\omega = \infty$ curve. For low densities the conductivity spans many orders (11 orders for $R_{po} = 25$). For $R_{po} = 4$ the $\omega = 0$ and $\omega = \infty$ curves touch. Thus for systems where $R_{po} < 4$ the conductivity is given by $\sigma(\infty)$ for all ω . This is the high density case discussed in Chapter 5.

§8.4 Comparison with Experimental Data

Our primary concern is with the conductivity of evaporated amorphous Germanium films which has been investigated by several authors (Gilbert and Adkins 1974; Chopra and Bahl 1970; Arizumi et al 1974; Hauser and Staudinger 1973, and Agarwal et al 1975). These authors investigate both the temperature dependence of dc conductivity and the frequency dependence of the ac conductivity. The symbols in Figure 28 indicate the extent of the dc data (for the symbol identification see Table 2 and Figure 20). From the values of g_o given in Table 2 we may deduce corresponding values for R_o using the expression $g_o = e^2 \beta R_o$. With one exception (Arizumi et al 1974) the values of R_o are in the order of 10^{16} Hz at 100 K. For a typical

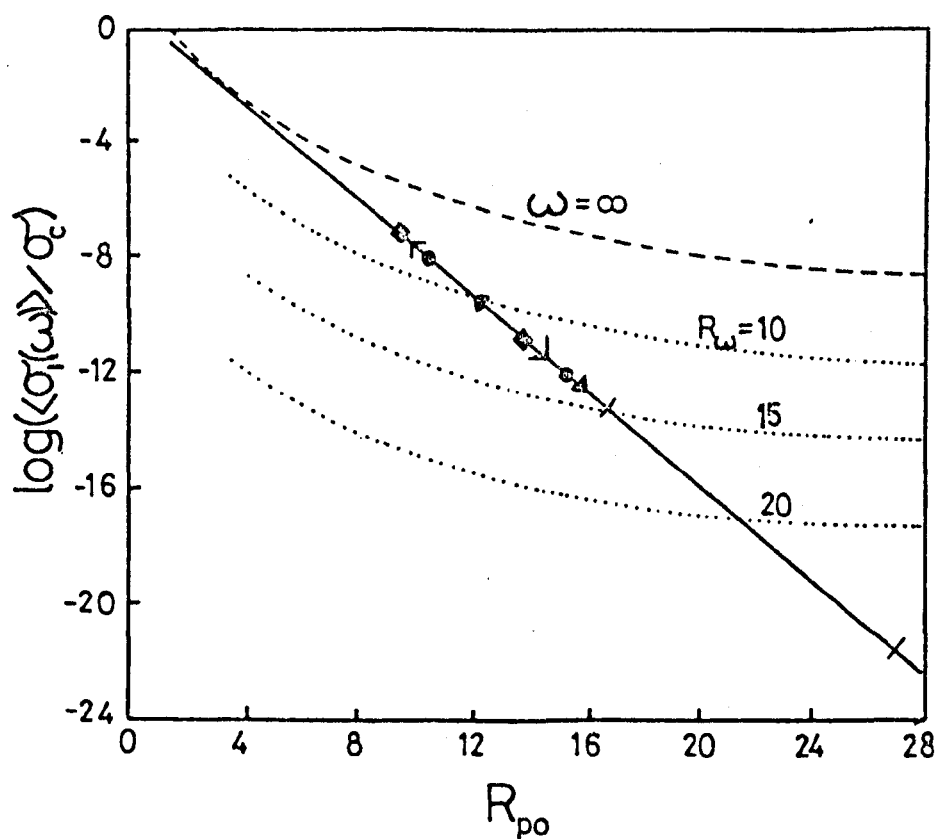


FIGURE 28 Plots of $\log (\langle \sigma_1(\omega) \rangle / \sigma_c)$ against R_{po} , where $\sigma_c = 5N_p^2 g_o \alpha / 6\pi$, $N_p = 2.1$ and $\nu = 2$. Full line: $\omega = 0$. Dashed line: $\omega = \infty$. Dotted lines: intermediate values of ω parameterised by the R_ω values indicated. The symbols on the full line indicate the extent of the dc experimental data for amorphous germanium, listed in Table 2.

frequency $\frac{\omega}{2\pi} = 10^4$ Hz we find from eqn. (8.3.3) that, for this value of R_o , $R_w \sim 17$. Hence we see from Figure 29 that most of the samples would be expected to show dc behaviour at 10^4 Hz.

The curve in Figure 29, shows $\log(\omega_c/2R_o)$ as a function of R_{po} . Data lying in the regime to the left of this line should be expected to show dc behaviour, whilst that region to the right describes the ac region. The vertical lines show the frequency range spanned by the ac data at the values of R_{po} appropriate to the different samples indicated in the legend. We see that the ac data of Chopra and Bahl, Arizumi et al and Agarwal et al lie in the regime for which dc behaviour is expected. The data of Hauser and Staudinger might be expected to show the transition from dc to ac behaviour. It appears to do so, but the ac conductivity is two orders of magnitude larger than one would expect for the values of ρ_F derived from the dc data. Finally, the data of Gilbert and Adkins should show Austin-Mott behaviour. The observed values of $\sigma_1(\omega)$ are indeed only about a factor of four larger than the predicted values. However the frequency and temperature dependence of the ac data are not consistent with the Austin-Mott formula (Gilbert and Adkins 1976).

§8.5 Discussion

The pair approximation, developed in this chapter, gives a simple form for the ac conductivity. It is, though, a low density theory. Whilst this has been recognized by many authors, no quantitative assessment of the regimes in which the Austin-Mott formula is valid has previously been made. This work is particularly useful in discussing recent arguments concerning the discrepancy between the density of states derived from the ac Austin-Mott formula and those

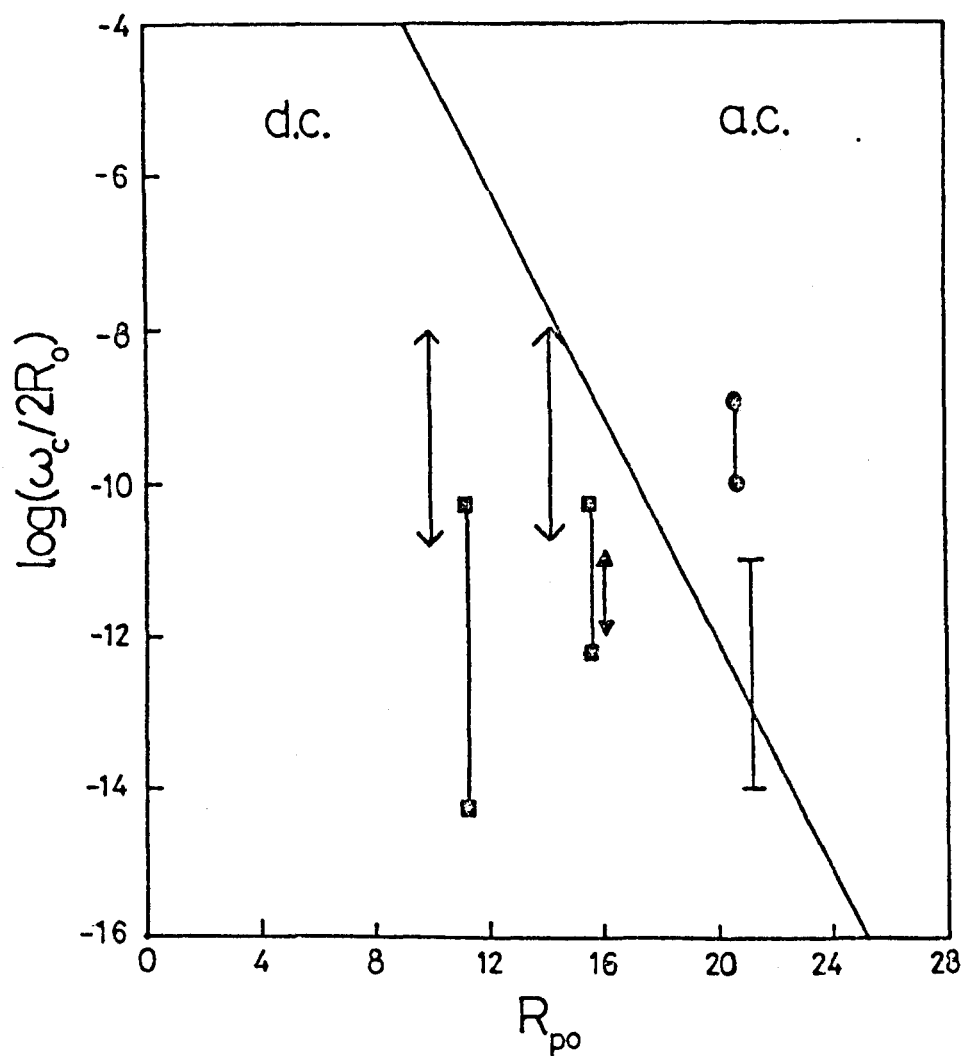


FIGURE 29 Plot of $\log (\omega_c/2R_o)$ against R_{po} (full line). The vertical lines show the span of the frequency dependent conductivity data for amorphous germanium listed in Table 2.

derived from the dc data. Abkowitz et al (1976) argue that the densities of states derived from the ac data are correct, whilst those deduced from the dc data are not. Their conclusions are based on an analysis without the benefit of the dc formula presented here. If we now consider the parameter values which they deduce from the ac data, namely, values of ρ_F 10 to 100 times larger than those found from dc data and a value of $R_0 = 10^{13}$ Hz, we find that the ac lines are put deeper into the dc region of Figure 29 because of the reduction of R_{po} . This inconsistency leads to one of two conclusions: either the pair approximation or the approximations necessarily made in deriving the formulae are in error, or the ac conductivity is due to some mechanism other than hopping near the Fermi level. The computer studies discussed in Section 8.3 show that the pair approximation gives accurate values for the ac conductivity. Although this comparison is made only for the energy independent case, our approximate treatment of the integral involved in (8.1.7) cannot be far removed from the correct answer. We have shown that for the densities involved in the experimental samples, given in Chapter 4, dc behaviour is expected for all frequencies over which the data applies. We conclude that the observed ac conductivity is due to some mechanism other than hopping near the Fermi level.

CHAPTER 9 - DISCUSSION

§9.1 Introduction

The purpose of this chapter is to discuss in some detail points raised both by this work and that of other authors in the study of conductivity of localized electrons. We begin by considering the basic formalism and then go on to discuss the percolation aspect of hopping conductivity. The comparison of the theoretical prediction with computational and experimental data is then investigated. Sections 9.6 and 9.7 deal with the transition rates and the ac conductivity respectively. Finally, in Sections 9.8 and 9.9 we discuss future work and state our conclusions concerning the work presented in the thesis as a whole.

§9.2 Basic Formalisms

As mentioned in Chapter 2, we introduce the rate equations in an intuitive manner. Recently, various authors, notably Capek (Capek 1972, 1973 and 1975; Capek, Koc and Zamek 1973) have challenged the validity of the rate equations. Our formulae for $\sigma_1(\infty)$, given in Section 3.4 are identical to the formulae for $\sigma_1(0)$ developed by Capek using a Green function formalism. Barker (1976) has shown that the above authors obtain this result because they neglect an infinite series of terms in the perturbation expansions. In Barker's treatment these terms are retained, the rate equation formalism is regained and $\sigma_1(0) \neq \sigma_1(\infty)$. Computer studies, presented in Chapters 4 and 5, show that our approximate formulae give good agreement with values of the conductivity deduced directly from the rate equations. Furthermore, our agreement with experimental data shows that the formulae accurately describe the hopping conduction process. We conclude from these observations that the rate equations provide a good description of the hopping process.

Our solution of the rate equations by the formal matrix approach is probably the most succinct for ac conductivity calculations. Its failure in the dc case is unfortunate. As we point out, it predicts a zero conductivity for any finite sized system. We have, in fact, solved the long time behaviour of the hopping system, but our choice of boundary conditions means we only predict the steady state polarization of the medium. By extending the system to infinite size, the boundary conditions become immaterial and a dc solution can be found. Unfortunately, this solution relies on a bridging theory since evaluating the infinite summations involved in G_{mn} becomes impossible.

§9.3 The Equivalent Network and Percolation

The equivalent network approach to the solution of the rate equations has a venerable history. This approach was originally introduced by Miller and Abrahams (1960). The transition from a microscopic to a macroscopic point of view is a useful one in that it allows one to view each conductance as being embedded in an assembly of surrounding conductances. One is, therefore, led to concentrate on the properties of the system as a whole. This leads quite naturally to a percolation argument, in contrast to single hop theories which are concerned with individual transitions. As outlined in Chapter 3, consideration of the power dissipated in each conductance leads to a percolation solution of the integral (3.2.1). It should be emphasised that in the actual hopping system, the electrons are not percolating, we merely use percolation theory to solve the equivalent conductance problem.

Fundamental to percolation theory are dimensional invariants such as N_p . Strictly speaking, although the primary dependence of N_p

is on the dimensionality of the percolation system, there is some residual dependence on the shape of the constant s surfaces in the percolation space. If we consider the r -percolation system where $s = 2\alpha r$, constant s surfaces are circles or spheres in two or three dimensions respectively. The values of N_p deduced by various authors (Seager and Pike 1974; Kirkijarvi 1974) using expanding circles or spheres are, therefore, the best ones to use in these hopping systems. If we now consider the more complicated energy dependent case, where $s = 2\alpha r + \frac{\beta}{2} [|\epsilon_1| + |\epsilon_2| + |\epsilon_1 - \epsilon_2|]$, the constant s surfaces are cylinders with cones at each end which we shall refer to as "bobs" (Seager and Pike 1974). One should therefore expand the bobs in the percolation space and determine a critical value such that infinite chains can be found.

Replacing the bobs by spheres or hyperspheres provides an approximate method of evaluating N_p . However, it conceals a very important concept. Consider a two-dimensional energy dependent system. The percolation space is defined by the vectors x_i , y_i and ϵ_i of the site i . Now consider Figure 31, where we have drawn just the (ϵ_i, x_i) -plane of the percolation space and for clarity have omitted any site for which y_i is non-zero. The equal s figures are drawn for the case of spheres (a) and the more accurate case (b) where s is given by $s = 2\alpha r + \frac{\beta}{2} [|\epsilon_i| + |\epsilon_j| + |\epsilon_i - \epsilon_j|]$. In the first case the volume enclosed by the constant s surface is the same for all ϵ_i . In the second case the volume goes to zero at $\beta\epsilon_i = s_0$. In fact, the volume enclosed by the shell about i is given by $V_i = V_0 [2 - 3x + x^3]$ where V_0 is a constant and $x = \epsilon_i / s_0 k_B T$. Sites with large energies, therefore, are unlikely to be in the percolation chain. This is exactly the behaviour found experimentally (see Chapter 6). One still obtains wide-band results even when $s_p k_B T$ lies well outside the energy band.

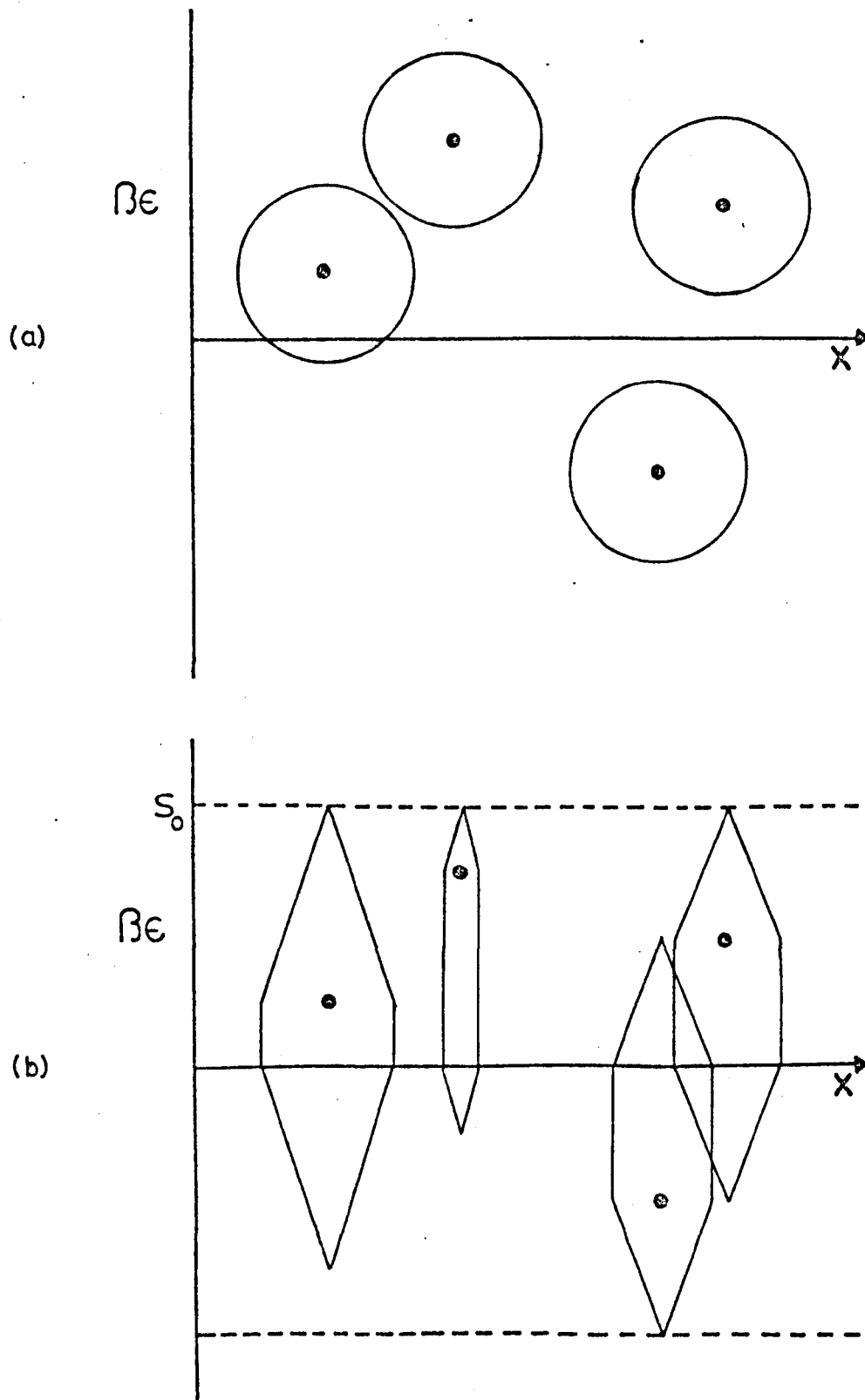


FIGURE 30 Schematic diagram of the constant s surfaces in the percolation space. Figure 30(a) shows the case when the constant s surfaces are approximated by spheres or circles and 30(b) shows the more accurate case when the constant s surfaces are "bobs".

This point was first raised by Pollak (1972) on dimensional grounds. It is worth emphasising, however, that the above argument relates to the percolation system, not to the real hopping system. In the actual hopping system large energy sites have less weight for the following reason. Consider an electron at site i , with other sites distributed around it. Many of the surrounding sites lie at approximately the same distance from site i . The electron will, therefore, be able to select a site whose energy minimizes s . Sites j with large energies do not count significantly since one has every chance of finding another site, whose distance from i is approximately the same as site j but whose energy is such that the electron will preferentially hop to this site rather than site j .

The effect of a bandwidth restriction is to limit the energy dimension in the percolation space. As pointed out above this makes little difference until $s_p k_B T$ is very much larger than the bandwidth. It would be very useful to test the ansatz regarding the temperature dependence of N_p (see Chapter 6) computationally. One may be able to do this by expanding the bobs as outlined above, but truncating any part which lies outside the permitted energy range. By applying the normal criterion for the determination of the percolation threshold, the dependence of N_p on the bandwidth and temperature could then be deduced.

§9.4 Comparison with Computer Data

The comparison of our analytical formulae with computer generated data shows that the approximate derivation of the formula from the rate equations is valid. The main criticism of this computer data is that the model system size is far from being infinite. The largest number of sites which can be handled is about 2000. For a three-dimensional system this necessarily means about

30% of the sites are on the surface and are therefore "anomalous". Attempts to remove surface effects by periodic repetition and other techniques do not alter the observed conductivity significantly. Indeed, increasing the number of sites from 200 to 2000 also has little effect on the conductivity of the system. We conclude that the number of surface sites is not significant and that systems with in excess of 1000 sites adequately model an infinite array of sites.

This lack of dependence on the number of surface sites may be readily understood in a semi-quantitative way. Consider an array of sites such that approximately 30% lies on the surface. This necessarily means we have "omitted" about 15% of the conductances which should connect this cluster to the infinite system. Furthermore, only about 10% of all the conductances in the network are of order $g_0 \exp[-s_p]$ and hence contributed significantly to $\langle \sigma \rangle$ (Shklovskii 1973; Pollak 1972). The effect of the surface sites is to remove about 1½% of the conductances which contributed to $\langle \sigma \rangle$. This effect is of the same order as that observed by increasing the number of sites from 200 to 2000.

§9.5 Interpretation of Experimental Data

In applying our formulae to the interpretation of experimental data a number of problems arise. The case of impurity conduction in crystalline semiconductors is the easiest to discuss. The Miller and Abrahams (MA) rates which we use were specifically calculated for this case. More recent calculations concerning multi-phonon effects, notably by Emin (1974), have shown that in this system the MA rates are valid. All the variable parameters, ν , ρ_F , α , and g_0 are well defined. The good agreement obtained with the data of Allen and Adkins is therefore to be expected.

Our analysis of impurity conduction in amorphous silicon does not have such a firm basis. As in all the interpretations of amorphous data,

we put $\nu = 2$ since this value arises naturally from consideration of the integral involved in calculating the overlap of the localized wave functions. Deviations from this value arise from the ellipticity of the constant k surfaces in the conduction band minima (Miller and Abrahams 1960). These concepts are ill-defined in the amorphous case and so we keep ν equal to two.

The system about which we know least is amorphous germanium. In that case a number of model approximations are necessary in the derivation of the basic formulae. We assume that the transition rate can be written in the MA form given in eqn. (4.1.1). The quantity R_0 is a variable parameter since we have no detailed knowledge of the electron-phonon interaction in these materials. We also assume that α is a constant independent of the energy of the state. Many authors have argued that this is not possible since $\alpha = 0$ at the mobility edge i.e. at an energy E_m (Abraham and Edwards 1972; Pollit 1976). These authors assume α is proportional to $(E - E_m)^n$, where $n \leq 1$. The effect of allowing an energy dependence for α could be calculated using the basic equations outlined in this work. For low temperatures, the effect should be small since the quantity $(E - E_m)$ will not vary significantly over the energy range of interest. Also, the power law dependence is much slower than the dominant exponential character of the important quantities arising in the integrands, which may justify our approximating α by a constant.

§9.6 The Transition Rates

Our approximate formula for the transition rates is open to severe criticism in amorphous semiconductors. Emin (1974) has calculated the rates for a more general case. He argues that multi-phonon contributions are significant for the temperatures at which the experiments on amorphous

materials are conducted (70 K to 300 K). It is, however, difficult to see how the $T^{\frac{1}{4}}$ law may be derived if the rates differ significantly from the MA form. It is not possible to obtain simple analytical formulae for the Emin type rates. However, Emin has shown the temperature dependence of the rates, computed numerically (Emin 1974). He argues that the $T^{\frac{1}{4}}$ law may follow directly from the fact that, under certain conditions, the logarithms of the rates themselves are proportional to $T^{\frac{1}{4}}$. This argument makes no appeal to the percolation aspect of hopping. If Emin's rates are correct, then the observed behaviour is due to a combination of the intrinsic temperature dependence of the rates and the effects discussed here.

The interpretation of some of the quantities arising in the MA rates needs revising in the case of disordered semiconductors. The energy difference $\Delta \equiv |\epsilon_i - \epsilon_j|$ which arises in these rates is usually interpreted as the energy associated with a single phonon, which gives rise to the transition. In our analysis the largest energy which enters into the calculation is $s_p k_B T$ although, as we point out above, the important energies are about $s_p k_B T/5$. For liquid helium temperatures (i.e. impurity conduction in crystalline semiconductors) this energy is less than the maximum phonon energy $\hbar\omega_{\max}$. There is, therefore, no effect when one introduces a realistic cut-off in the value of Δ . In the case of amorphous semiconductors, however, the value of $s_p k_B T/5$ is much greater than $\hbar\omega_{\max}$. We, therefore, have to discuss the effect of introducing a maximum value for Δ into the calculations. The effect is similar to that due to the bandwidth restriction described in Chapter 6. However, in this case, the permitted energy area in the (ϵ_1, ϵ_2) -plane has diagonal form running from lower left to upper right of this plane. The intercepts on the $\epsilon_1 = 0$ line are $\epsilon_2 = \pm W$, where $W \equiv \hbar\omega_{\max}$. Thus $A(q)$, for $q > W$, becomes the area of a rectangle lying

at 45° to the $\epsilon_1 = 0$ axis with isosceles triangles at each end. Preliminary investigations show that adopting this form for $A(q)$ leads to deviations from the $T^{\frac{1}{4}}$ law for parameter values appropriate to amorphous semiconductors. Our derivation of the basic formulae describing degenerate hopping in these systems must, therefore, rely on some other interpretation of the energy difference Δ . Whilst firm conclusions must await a detailed analytical calculation of the transition rates, we may tentatively suggest that for amorphous semiconductors, Δ should be associated with an energy difference arising from multiphonon contributions rather than single phonon processes.

Finally, we wish to discuss the parameter R_0 . We see from eqns. (4.1.3) and (4.3.1) that for n-type crystalline germanium g_0 is independent of T , whilst R_0 is proportional to T . We have assumed that this is so for all the systems we have investigated. Most authors quote the characteristic hopping frequency R_0 instead of g_0 . In fact $R_0 = 5.4 \times 10^{11} T$ H when $g_0 = 1$ mS. It follows from Table 2 that $R_0 \sim 10^{11}$ Hz for n-type crystalline germanium. For the n-channel and p-channel devices, the inversion layer experiments show $R_0 \sim 10^{12}$ Hz and 10^9 Hz respectively for tail state hopping. For impurity conduction in the n-channel device $R_0 \sim 10^{13}$ Hz. Finally, the values for R_0 obtained from Table 2 for amorphous germanium imply that $R_0 \sim 10^{15} \rightarrow 10^{16}$ Hz for $T \sim 100$ K. This last value may seem high because it is often assumed that R_0 is in the order of a typical phonon frequency ν_{ph} (see, for example, Mott and Davis 1971). There seems little reason to suppose that this is generally valid. The assumption that $R_0 \sim \nu_{ph}$ arises from the observation that R_0 is of the order of the maximum possible hopping rate permitted in the theory which cannot be greater than ν_{ph} . However, the hops which are significant in determining $\langle \sigma \rangle$ are those between

sites having energy values and intersite separations in the immediate neighbourhood of the critical percolation surface and these proceed at a rate many orders of magnitude below R_0 . Thus while the model formally allows hop rates of the order 10^{15} Hz in amorphous germanium, they do not affect the calculated values of the conductivity.

We see that to obtain rates in the order of R_0 , the sites i and j must have $\epsilon_i \approx \epsilon_j$ and very small intersite separation r_{12} . This second criterion totally invalidates the MA calculation, which assumes large site separations. Furthermore the MA rates rely on the energy difference arising primarily through the random potential fluctuation. For small r , this will not be the case because the resonance energy becomes large. In Appendix 3 we calculate the transition rates for all values of the parameter Δ/W . The results, shown in Figure 32, indicate that all transitions occur at rates many orders below R_0 . Thus the value of the parameter $R_0 = 10^{15}$ which arises as a consequence of our model in amorphous germanium does not signify the maximum hopping rate possible in such a system.

§9.7 The AC Conductivity

The pair approximation given in Chapter 8 is fundamental to the study of $\langle \sigma_1(\omega) \rangle$. It is exact for $\omega \rightarrow \infty$ and for $n_s \rightarrow 0$. It has long been recognized in the literature that the pair approximation is a low density formula, but there has been no attempt to quantify what is meant by "low density". We see that only sites a distance R_ω apart contribute to $\langle \sigma_1(\omega) \rangle$. The pair approximation is only valid if $R_\omega < \alpha n_s^{-1/3}$. When R_ω approaches the average intersite separation (i.e. as $\omega \rightarrow 0$), contributions from clusters of three and four sites and so on, become important. However, the transition to dc behaviour is rather rapid since R_p is also in the order of the average intersite

separation. We would, therefore, expect the transition from a regime where the pair approximation is valid, to one where the dc formulae are applicable to be rapid. It is for this reason we feel secure in writing $\sigma = \sigma_1(0) + \sigma_1^p(\omega)$. We wish to emphasise the point made in Chapter 8 concerning the inconsistency between the ac and dc data obtained from studies in amorphous germanium. The observed ac behaviour occurs at a frequency such that $R_\omega > R_p$, which is somewhat unphysical. We would expect the dc-ac transition at a much higher frequency.

The general shape of the $\sigma(\omega)$ versus ω curve, shown in Figure 27, has two "shoulders" at frequencies ω_1 and ω_2 where $\omega_1 < \omega_2$. We would expect the first shoulder to occur at a frequency ω_1 such that $R_p \approx R_\omega$ i.e. $\omega_1 \approx R_0 \exp[-R_p]$. The second shoulder should occur at $\omega_2 \approx R_0$. The frequency ω_1 is higher than that observed experimentally, whilst no studies have shown saturation. As pointed out in Chapter 8, reducing R_0 does not remove the inconsistency, since using the values of ρ_F deduced from the ac data, also reduces R_p .

We are therefore led to the following conclusions. Firstly, a more detailed treatment of ac conductivity is needed. Secondly, the observed ac conductivity in amorphous germanium, described in Chapter 8, cannot be interpreted on the basis of the Austin-Mott formula. The experimental densities are such that we predict dc behaviour in a regime where ac behaviour is observed. This observed conductivity must therefore be attributed to some process other than the simple Fermi level hopping described by the Austin-Mott formula.

§9.8 Future Work

There are a number of outstanding problems basic to transport processes in systems of localised states. The development necessary in order to acquire a deep understanding of the physical processes

involved is daunting. Here, we shall merely list some areas of interest.

An understanding of the role of the structure of materials on the electron statistics is fundamental (for example, in studies of the Hubbard energy and double occupancy). The electron statistics in turn have a great effect on transport properties such as the electrical conductivity. It would therefore be of great interest to perform a more general analysis concerning different site location and energy statistics.

The introduction of more realistic density of states profiles should also receive attention. This is particularly true in the case of inversion layer studies, where the variable Fermi level is a powerful tool. Combined with a realistic density of states calculation, it should enable one to study the relevant strengths of the different transport processes, such as hopping and activation to the mobility edge, which occur in these devices.

Fundamental to the study of hopping conduction are the transition rates. For the case of impurity conduction in n-type crystalline semiconductors the rates of Miller and Abrahams (1960) are applicable. In all other cases studied in this work, the rates are introduced in a somewhat ad hoc manner. A study of the transition rates in disordered materials, inversion layers and p-type semiconductors would be invaluable in this context. Presumably such a calculation would remove such worrying features as the large energy differences and R_0 values obtained from the studies of amorphous germanium reported here. As emphasised earlier, the ac conductivity should be reviewed in an attempt to remove the inconsistencies which arise in the study of the ac and dc data obtained from a variety of materials.

Transport coefficients other than the conductivity should receive attention. Notable amongst these are the Hall constant and the thermopower, both of which are very poorly understood.

§9.9 Conclusion

We conclude that this work develops the simple hopping theory, which adequately describes experimental data obtained from a variety of systems, notably impurity conduction in crystalline and amorphous semiconductors, hopping conductivity in inversion layers, and the basic conduction process in amorphous semiconductors. Various problems have been isolated, which relate to the model adopted rather than any approximations inherent in the deduction of the analytical formulae. It is hoped that future work will lead to considerations of other transport coefficients and more physically meaningful models.

References

- ABKOWITZ M, LE COMBER P G and SPEAR W E 1976 Com. on Phys. 1 175.
- ABRAM R A and EDWARDS S F 1972 J. Phys. C. 5 1183
- AGARWAL S C, GUTTA S and NARAZIMHAN K L 1975 J. Non-Crys. Sol. 18 429.
- ALLEN F R and ADKINS C J 1972 Phil. Mag. 26 1027.
- AMBEGAOKAR V, COCHRAN S and KURKIJARVI J S 1973 Phys. Rev. B8 3682.
- AMBEGAOKAR V, HALPERIN B I and LANGER J S 1971 Phys. Rev. B4 2612.
- ANDERSON P W 1958 Phys. Rev. 109 1492.
- ARIZUMI T, YOSHIDA A, BABA T, SHIMUKAWA K and NITTA S 1974
- Tetrahedrally Bonded Amorphous Semiconductors. Eds. M H Brodsky,
S. Kirkpatrick and D. Weaire (New York, A.I.P. 1974) 363.
- ATKINS K R, DONOVAN R and WALMSEY R H, 1960 Phys. Rev. 118 411.
- AUSTIN I G and MOTT N F 1969 Adv. in Phys. 18 41.
- BARKER J R 1977 J. Phys. C. 9 4397.
- BLAKEMORE J S 1962 Semiconductor Statistics (Oxford - Pergamon Press).
- BRENIG W, DOHLER G and WOLFE P 1971 Z. Phys. 246 1.
- BUTCHER P N 1972 J. Phys. C: Solid St. Phys. 5 1817.
- BUTCHER P N 1973 J. Phys. C: Solid St. Phys. 6 2147.
- BUTCHER P N 1974 J. Phys. C: Solid St. Phys. 7 2645.
- BUTCHER P N 1976a Linear and Nonlinear Electronic Transport in Solids.
Eds. J T DeVreese and V E van Doren (New York: Plenum Press) 341-381.
- BUTCHER P N 1976b Proc. Sixth Int. Conf. on Amorphous and Liquid Semiconductors.
Ed. Kolomiets (Leningrad: Nauka) 89-94.
- BUTCHER P N, CLARK J D, HAYDEN K J and McINNES J A 1978. To be published
in the Proc. of the 14th Int. Conf. on the Physics of Semiconductors.
- BUTCHER P N and HAYDEN K J 1977 Proc. 7th Int. Conf. on Amorphous and
Liquid Semiconductors. Ed. W E Spear (Edinburgh: The University) 234.
- BUTCHER P N, HAYDEN K J and McINNES J A 1977 Phil. Mag. 36 19.
- BUTCHER P N and McINNES J A 1978 Phil. Mag. 37B 249.
- BUTCHER P N and MORYS P L 1973 J. Phys. C: Solid St. Phys. 6 2147.

- CAPEK V 1972 J. Phys. B22 1122.
- CAPEK V 1973 Phys. Stat. Sol. B60 K5.
- CAPEK V 1975 J. Phys. C: Solid St. Phys. 8 479.
- CAPEK V, KOC S and ZAMEK J 1975 J. Non-Cryst. Solids 18 95.
- CHOPRA K L and BAHL S K 1970 Phys. Rev. B1 3545.
- CLARK A H 1967 Phys. Rev. 154 750.
- CONWELL E M 1956 Phys. Rev. 103 51.
- COSTATO M, GAGLIANI G, JACOBINI C and REGGIANI L 1974 J. Phys. Chem. Solids 35 1605.
- DAVIS E A and DALE COMPTON W 1965 Phys. Rev. 140A 2183.
- DWIGHT H B 1969 Tables of Integrals and Other Mathematical Data. (Toronto - MacMillan).
- EMIN D 1974 Phys. Rev. Lett. 32 303.
- FOWLER A B and HARSTEIN A 1977 Proc. 2nd Int. Conf. on the Electronic Properties of Two-Dimensional Systems. Eds J F Koch and G. Landwehr (Warburg: The University) 27-42.
- FRITZSCHE H 1959 J. Phys. Chem. Solids 6 69.
- FRITZSCHE H 1960 Phys. Rev. 120 1120.
- FRITZSCHE H and CUEVAS M 1960 Phys. Rev. 119 1238.
- FRITZSCHE H and LARK-HOROWITZ K 1959 Phys. Rev. 113 999.
- GILBERT M H and ADKINS C J 1976 Phil. Mag. 34 143.
- GOLIN 1963 Phys. Rev. 132 178.
- HARSTEIN A and FOWLER A B 1975a J. Phys. C. 8 L249.
- HARSTEIN A and FOWLER A B 1975b Phys. Rev. Lett. 34 1435.
- HARSTEIN A and FOWLER A B 1976 Proc. of the 13th Int. Conf. on Phys. of Semiconductors Rome. Ed. F. Fumi 741.
- HARSTEIN A, NING T H and FOWLER A B 1975 Surface Sci. 58 178.
- HAUSER J J and STAUDINGER A 1973 Phys. Rev. B8 607.
- KAHLERT H and LANDWEHR G 1976 Z. Phys. B24 361.
- KEYES R W and SLADEK R S 1956 J. Phys. Chem. Solids 1 143.

- KIRKPATRICK S 1973 Rev. Mod. Phys. 45 574.
- KOHN W 1957 Solid State Physics. Eds. F Seitz and D Turnbull 258.
- KUBO R 1957 J. Phys. Soc. Japan 12 570.
- KURKIJARVI J 1974 Phys. Rev. B9 770.
- LE COMBER P G, JONES D I and SPEAR W Phil. Mag. 35 1173.
- MASCHKE K, OVERHOF H and THOMAS P 1974 Phys. Stat. Sol. B62 113.
- MILLER A and ABRAHAMS E 1960 Phys. Rev. 120 745.
- MOTT N F 1956 Can. J. Phys. 34 1356.
- MOTT N F 1969 Phil. Mag. 19 835.
- MOTT N F 1972 J. Non-Cryst. Solids 8-10 1.
- MOTT N F and DAVIS E A 1971 Electronic Processes in Non-Crystalline Materials. (Oxford: Clarendon Press).
- MOTT N F, PEPPER M, POLLIT S, WALLIS R H and ADKINS C J 1975 Proc. Roy. Soc. A345 169.
- McINNES J A and BUTCHER P N 1978. Submitted to Phil. Mag.
- NUNOSHITA M, ARAI J, TANEKI T and HAMAKAWA Y 1973 J. Non-Cryst Solids 12 339.
- OKAMATO H and HAMAKAWA Y 1977 Sol. State Comm. 24 23.
- PEPPER M 1977 Contemp. Phys. 18 423.
- PEPPER M, POLLIT S and ADKINS C J 1974 Phys. Letts 48A 113.
- PEPPER M, POLLIT S, ADKINS C J and OAKLEY R E 1974 Phys. Lett. 47A 71.
- PIKE G E and SEAGER C H 1974 Phys. Rev. B10 1421.
- POLLAK M 1972 J. Non-Cryst Solids 11 1.
- POLLAK M and GEBALLE T H 1961 Phys. Rev. 122 1742.
- POLLIT S 1977 Commun. Phys. 1 207.
- REGGIANI L 1976 J. Phys. Chem. Solids 37 293.
- SCHER H and LAX M 1973 Phys. Rev. B7 4491 and 4502.
- SCHRIEFFER J R 1957 Semicond. Surf. Phys. 55.
- SEAGER G E and PIKE C H 1974 Phys. Rev. B10 1435.
- SHANTE V K S 1978 Phys. Rev. B16 2597.
- SHANTE V K S and KIRKPATRICK S 1971 Adv. in Phys. 20 325.

- SHKLOVSKII B I 1973 Sov. Phys. Semicond. 6 1053.
- SKAL A S and SHKLOVSKII B I 1975 Sov. Phys. Semicond. 8 1029.
- STERN F 1972 Phys. Rev. B5 4891.
- STERN F 1974 Phys. Rev. B9 2762.
- STREET R A and MOTT N F 1975 Phys. Rev. Lett. 35 1293.
- THOULESS D J 1977 J. Phys. C. 9 L603.
- THOULESS D J and LICCIARDELLO D 1977 Comm. in Phys. 2 1459.
- WALLEY P A and JONSCHER A K 1968 Thin Solid Films 1 367.
- YOFFA E J and ADLER D Phys. Rev. B15 2311.

APPENDIX 1 EVALUATION OF THE INTEGRALS INVOLVED IN $2B$, σ_p AND
 $\langle \sigma_1(\infty) \rangle$ FOR HOPPING IN VERY WIDE BANDS

A1.1 Evaluation of the Integral Involved in $2B$

We see from (5.1.5) that

$$A'(q) = (k_B T)^2 [4 + 6q + 4 \ln q] \quad (A1.1.1)$$

Hence the integral involved in (5.1.2) is $(k_B T)^2 \alpha^{-3} J(R_p)$ with

$$J(R_p) = \int_0^{R_p} R^2 (2R - v) (4 + 6q + 4 \ln q) dR \quad (A1.1.2)$$

where $q = s_p - 2R + v \ln R$ and we have put $r'_p = 0$. We may therefore write

$$J(R_p) = J_1(R_p) + J_2(R_p) + J_3(R_p)$$

where the terms on the right are the contributions from 4, 6q and 4lnq in (A1.1.2) respectively. The evaluation of $J_1(R_p)$ is trivial:

$$J_1(R_p) = 2R_p^3 \left[R_p - \frac{2v}{3} \right] \quad (A1.1.4)$$

The evaluation of $J_2(R_p)$ is less trivial but is nevertheless elementary. When (5.1.11) is used to eliminate s_p we find that

$$J_2(R_p) = 6R_p^3 \left[\frac{1}{5} R_p^2 + \frac{1}{2} R_p (q_m - \frac{7v}{12}) + \frac{v}{3} (\frac{v}{3} - q_m) \right] \quad (A1.1.5)$$

The integral $J_3(R_p)$ cannot be evaluated by elementary methods. We therefore approximate q by $a - fR$ with a and f chosen to match the magnitude and slope of q at $R = R_p$. Hence $f = 2 - v/R_p$ and $a = q_m + fR_p$ where we have used (5.1.11). With this approximation, $J_3(R_p)$ may be evaluated by elementary (but tedious) methods. We find that

$$J_3(R_p) = 2R_p^4 \left[\ln q_m - \frac{1}{4} \right] - R_p^3 \left[\frac{4v}{3} \ln q_m \right] - 2 \left(\frac{a}{f} - \frac{2v}{3} \right) \left[\frac{1}{3} R_p^3 + \frac{1}{2} R_p^2 \frac{a}{f} + R_p \left(\frac{a}{f} \right)^2 + \left(\frac{a}{f} \right)^3 \ln \frac{q_m}{a} \right] \quad (A1.1.6)$$

For a two-dimensional system the corresponding integral is given by (A1.1.2) with

$$J_1(R_p) = \frac{8}{3} R_p^2 (R_p - \frac{3}{4}v) \quad (A1.1.7)$$

$$J_2(R_p) = 2R_p^2 \left[R_p^2 + R_p (2q_m - \frac{5}{3}v) + \frac{3}{4}v(v - 2q_m) \right] \quad (A1.1.8)$$

$$J_3(R_p) = R_p^3 \frac{8}{3} (\ln q_m - \frac{1}{3}) - R_p^2 \left[2v \ln q_m \right] + \left[R_p^2 + R_p \frac{2a}{f} + 2 \left(\frac{a}{f} \right)^2 \ln \left(\frac{q_m}{a} \right) \right] \left[v - \frac{4a}{3f} \right] \quad (A1.1.9)$$

A1.2 Evaluation of the Integral Involved in σ_p

With the aid of eqn. (A1.1.1) we see that the integral involved in (5.1.4) is $(k_B T)^2 \alpha^{-5} K(R_p)$ where

$$K(R_p) = \int_0^{R_p} R^4 (4 + 6q + 4 \ln q) dR$$

$$= K_1(R_p) + K_2(R_p) + K_3(R_p) \quad (A1.2.1)$$

where the successive terms in the second line are the contributions from 4, 6q and 4lnq in the first line. Proceeding as in A1.1 we find that

$$K_1(R_p) = \frac{4}{5} R_p^5 \quad (A1.2.2)$$

$$K_2(R_p) = \frac{2}{5} R_p^5 R_p + 3(q_m - \frac{1}{5}v) \quad (A1.2.3)$$

$$K_3(R_p) = \frac{4}{5} \left[R_p^5 \ln q_m - \left\{ \frac{1}{5} R_p^5 + \frac{1}{4} R_p^4 \frac{a}{f} + \frac{1}{3} R_p^3 \left(\frac{a}{f} \right)^2 + \frac{1}{2} R_p^2 \left(\frac{a}{f} \right)^3 + R_p \left(\frac{a}{f} \right)^4 + \left(\frac{a}{f} \right)^5 \ln \left(\frac{q_m}{a} \right) \right\} \right] \quad (A1.2.4)$$

For a two-dimensional system the corresponding integral is given by (A1.2.1) with

$$K_1(R_p) = R_p^4 \quad (A1.2.5)$$

$$K_2(R_p) = \frac{2}{5} R_p^4 \left[R_p + \frac{5}{2}(q_m - \frac{1}{4}) \right] \quad (A1.2.6)$$

$$K_3(R_p) = R_p^4 \left[\ln q_m - \frac{1}{4} \right] - \frac{a}{f} \left[\frac{1}{3} R_p^3 + \frac{1}{2} R_p^2 \frac{a}{f} + R_p \left(\frac{a}{f} \right)^2 + \left(\frac{a}{f} \right)^3 \ln \left(\frac{q_m}{a} \right) \right] \quad (A1.2.7)$$

A1.3 Evaluation of $\langle \sigma_1(\infty) \rangle$

To calculate $\langle \sigma_1(\infty) \rangle$ we set s_p equal to the minimum value of s in (3.2.5). Then the modulus sign may be removed from $|s-s_p|$ and $r_a = r$ throughout the range of integration. We assume that the density of states has a constant value ρ_F and make the changes of integration variables: $R = \alpha r$, $x = \beta \epsilon_1/2$ and $y = \beta \epsilon_2/2$. Hence, using (3.2.4), (4.1.2), (4.1.4) and (4.1.5) we obtain

$$\langle \sigma_1(\infty) \rangle = g_o \frac{2\pi}{3} \frac{(\rho_F k_B T)^2}{\alpha^5} I_1 I_2 \quad (A3.1.1)$$

where

$$I_1 = \int_0^\infty R^{4+\nu} e^{-2R} dR \quad (A3.1.2)$$

and

$$I_2 = \int_{-\infty}^\infty \int_{-\infty}^\infty \frac{(x-y) dx dy}{\cosh x \cosh y \sinh(x-y)} \quad (A3.1.3)$$

The integral I_1 is just $\Gamma(5+\nu)/2^{5+\nu}$ (Dwight 1969). To evaluate

I_2 we make the further change of variable $\xi = (x+y)$ and $\eta = x-y$.

Then we have

$$\begin{aligned} I_2 &= \frac{1}{2} \int_{-\infty}^\infty dy \frac{\eta}{\sinh \eta} \int_{-\infty}^\infty \frac{d\xi}{\cosh \xi + \cosh \eta} \\ &= \frac{1}{2} \int_{-\infty}^\infty d\eta \frac{\eta}{\sinh \eta} \cdot \frac{4\eta}{\sinh \eta} \\ &= 2\pi^2/3. \end{aligned} \quad (A3.1.4)$$

In the second line we have evaluated the elementary integral over ξ and in the last line we use the value of the remaining integral quoted by Dwight (1969).

When these results are substituted into (A3.1.1) we obtain, with the aid of eqn. (5.1.6), the result (5.3.1) for a three-dimensional system quoted in the text. The evaluation of $\langle \sigma_1(\infty) \rangle$ for a two-dimensional system proceeds in an almost identical way and yields eqn. (5.4.1).

APPENDIX 2 EVALUATION OF s_p AND σ_p FOR HOPPING IN BANDS OF FINITE WIDTH

A2.1 Fermi level lying at the centre of the band

In this section we evaluate the expressions (3.3.2), (5.1.2) and (5.1.4) for S , $2B$ and σ_p for the intermediate bandwidth case discussed in Chapter 6. We suppose a rectangular band of states whose width is W . The effect of the bandwidth restriction is to introduce a permissible energy square in the (ϵ_1, ϵ_2) -plane as shown in Figure 32. The shaded area is $A(q)$ where $q = s_p - 2R$ with $R = \alpha r$. $A'(q)$ depends on the relative sizes of q and $W' = W/2k_B T$. From the diagram we deduce that

$$\left. \begin{aligned} A'(q) &= (k_B T)^2 6q & 0 < q < W' \\ A'(q) &= (k_B T)^2 (4W' - 2q) & W' < q < 2W' \\ A'(q) &= 0 & 2W' < q \end{aligned} \right\} \quad (A2.1.1)$$

Since q varies from 0 to $q_{\max} = s_p$ we may write, using eqns. (5.1.2) and (A2.1.1)

$$2B = \frac{2\pi(\sigma_F k_B T)^2}{\alpha^2} \left[\int_a^b 6(s_p - 2R) 2R^2 dR + \int_c^d R^2 (4W' - 2s_p + 4R) dR \right] \quad (A2.1.2)$$

where

$$\begin{aligned} a &= \frac{1}{2}(s_p - W)\theta(s_p - W) \\ b &= s_p/2 \\ c &= \frac{1}{2}(s_p - 2W)\theta(s_p - 2W') \\ d &= \frac{1}{2}(s_p - W)\theta(s_p - W') \end{aligned} \quad (A2.1.3)$$

with $\theta(x)$ denoting the unit step function. Hence:

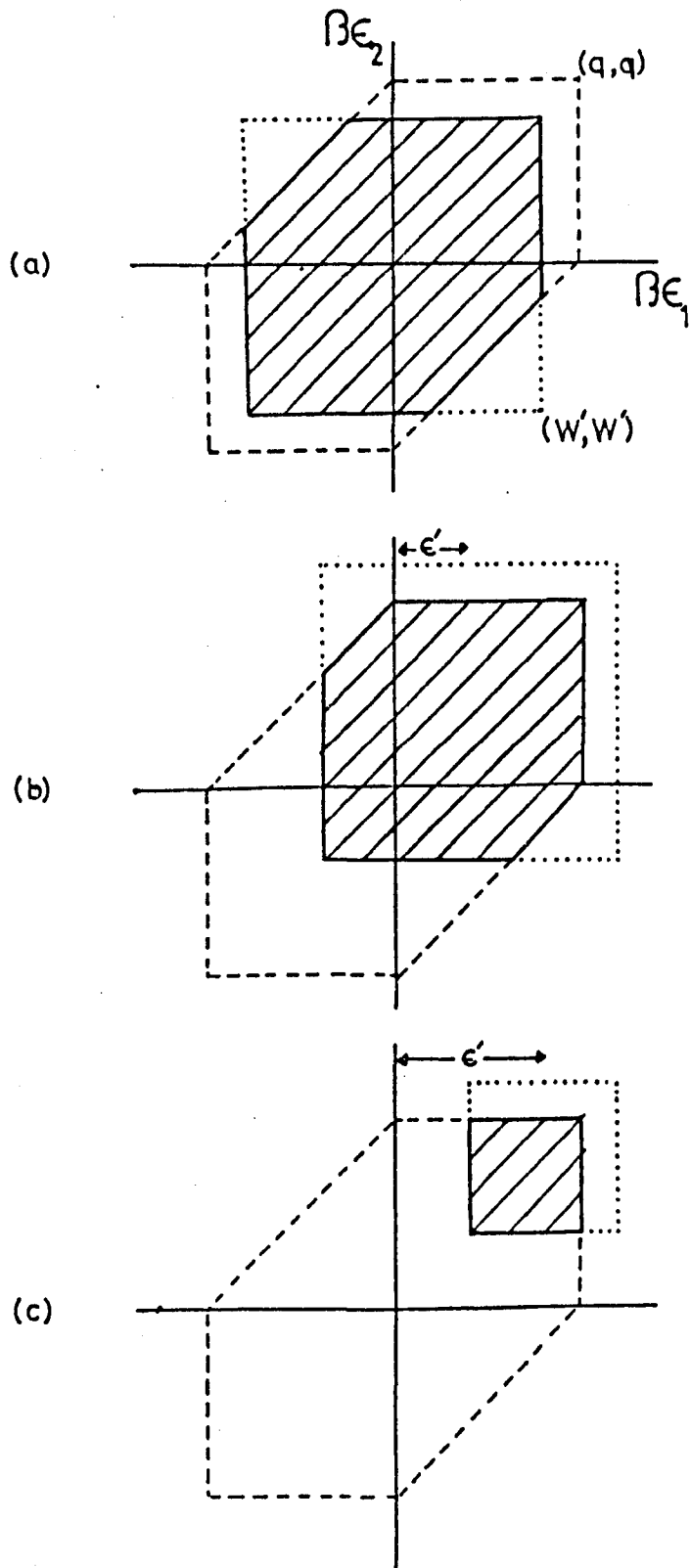


FIGURE 31 Schematic diagram of the $q(\epsilon_1, \epsilon_2) = q$ contours for the case of a finite bandwidth. Figure (a): Fermi level lying at the centre of the band. (b): Fermi level in the band but off-centre. (c): Fermi level outside the band. In each case $A(q)$ is shown shaded and the dots indicate the permitted energy square in the $(\epsilon_1 - \epsilon_2)$ -plane.

$$2B = \frac{\pi(\rho_F k_B T)^2}{24\alpha^2} \begin{cases} x (3s_p^4) & s_p > W' \\ x (-s_p^4 + 8s_p^3 W' - 8s_p^2 W'^3 + 4W'^4) & W' < s_p < 2W' \\ x (24s_p^2 W'^2 - 40s_p W'^3 + 20W'^4) & 2W' < s_p \end{cases} \quad (A2.1.4)$$

The quantity S is easily evaluated to give

$$S = \begin{cases} 2\rho_F k_B T s_p & s_p < W' \\ 2\rho_F k_B T W' & W' < s_p \end{cases} \quad (A2.1.5)$$

Combining equations (A2.1.4) and (A2.1.5) using (3.3.3) we obtain polynomial equations for s_p , the solutions of which are discussed in Chapter 6.

The evaluation of the prefactor proceeds in a similar way.

Using

$$\sigma_p = \frac{g_o \pi(\rho_F k_B T)^2}{160\alpha^4} \begin{cases} (3s_p^5) & s_p > W' \\ (-s_p^5 + 10s_p^4 W' - 20s_p^2 W'^3 + 20s_p W'^6 - 6W'^5) & W' < s_p < 2W' \\ (40s_p^3 W'^2 - 100s_p^2 W'^3 + 100s_p W'^4 - 38W'^5) & 2W' < s_p \end{cases} \quad (A2.1.6)$$

We note that the expression for σ_p reduces to those given in Chapter 4 and Chapter 5 in the limits of very narrow bands ($s_p \gg W'$) and very wide bands ($s_p < W'$).

A2.2 Evaluation of s_p and σ_p when the Fermi level does not lie in the centre of the band

We may readily extend the arguments presented above to the case when the Fermi level does not lie in the centre of the band of localized states. Once we have deduced $A(q)$ for the different cases, the integrals are trivial but tedious. We suppose that the bandwidth is W and that the Fermi level is displaced by an energy ϵ from the

centre of the band. It is convenient to distinguish two regimes: the Fermi level lying in the band ($\frac{W}{2} - \epsilon > 0$) and the Fermi level lying outside the band ($\frac{W}{2} - \epsilon < 0$).

1. Fermi level outside the band

The effect of moving the Fermi level below the centre of the band is to offset the permissible energy square in the (ϵ_1, ϵ_2) -plane towards the upper right quadrant (see Figure 31). If $\epsilon > W/2$ then the square lies entirely in this quadrant. In this case

$$\left. \begin{aligned} A'(q) &= 0 & q &< \epsilon' - W' \\ A'(q) &= (k_B T)^2 [q - (\epsilon' - W')] & \epsilon' - W' &< q < \epsilon' + W' \\ A'(q) &= 0 & \epsilon' + W' &< q \end{aligned} \right\} \quad (A2.2.1)$$

where $W' = W/2k_B T$ and $\epsilon' = \epsilon/k_B T$. We see from eqn. (A2.2.1) that the lower limits on the integrals involving $A'(q)$ depend on whether $s_p < \epsilon' + W'$ (lower limit = 0) or $s_p > \epsilon' + W'$ (lower limit = $\frac{1}{2}[s_p - \epsilon' - W']$). When $s_p k_B T$ lies within the band, we obtain

$$s_p = \left(\frac{24\alpha^2 N_p}{\pi \rho_F k_B T} \right)^{1/3} + \left(\frac{\epsilon - W/2}{k_B T} \right) \quad (A2.2.2)$$

We may interpret the two terms in this equation as follows. The second term arises because of carrier activation from the Fermi level to the edge of the band of localized states. The first term describes the resulting hopping conductivity that takes place and, since $s_p k_B T$ lies within the band, s_p has a $T^{-1/3}$ dependence. We note that T_0 is 50% larger than when the Fermi level lies at the centre of the band. Above a temperature θ' , s_p becomes greater than $\epsilon' + W'$ and eqn. (A2.2.2) is no longer valid. We may readily deduce that

$$\theta' = \left(\frac{W^3 \pi \rho_F}{24\alpha^2 N_p k_B^2} \right)^{1/3} \quad (A2.2.3)$$

For temperatures greater than θ' , s_p is given by a quadratic equation, which is easily solved to give

$$s_p = \frac{W + 6\epsilon}{6k_B T} + \left(\frac{4\alpha_N^2}{\pi n_s} \right)^{\frac{1}{2}} \left[1 - \frac{\pi n_s W^2}{72\alpha_N^2 k_B^2 T^2} \right]^{\frac{1}{2}} \quad (\text{A2.2.4})$$

The term in the square bracket is very nearly unity and so we may write

$$s_p = s_{p^\infty} + \frac{E^{(1)}}{k_B T} \quad (\text{A2.2.5})$$

where $E^{(1)} = \epsilon + W/6$ (we have ignored the small correction due to the temperature dependence of N_p). We see, therefore, that the conductivity will be activated, with an activation energy $E^{(1)}$.

2. Fermi level within the band

If the Fermi level lies within, but below the centre of, the band then the permissible energy square is displaced towards the upper right hand quadrant but is not contained wholly within it. In this case

$$\left. \begin{aligned} A'(q) &= (k_B T)^2 6q & 0 < q < W' - \epsilon' \\ A'(q) &= (k_B T)^2 [2q + 2(W' - \epsilon')] & W' - \epsilon' < q < W' + \epsilon' \\ A'(q) &= (k_B T)^2 (4W' - 2Q) & W' < q < 2W' \\ A'(q) &= 0 & 2W' < q \end{aligned} \right\} \quad (\text{A2.2.5})$$

Because of the many regimes that exist, we have tabulated the results in Tables 4 and 5 where for completeness we have also given the cases when $\epsilon > W/2$. We see that for sufficiently low temperatures we have a $T^{-1/3}$ law. For $T > \theta^{(4)}$ we have an activated behaviour and the activation energy depends on W and ϵ . At intermediate temperatures (regions II and III) the temperature dependence of s_p is more involved, but the temperature range covered by these regions is small compared with that covered by I and IV.

TABLE 4 Table indicating the dependence of the critical percolation exponent s_p and the prefactor σ_p on the system parameters. Section A deals with the case of the Fermi level lying outside the band. Section B deals with the case when the Fermi level lies inside the band, at an energy ϵ below the centre. For each case the solution/equation for s_p and σ_p are given under the temperature regime for which they are valid. Here $\sigma_p' = g_o \pi (\rho_F k_B T)^2 160 \alpha^4$, $K = W' - \epsilon'$, and $J = W' + \epsilon'$, with $W' = W/2k_B T$ and $\epsilon' = \epsilon/k_B T$.

A: FERMI LEVEL OUTSIDE THE BAND

$$\underline{0 < T < \theta^{(1)}}$$

$$s_p = \left[\frac{24\alpha_N^2}{\pi\rho_F k_B T} \right]^{\frac{1}{2}} + \frac{(\epsilon - W/2)}{k_B T}$$

$$\sigma_p = \sigma_p' (s_p + K)^5$$

$$\underline{\theta^{(1)} < T}$$

$$s_p = \frac{E^{(1)}}{k_B T} + s_{p\infty}$$

$$\sigma_p = \left[(s_p + K)^5 - 5(s_p + K)(s_p - J)^4 + 4(s_p - J)^5 \right]$$

B: FERMI LEVEL INSIDE THE BAND

$$\underline{0 < T < \theta^{(2)}}$$

$$s_p = \left[\frac{16\alpha_N^2}{\pi\rho_F k_B T} \right]^{\frac{1}{2}}$$

$$\sigma_p = \sigma_p' 3s_p^5$$

$$\underline{\theta^{(2)} < T < \theta^{(3)}}$$

$$\left[\frac{16\alpha_N^2}{\pi\rho_F k_B T} \right] = \left[6s_p^4 - 4(s_p - K)^3(s_p + K) \right] / (s_p + K)$$

$$\sigma_p = \sigma_p' \left[3s_p^5 - (3K - 2s_p)(s_p - K)^4 \right]$$

$$\underline{\theta^{(3)} < T < \theta^{(4)}}$$

$$\left[\frac{16\alpha_N^2}{\pi\rho_F k_B T} \right] = \left[6s_p^4 - 4(s_p - K)^3(s_p + K) - 8(s_p + K)(s_p - J)^3 - 4(s_p - J)^4 \right] / (J + K)$$

$$\sigma_p = \sigma_p' \left[3s_p^5 - (3K - 2s_p)(s_p - K)^4 - (3J + 2s_p)(s_p - J)^4 \right]$$

$$\underline{\theta^{(4)} < T}$$

$$s_p = \frac{E^{(2)}}{k_B T} + s_{p\infty}$$

$$\sigma_p = \sigma_p' \left[3s_p^5 - (3K - 2s_p)(s_p - K)^4 - (3J + 2s_p)(s_p - J)^4 - (s_p - J - K)^5 \right]$$

TABLE 4

$\theta^{(1)}$	$\left[\frac{W^3 \pi \rho_F}{24 \alpha_N^2 k_B^2} \right]^{\frac{1}{2}}$
$\theta^{(2)}$	$\left[\frac{(W - 2\epsilon)^3 \pi \rho_F}{128 \alpha_N^2 k_B^2} \right]^{\frac{1}{2}}$
$\theta^{(3)}$	NOTE A
$\theta^{(4)}$	NOTE A
$E^{(1)}$	$\epsilon + W/6$
$E^{(2)}$	$\left[\frac{8 - 3(1 - \frac{4\epsilon^2}{W^2})}{12} \right] W$

TABLE 5 Table giving the expressions for the temperatures $\theta^{(i)}$ and energies $E^{(i)}$ in terms of the system parameters.

Note A

The temperatures $\theta^{(3)}$ and $\theta^{(4)}$ are determined numerically by solving the polynomial equations for s_p , and then determining at what temperatures $s_p = W + \epsilon$, ($\theta^{(3)}$), and $s_p = 2W$, ($\theta^{(4)}$), respectively, in a self-consistent manner.

APPENDIX 3 THE TRANSITION RATES

A fundamental quantity in the study of hopping conduction is the equilibrium transition rate R_{12} between sites 1 and 2. In particular, we wish to discuss the single phonon rates, originally calculated by Miller and Abrahams (1960). Their general method of calculation is as follows. They have a variational calculation of the pair wavefunction and then calculate transition rates using the deformation potential interaction between two pair states of different energies. These rates are then averaged over all directions. The resultant form for R_{12} is given by eqns. (4.1.1) and (4.3.1).

Miller and Abrahams make a number of model assumptions and approximations. Perhaps the most important from the point of view of this work is the low density approximation. By low density Miller and Abrahams mean that the resonance energy W , arising through the overlap of the component states, is much less than Δ , the energy difference arising from the random potential field associated with neighbouring donors and acceptors. For small site separations or slowly varying potentials, the approximation $W \ll \Delta$ is not valid. It is of interest to calculate the transition rates for all values of W/Δ .

The following analysis follows that of Miller and Abrahams very closely. We generalise the arguments, however, by keeping the exact wavefunctions which result from the variational calculation of the pair states. We suppose that a sufficient basis for the one electron pair wavefunction Ψ is a linear combination of the hydrogen-like wavefunctions ψ of each isolated state. A straightforward but tedious variational calculation then gives

$$\psi_i = \frac{D^+ \psi_i + \psi_j}{(T^+)^{\frac{1}{2}}} \quad (\text{A3.1})$$

$$\psi_j = \frac{D^- \psi_i + \psi_j}{(T^-)^{\frac{1}{2}}} \quad (\text{A3.2})$$

where

$$D^\pm = (D/2W)(1 \pm F) \quad (\text{A3.3})$$

$$T^\pm = 1 + 2D^\pm S + D^{\pm 2} \quad (\text{A3.4})$$

$$F = (1 + 4WS/\Delta + 4W^2/\Delta^2)^{\frac{1}{2}} \quad (\text{A3.5})$$

Here Δ is the energy difference due to the local environmental potential, and is given by $\Delta \equiv \Delta_i - \Delta_j = \langle \psi_i | V | \psi_i \rangle - \langle \psi_j | V | \psi_j \rangle$. W is the resonance energy between the two sites and $S = \langle \psi_i | \psi_j \rangle$. We now wish to calculate the matrix elements

$$\langle H \rangle = \langle \psi_j | E_1 \eta | \psi_i \rangle \quad (\text{A3.6})$$

where E_1 is the deformation potential and η is the dilation which we may write in terms of the annihilation and creation operators for phonons of wavelength q , b_q and b_q^+ as

$$\eta = i \left(\frac{h}{2\rho_0 V_s} \right)^{\frac{1}{2}} \sum_q q^{\frac{1}{2}} \left[b_q e^{i\mathbf{q} \cdot \mathbf{r}} - b_q^+ e^{-i\mathbf{q} \cdot \mathbf{r}} \right] \quad (\text{A3.7})$$

For phonon absorption,

$$\langle H \rangle = iE_1 \left(\frac{hqn_q}{2\rho_0 V_s} \right)^{\frac{1}{2}} \left[\langle \psi_j | e^{i\mathbf{q} \cdot \mathbf{r}} | \psi_i \rangle \right] \quad (\text{A3.8})$$

The term in the square bracket may be written as

$$[] = \frac{1}{(T^+ T^-)^{\frac{1}{4}}} (D^+ D^- + e^{i\mathbf{q} \cdot \mathbf{R}}) \quad (\text{A3.9})$$

where we have dropped a small term involving an overlap integral between the two sites and assumed $q \gg \alpha$. Here R is the intersite separation. The total transition rate is then

$$R_{ij} = \frac{2\pi}{\hbar} \frac{V}{8\pi^3} \int |H|^2 \delta(\hbar s q - \epsilon_j + \epsilon_i) d^3 q \quad (\text{A3.10})$$

Thus

$$R_{ij} = \frac{E_1^2}{2\rho_0 s \pi} \int q^3 n_q \frac{[(\Delta^+ \Delta^-)^2 + 1]}{T^+ T^-} \delta(\hbar s q - \epsilon_j + \epsilon_i) dq \quad (\text{A3.11})$$

where we have dropped an oscillatory contribution to the integral.

The variation calculation gives the energy difference $\epsilon_j - \epsilon_i = \Delta F(1 - S^2)$.

We may therefore write (A3.11) as

$$R_{ij} = \frac{E_1^2}{\rho_0 s^5 \pi \hbar^4} \left(\frac{\Delta F}{1 - S^2} \right)^3 \frac{[(\Delta^+ \Delta^-)^2 + 1]}{2T^+ T^-} \bar{n}_q \quad (\text{A3.12})$$

where $\bar{q} = \Delta F / (1 - S^2) \hbar s$. It is instructive to put (A3.12) in terms of the quantities W , S , Δ , using (A3.3), (A3.4) and (A3.5). Thus, with $x = \beta \Delta F / (1 - S^2)$

$$R_{ij} = R_0 \frac{x}{e^x - 1} F^2(\alpha r) \frac{1}{(1 - S^2)^3} \left[\frac{S^2 \Delta^2}{2W^2} + \frac{S\Delta}{W} + 1 \right] \quad (\text{A3.13})$$

where R_0 is given by (4.3.1). Here $F(\alpha r)$ is defined by writing $W = (e^2 \alpha / 6\pi \epsilon \epsilon_0)^{-1} F(\alpha r) = W_0 F(\alpha r)$. To regain MA rates we put $S = 0$ and assume $\Delta \gg W$. Eqn. (A3.13) then reduces to the MA rates given by eqns. (4.1.1) and (4.3.1). However, both S and W have primarily the same r -dependence, so strictly speaking the MA rates are only valid if $W_0 \gg \Delta \gg W$ which is true for large separations.

In Figure 32 we show plots of $\log(R_{ij}/R_0)$ against αr for various values of the parameter Δ/W_0 . We see that for all values of αr and Δ/W_0 the hopping rates R_{ij} are many orders less than R_0 . For the site separations which are important in determining the conductivity, however, the MA rates are valid. In this region the parameter R_0 is a sensible characteristic frequency. The purpose of this section has been to illustrate the derivation of the MA rates and to point out rates in the order of R_0 cannot occur in a realistic hopping system.

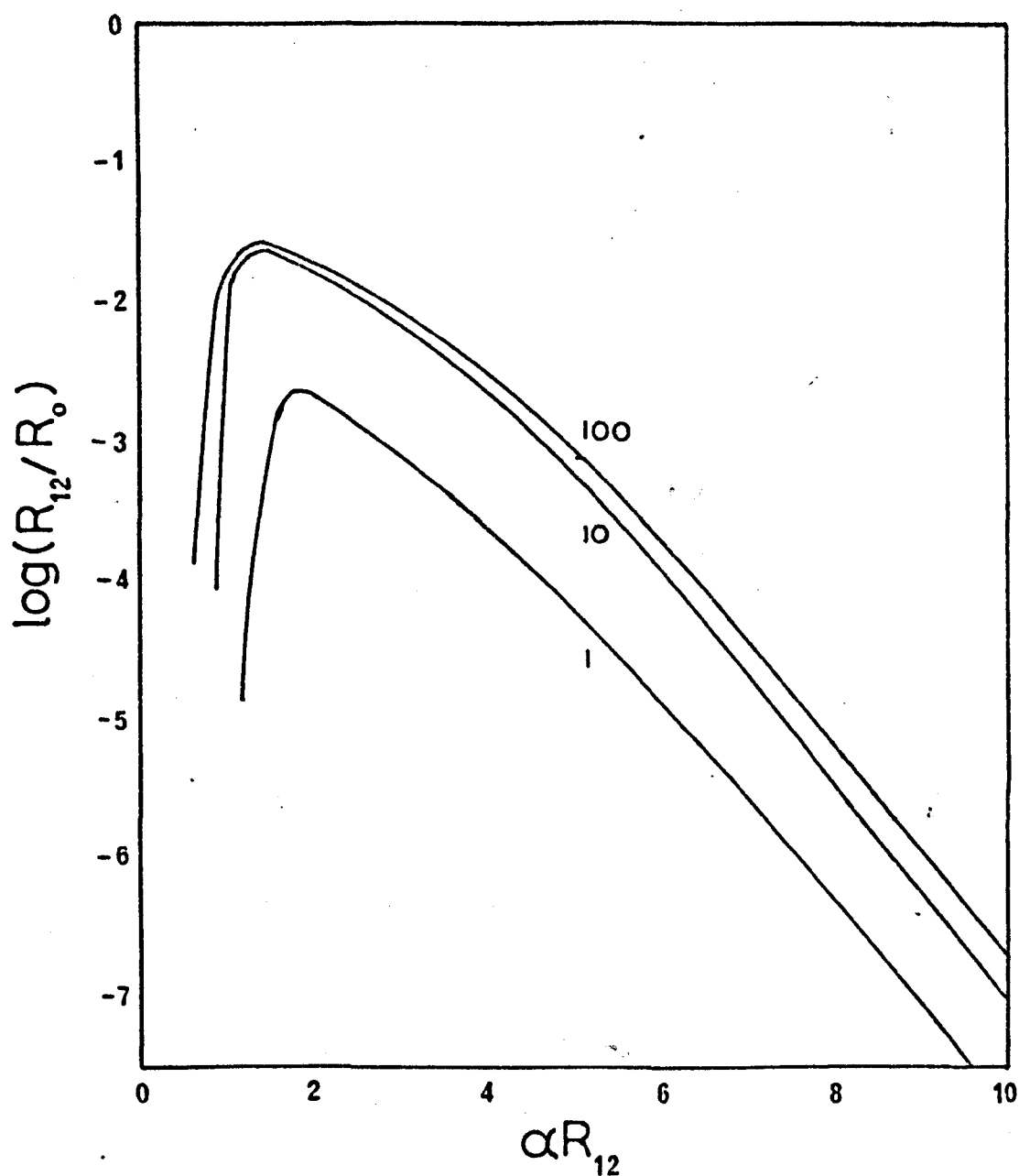


FIGURE 32 Plot of $\log(R_{12}/R_0)$ against the site separation. The numbers on each curve give the relevant value for W_0/Δ . The remaining parameter values were chosen to be $\alpha^{-1} = 1.4$ nm, $T = 200$ K.